ROCK PHYSICS MODELING AND INVERSION IN GLACIAL ORDOVICIAN RESERVOIRS

BY

Ahmed Naseem Al-Dawood

A Thesis Presented to the

DEANSHIP OF GRADUATE STUDIES

KING FAHD UNIVERSITY OF PETROLEUM & MINERALS

DHAHRAN, SAUDI ARABIA

In Partial Fulfillment of the
Requirements for the Degree of

MASTER OF SCIENCE

In

GEOPHYSICS

DECEMBER 2019

KING FAHD UNIVERSITY OF PETROLEUM & MINERALS

DHAHRAN- 31261, SAUDI ARABIA

DEANSHIP OF GRADUATE STUDIES

This thesis, written by **Ahmed Al-Dawood** under the direction of his thesis advisor and approved by his thesis committee, has been presented and accepted by the Dean of Graduate Studies in partial fulfillment of the requirements for the degree of **MASTER OF SCIENCE IN GEOPHYSICS.**

Prof. Abdullatif Al-Shuhail
(Advisor)

Prof. Abdullatif Al-Shuhail
Department Chairman

Dr. Khalid Al-Ramadan
(Member)

Prof. Salam A. Zummo
Dean of Graduate Studies

Dr. Saleh Al-Dossary
(Member)

22/12/09
Date

This thesis is dedicated to my family for their inspiration and support

ACKNOWLEDGMENTS

I would like to thank my advisor Professor Abdullatif Al-Shuhail for his continuous guidance and support throughout this project.

I would like to express my sincere gratitude to the thesis committee members Dr. Saleh Al-Dossary and Dr. Khalid Al-Ramadan for their recommendations and comments especially with the data analysis.

I would like to convey special thanks to Saudi Aramco for providing me with the data and allowing me to allocate time to work on this project.

I would like to extend my appreciation to Hamad Al-Ghenaim for his recommendations and mentorship.

TABLE OF CONTENTS

LIST OF FIGURES

LIST OF ABBREVIATIONS

3D	:	Three Dimensional
AVO	:	Amplitude Variation with Offset
AVA	:	Amplitude Variation with Angel
P-wave	:	Compressional Body Wave
S-wave	:	Shear Body Wave
ρ	:	Density
V_{shale}	:	Volume of Shale
AI	:	Acoustic Impedance
Vp	:	Compressional Body Wave Velocity
Vs	:	Shear Body Wave Velocity
PHIT	:	Total Porosity
SGT	:	Total Gas Saturation
NT	:	Neural Network
RP	:	Rock Physics

ABSTRACT

Full Name : [Ahmed Al-Dawood]

Thesis Title : [ROCK PHYSICS MODELING AND INVERSION IN GLACIAL ORDOVICIAN RESERVOIRS]

Major Field : [Geophysics]

Date of Degree : [December, 2019]

This research aims to investigate the use of post-stack seismic data directly to characterize reservoir fluids by applying rock physics and AVO analysis on the estimated parameters from seismic data.

This research falls into two parts. The first part is using the well logs cross plots for rock physics modeling to get the feasibility study and pay zone through gas fluid substitution utilizing Gassmann's fluid substitution equation. Then, inversion analysis is generated to predict properties such as porosity and gas saturation zones. The second part is to assume there are no drilled wells in the seismic block and the wells there are future planned wells and we would like to know if the reservoir is porous and gas saturated. A synthetic seismogram is created to match the seismic response at the location of interest by forward modeling of P-wave interval velocity and density. Inversion analysis is run on the synthetic wells. Property prediction is done by a feasibility study and pay zone calculation by rock physics modeling of the nearest well to our seismic block, which is about 60 km away from the block. Predicted properties from the two inversion results are

then compared with each other. Also, the results of the estimated parameters studies are validated with the actual well results.

This new approach aims in helping to characterize fluids in the Ordovician reservoir channels in Saudi Arabia as a main challenge in targeting these reservoirs is not being able to characterize the reservoir fluid type. This is mainly because geophysicists are not able to do pre-stack inversion because of the lack of well control in these blocks and the poor quality of the pre-stack gathers.

ملخص الرسالة

يهدف هذا البحث إلى دراسة استخدام البيانات السيزمية مباشرة لوصف سوائل المكمن من خلال تطبيق فيزياء الصخور واختلاف مدى الطاقة بالنسبة إلى البعد على الخصائص المقدرة من البيانات السيزمية.

ينقسم هذا البحث إلى جزئين. الجزء الأول هو استخدام سجلات قطع الآبار لنمذجة فيزياء الصخور للحصول على دراسة جدوى ومنطقة الربح المرغوبة من خلال استبدال السوائل بالغاز داخل المكمن بعد ذلك يتم إنشاء تحليل الانعكاس للتنبؤ بالخصائص مثل المسامية ومناطق التشبع بالغاز.

الجزء الثاني هو افتراض أن ليس لدينا آبار في الكتلة السيزيمة ولكن تم التخطيط لحفرها في المستقبل ونود أن نعرف ما إذا كان المكمن مسامياً ومشبعاً بالغاز.

يتم اصطناع بيانات سيزمية لتماثل مدى طاقة البيانات السيزمية في المكان المرغوب عن طريق التحليل الأمامي لسرعة الموجات الأولية والكثافة. بعد ذلك يتم إنشاء تحليل الانعكاس على البيانات السيزمية المصطنعة. يتم التنبؤ بالخصائص من خلال تطبيق فيزياء الصخور على أقرب بئر للمنطقة السيزمية على بعد 60 كم للحصول على دراسة جدوى ومنطقة الربح المرغوبة. بعد ذلك يتم مقارنة نتائج تحليلي الانعكاس مع بعضهما وأيضاً يتم مقارنة نتائج دراسة الخصائص المقدرة مع نتائج البئر الفعلية.

تهدف هذه الطريقة إلى المساعدة في وصف السوائل في المكامن في القنوات الاودوفيشية في المملكة العربية السعودية بسبب وجود صعوبات في وصف السوائل في هذه المكامن ويعود السبب في ذلك إلى عدم تمكن الجيوفيزيائيون من تحليل الانعكاس لقلة الآبار المحفورة في هذه المناطق السيزمية بالإضافة إلى قلة الجودة في البيانات السيزمية.

الاسم الكامل: أحمد نسيم الداوود

عنوان الرسالة: تحليل فيزياء الصخور والانعكاس في المكامن الاوردفيشية الجليدية

التخصص: ماجستير في الجيوفيزياء

تاريخ الدرجة العلمية: ديسمبر 2019

CHAPTER 1

INTRODUCTION

1.1 Background

Reflection seismic data plays a major role in hydrocarbon exploration and field development. There have been advances in the oil industry to increase the rate of successful wells as well as increase hydrocarbon reserves. These advances include improvements of drilling practices, which optimized well costs and drilling time, and 3-D seismic acquisition, which improved mapping of faults, horizons, and structure. Seismic quality improvements allowed for better interpretation of structural and stratigraphic traps, bright spots, and amplitude variation with offset (AVO).

Identification of reservoir fluids is essential for interpreters to place their prospects at the maximum hydrocarbon accumulation trap in the reservoir. Hydrocarbon-filled reservoirs are characterized with lower acoustic impedance as they have lower density and lower velocity than the surrounding water-filled rocks. There are different methods to characterize fluid properties in the reservoir such as, well logs, AVO inversion, rock physics, and seismic inversion.

One of the challenges of targeting Ordovician formation channels in 3-D seismic blocks in the study area is not being able to characterize the reservoir fluid type. This is mainly because geophysicists are not able to do pre-stack inversion because of the lack of well control in these blocks and the poor quality of the pre-stack gathers.

1.2 Study Area

Paleozoic rocks are exposed along the eastern margin of the Arabian Shield, in addition to northwestern and central Arabia. Central Arabia went through a series of epirogenic movements associated with global tectonic events. The three main regional tectonic episodes were Taconic, Acadian, and Hercynian movements. Sub-Middle Ordovician and sub-Upper Silurian unconformities are a result of these epirogenic phases (Laboun, 2009).

During Middle Ordovician, sediments were deposited in stable marginal shelf conditions as a result of tectonic quiescence (Senlap & Al-Duaiji, 2001). The area went through an uplift and tilt following that deposition during late Ordovician. Lower Ordovician and Middle Ordovician formations were exposed and eroded. Upper Ordovician glaciation affected the Arabian Plate that was sitting on the margin of the Gondwana supercontinent during the Upper Ordovician, which resulted in the deposition of glacial sandstone Formation across the Arabian Plate. In the outcrop, the Upper Ordovician glacial sandstone formation is a confined underfilled valley with very fine to conglomeratic sand dominated glaciogenic deposits. In the subsurface, deposits are unconfined overfilled valley with glaciomarine sandstones.

The Upper Ordovician deformed unit (Melvin, 2015) was also deposited along with Upper Ordovician glacial sandstone formation as a result of sea level fall and glaciation. The Upper Ordovician deformed unit is composed of a repetition of tillite, boulder-clay, and fined grained micaceous sandstone lithofacies. The Upper Ordovician glacial sandstone formation consists of fine to coarse grained trough cross-bedded fining upward sandstone. The glaciation events subdivide the Cambrian – Ordovician – Silurian

succession into three depositional cycles: pre-glaciation cycle (Lower and Middle Ordovician formations), syn-glaciation cycle (Upper Ordovician Formation), and post-glaciation cycle (Upper Ordovician and Lower Silurian units) as seen in Figure 1.1 (Laboun, 2009).

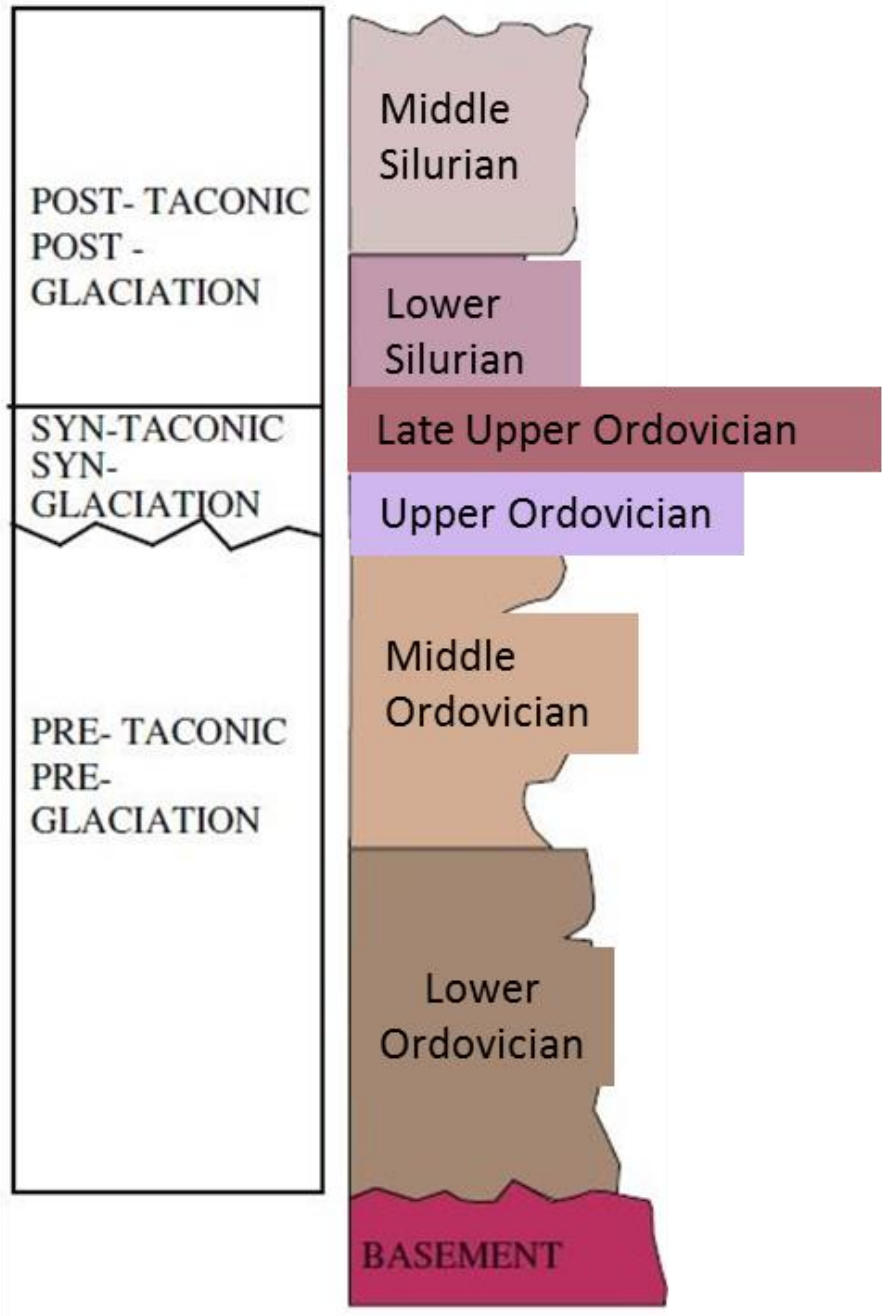

Figure 1.1: The three deposition cycles associated with the glaciations (Modified after Laboun, 2009)

The Upper Ordovician glacial sandstone formation is believed to be deposited in a range of fluvio-glacial and glaciomarine environments. Palynological data from core analysis in the study area indicate glacio-marine conditions where sub-glacial erosion of tunnel

valleys fed glacial outwash fans that were developed during ice maxima low-stand phases separated by extended narrow channels (Figure 1.2). The Upper Ordovician post glacial unit unconformity of the fluvial and shallow marine and isostatic rebound caused regional instability. Upper Ordovician post glacial unit sedimentation was deposited above the unconformity as a result of differential unloading and fault reactivation. In this area, the Upper Ordovician post glacial unit is shallow marine and dominated by tidal features. The Lower Silurian unit overlies Upper Ordovician post-glacial unit and is characterized by gray to black color, organic rich, mudstones, and claystones as the eustatic sea level rose on Gondwanan ice sheet during Lower Silurian. Glacial margin flooded and Lower Silurian unit sediments were deposited (Craigie, Rees, MacPherson, & Berman, 2016).

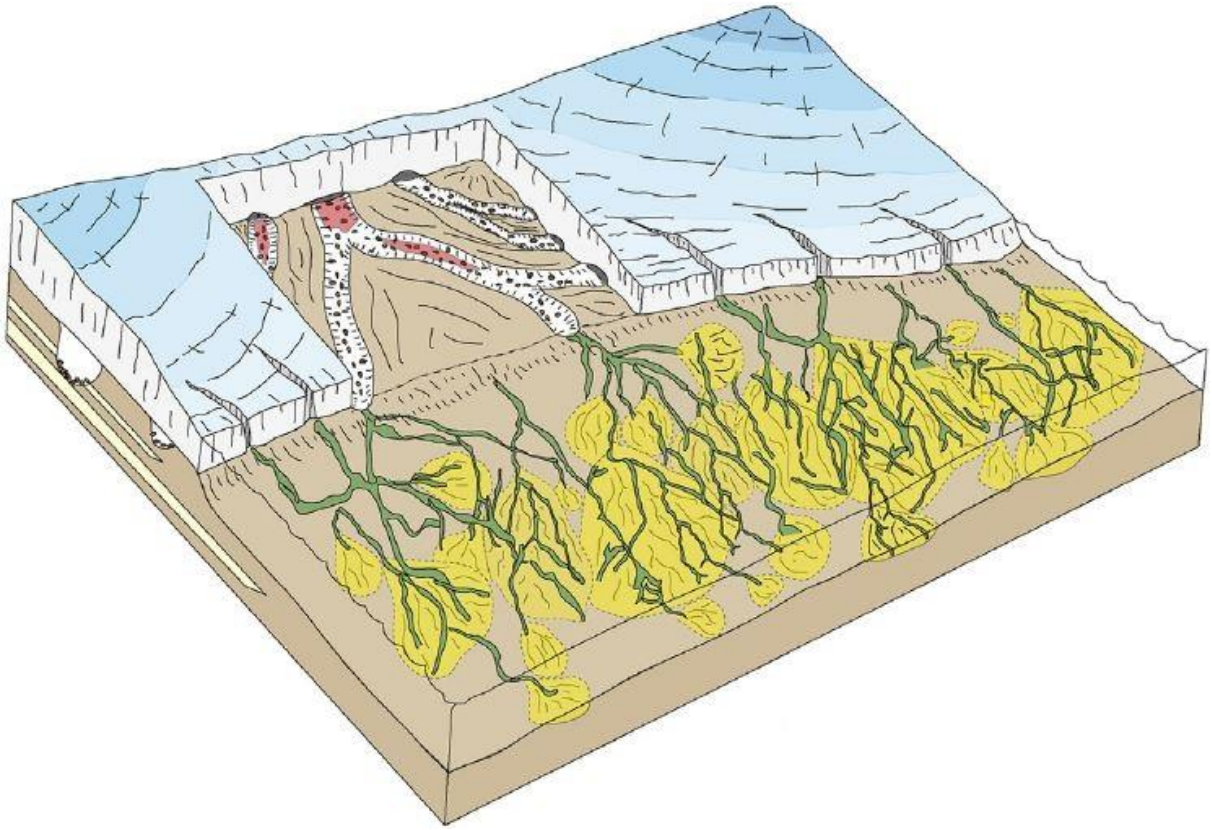

Figure 1.2: A model of sub-glacial tunnel valleys feeding glacial outwash fans separated by extended narrow channels (Craigie, Rees, MacPherson, & Berman, 2016)

1.3 Objective

This research aims to investigate the use of post-stack seismic data to characterize reservoir fluids. Acoustic impedance and P-wave interval velocity are used to calculate a synthetic seismogram that matches the seismic response at the target reservoir in the well location. This method will be applied to different fluid-saturated reservoirs where there are wells to validate this method. Rock physics modeling and two models of inversion are generated. The first model is generated using estimated parameters and the second model using real parameters from a well. Results of the two models are compared.

1.4 Literature Review

1.4.1 Well Logs Interpretation

In the oil industry, a log means a recording against depth of any of the rock characteristics of the rock formations traversed by a measuring apparatus in the wellbore (Serra, 1984). Wireline logs are measured by lowering the logging tools in the wellbore by a cable. Measurements then are transferred to a computer unit where they get recorded to construct the well log. Different logs are run, each one of them records a different property of the rocks surrounding the wellbore. Well logs present a detailed plot of formation parameters versus depth. The plots are interpreted to identify formations properties such as lithology, porosity, resistivity, and fluid zones.

Electric logs measure formation resistivity. Resistivity measures the electric current flow in a rock. Its unit is ohm.m. Resistivity is the reciprocal of conductivity. Electrical current conductivity is a function of the conductivity of the water contained in the rock's pore space. Fresh water has low conductivity and high resistivity. However, if the formation

water contains salt ions, then conductivity will be high, and resistivity will be low. If the rock's pore space is filled with hydrocarbon, then resistivity will be high as hydrocarbons are non-conductive (Varhaug, 2016).

The spontaneous potential log (SP) measures the voltage difference between a wellbore's movable electrode and a fixed electrode at the surface. While drilling, drilling mud filtrate invades permeable rocks around the wellbore. SP baseline is established across impermeable shale formations. If the formation fluids are more saline than the filtrate, negatively charged chlorine ions will shift the SP curve to the left. If the formation contains fresher water than the filtrate, SP curve will shift to the right. Permeability, porosity, formation water salinity, and mud filtrate properties influence the magnitude of the SP curve shift. SP curve indicates permeable formations (Varhaug, 2016).

Gamma ray (GR) log measures the formation's natural occurring radioactivity. GR is used to differentiate between shales and clays from reservoir rocks. Shales and clays are more radioactive than carbonates and sandstones as they contain radioactive elements such as potassium, uranium, and thorium (Varhaug, 2016).

Density log is measured by emitting gamma ray into the formation, which collides with the formation's electrons. The number of collisions is related to the number of electrons in the formation. Gamma rays reach the detectors more in a low-density than in a high-density formation. Generally, the rock's density is inversely proportional to the porosity (Varhaug, 2016).

In neutron logs, a chemical source or an electronic neutron generator emits neutrons that collide with hydrogen atoms in a formation where they slow down as they lose energy at a rate that is proportional to the hydrogen index (HI). HI is measured by neutron porosity

tools. The formation's porosity's fluids are determined by hydrogen atoms concentration (Varhaug, 2016).

The sonic log measures the time it takes for a sound wave to travel through a formation. Porosity, lithology, and fluid content affect the travel time of the wave in a formation. Figure 1.3 illustrates different logs measurements with different fluids.

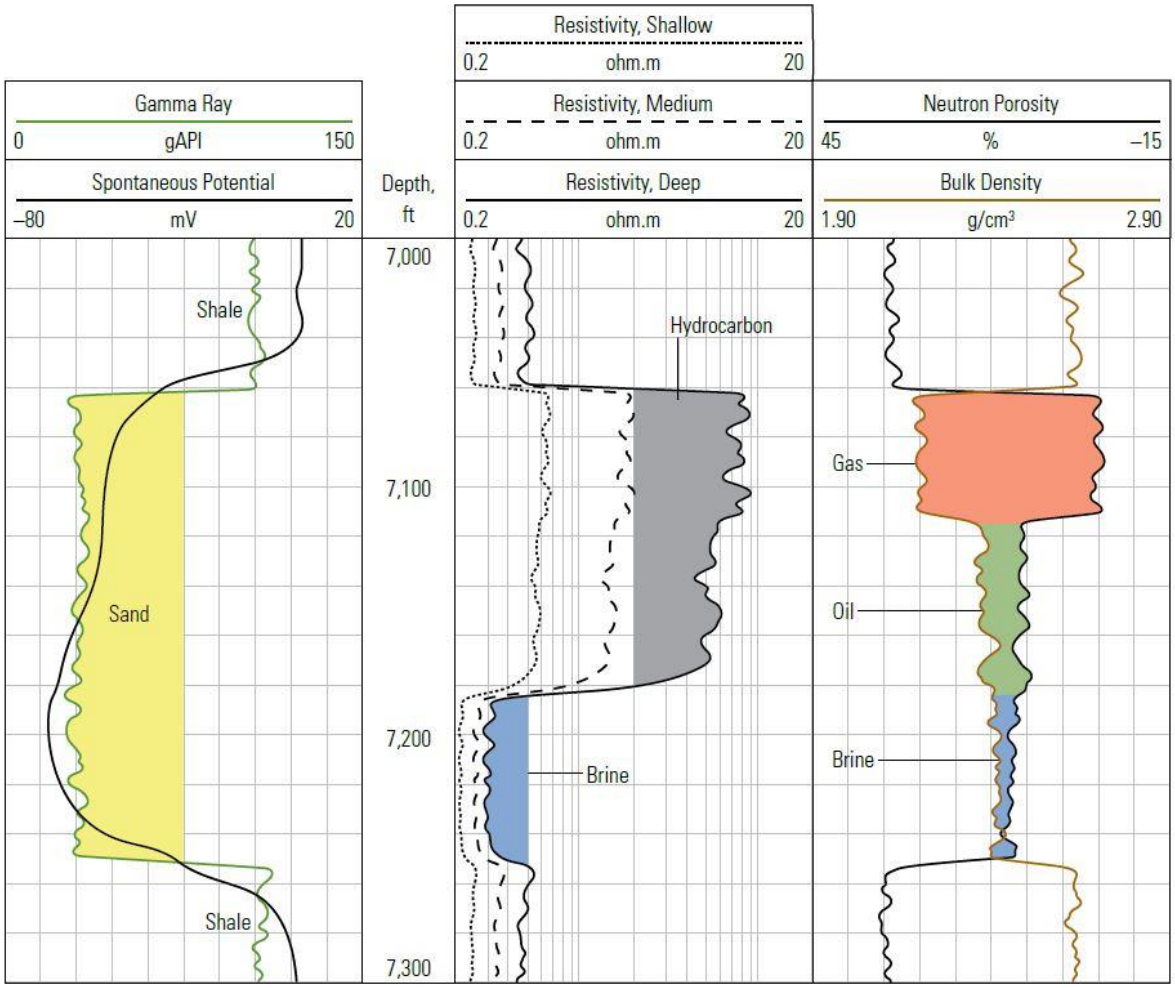

Figure 1.3: Different log measurements with different fluids (Varhaug, 2016)

1.4.2 Seismic Inversion

In forward modeling, we apply a mathematical simulation on earth properties such as Vp, Vs, and density to generate synthetic seismic data (Figure 1.4). In seismic inversion (Figure 1.5), seismic reflectivity data is converted to rock properties such as acoustic impedance, Vshale, porosity, and water saturation (Barclay, 2008).

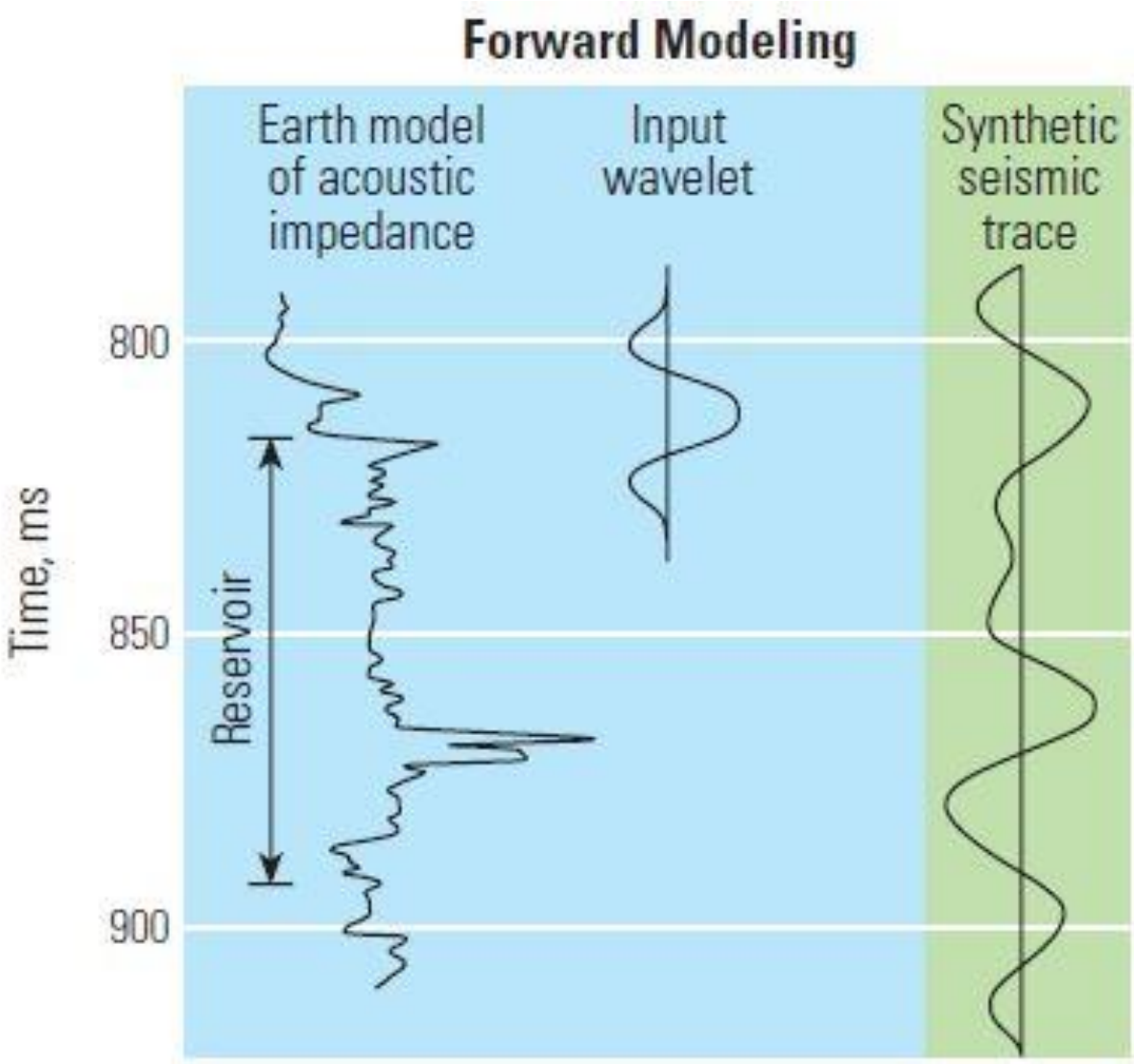

Figure 1.4: Forward Modeling (Barclay, 2008)

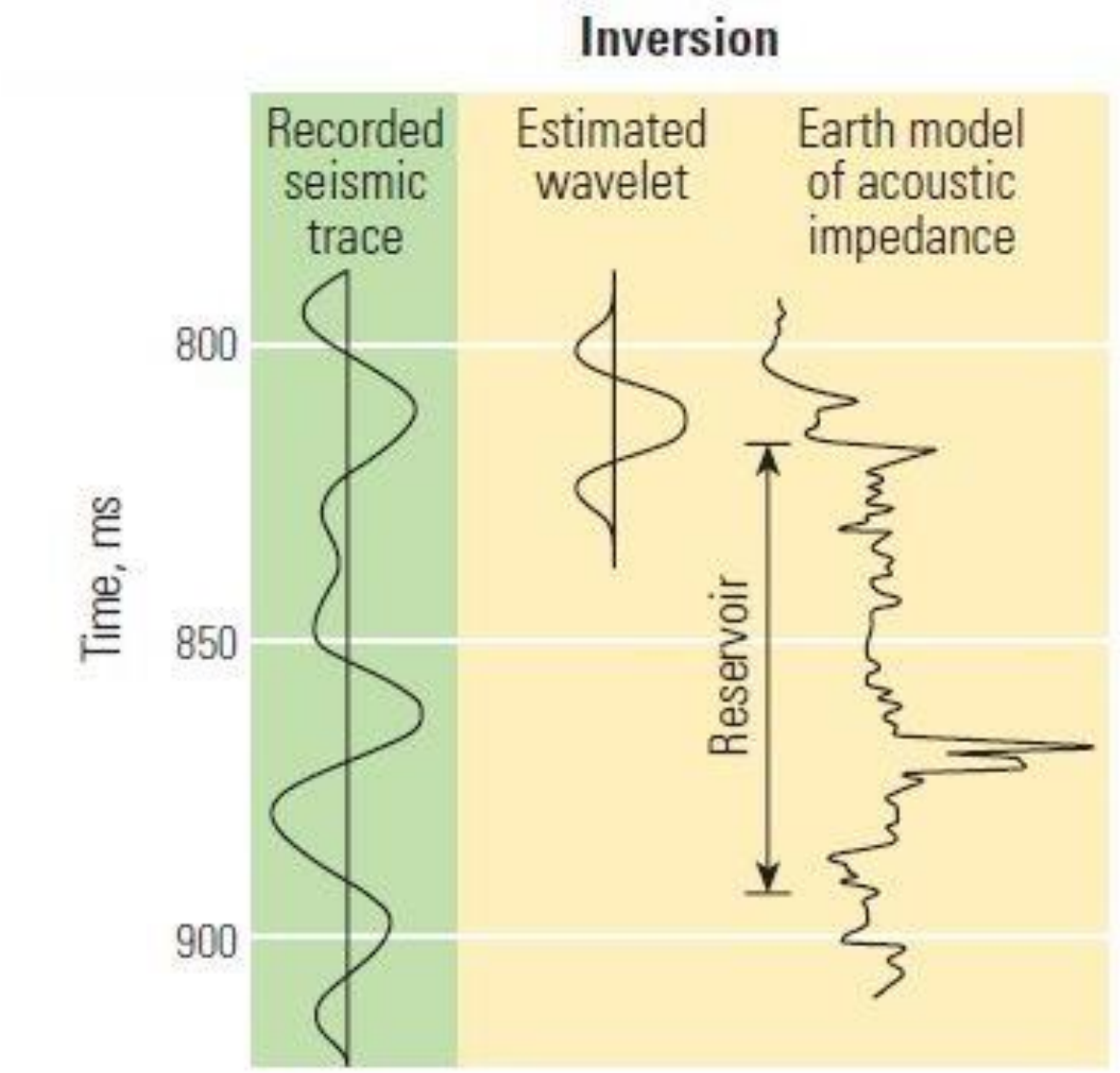

Figure 1.5: Inverse modeling (Barclay, 2008)

Seismic inversion is classified according to the type of seismic data used: pre-stack or post-stack data. Post-stack data is used to invert for acoustic impedance. Pre-stack data is used to invert for P-impedance, S-impedance, and density (Altowairqi, 2015). Log data have to be conditioned and QC'ed before they are utilized. In Figure 1.6, in the left plot,

washouts and borehole collapse effect the data quality in the top right plot. After corrections, the rock physics trend is clearer as shown in the bottom right plot.

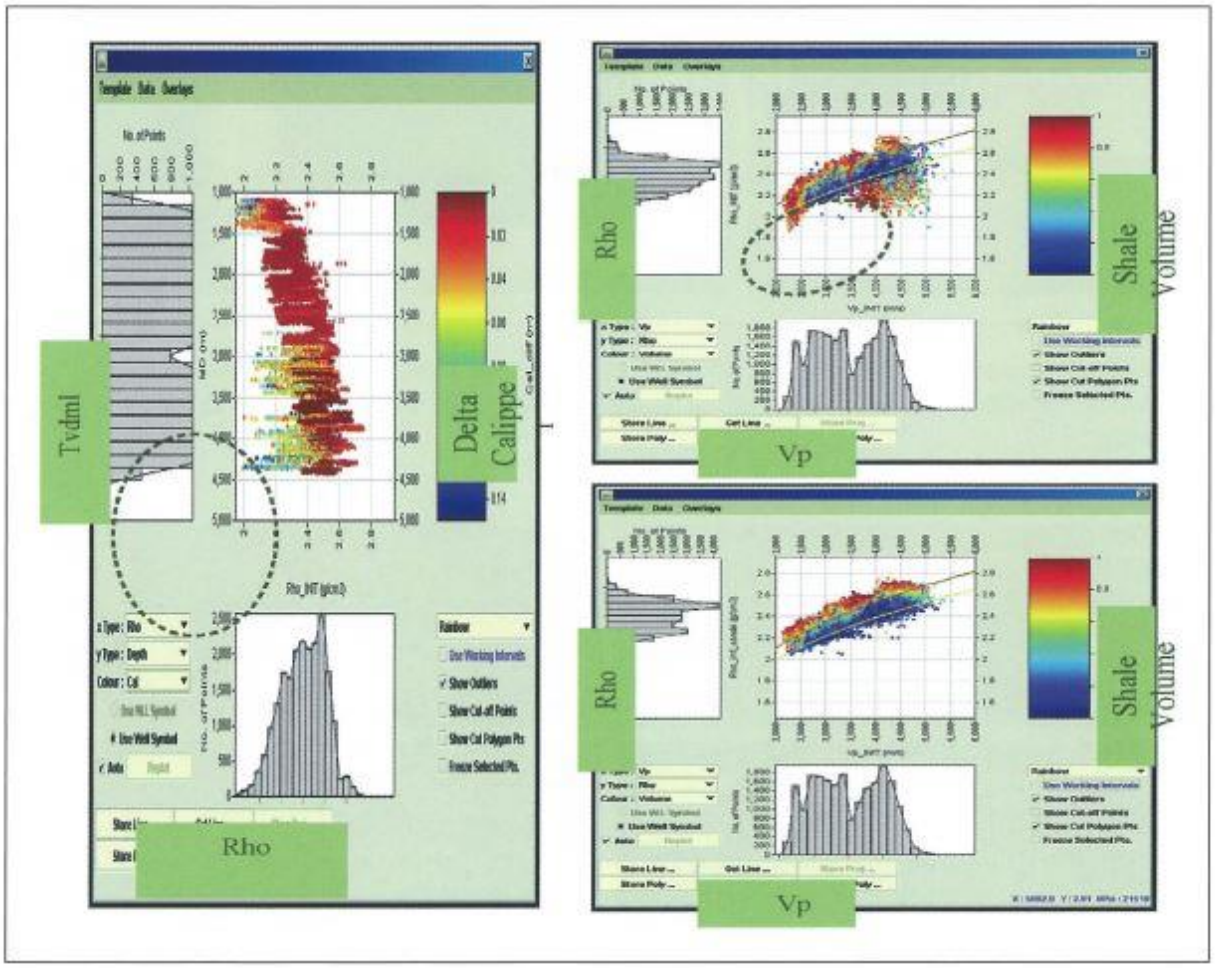

Figure 1.6: Log data conditioning effect on the rock physics trend (Kemper, 2010)

To perform an acoustic impedance inversion modeling, we start with an earth model with estimated formation depths, velocities, and thicknesses derived from well log data. This model is convolved with a wavelet from the seismic to generate a synthetic seismic data. Inversion takes place by iterating between the synthetic forward model and the real seismic data to get the best fit model (Barclay, 2008).

Seismic data is band-limited. Low frequency models are generated from well log data to constrain the inversion and add high frequency beyond the seismic band (Kemper, 2010). Combining relative acoustic impedance derived from seismic and low frequency model derived from well logs generate an absolute acoustic impedance model (Figure 1.7). Absolute acoustic impedance is required to obtain reservoir properties such as velocity and density (Barclay, 2008).

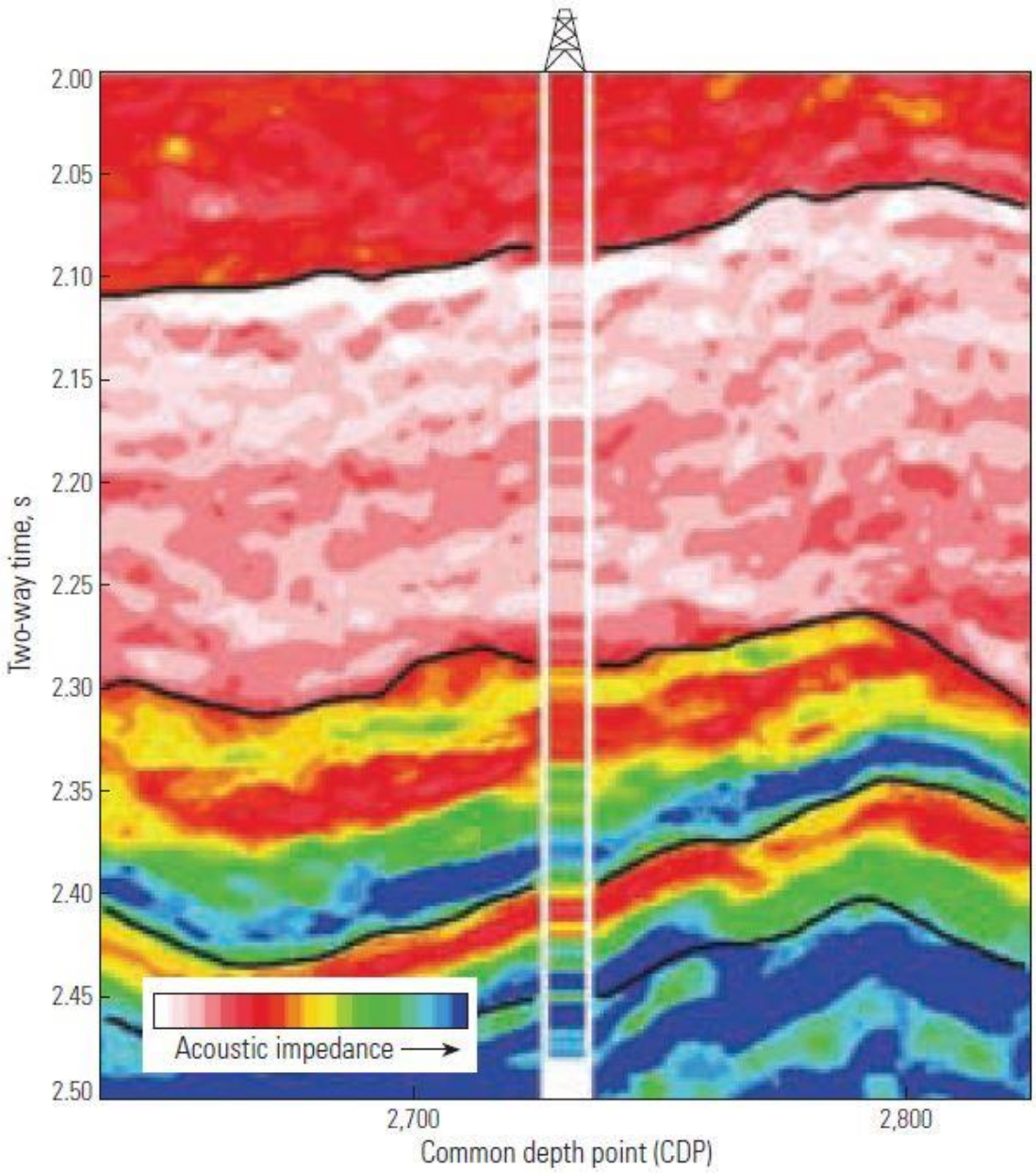

Figure 1.7: Absolute acoustic impedance model (Barclay, 2008)

1.4.3 AVO

Amplitude variation with offset (AVO) analysis is a technique used for hydrocarbon identification by validating seismic reflection amplitude anomalies. Zoeppritz equations are used to derive the amplitudes of a reflected P-wave as a function of incidence angle.

These equations are too complicated to be used for explaining the relationship between amplitudes and the physical parameters. There have been several approximations of Zoeppritz equations over the years. Bortfeld (1961) emphasized the fluid and rigidity terms, which helped in interpreting fluid-substitution problems. Aki and Richards (1980) emphasized on P- and S- wave velocities and densities. Shuey (1985) modified the equations to include Poisson's ratio and found a relationship between angle stacks and rock properties. The first term in Shuey's equation is the normal incident reflectivity and it dominates at small incidence angles (0-15^0). The second term dominates at intermediate incidence angles (15-30^0). The third term dominates at large incidence angles (30-45^0). The third term is insignificant as most incidence angles are below 30^0 (Feng & Bancroft, 2006).

Shuey's approximation is given by:

$$R(\theta) = A + B \sin^2 i + C(\tan^2 i - \sin^2 i) \quad (1)$$

$$A = \frac{\Delta V_P}{2V_P} + \frac{\Delta \rho}{2\rho} \quad (2)$$

$$B = \frac{\Delta V_P}{2V_P} - 4\frac{{V_S}^2}{{V_P}^2}\left(\frac{\Delta \rho}{2\rho} + \frac{\Delta V_S}{2V_S}\right) \quad (3)$$

$$C = \frac{\Delta V_P}{2V_P} \quad (4)$$

where

θ = average of incidence and transmission angles across the interface

V_P = average of P-wave velocities across the interface

V_S = average of S-wave velocities across the interface

ρ = average of densities across the interface

Gas sand reflections have been divided into four classes based on their AVO characteristics (Figure 1.8). Intercept and gradient are plotted to view different trends of elastic properties as viewed in Figure 1.9.

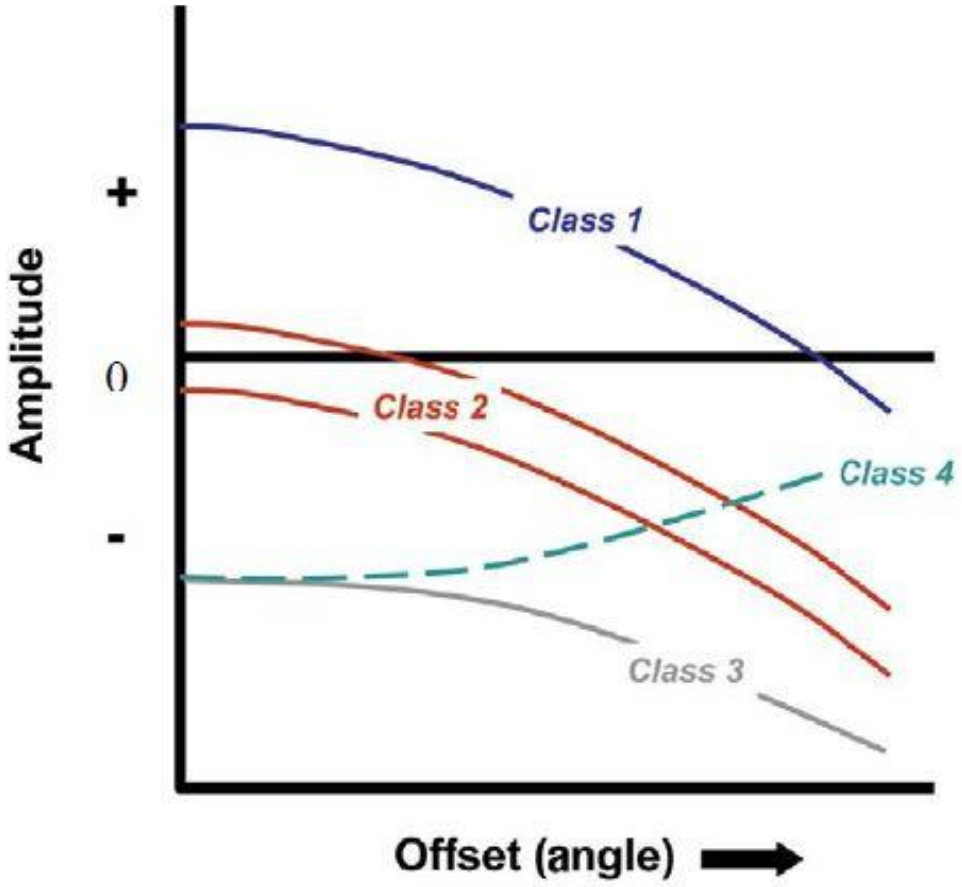

Figure 1.8: AVO classes (Rutherford & Williams, 1989)

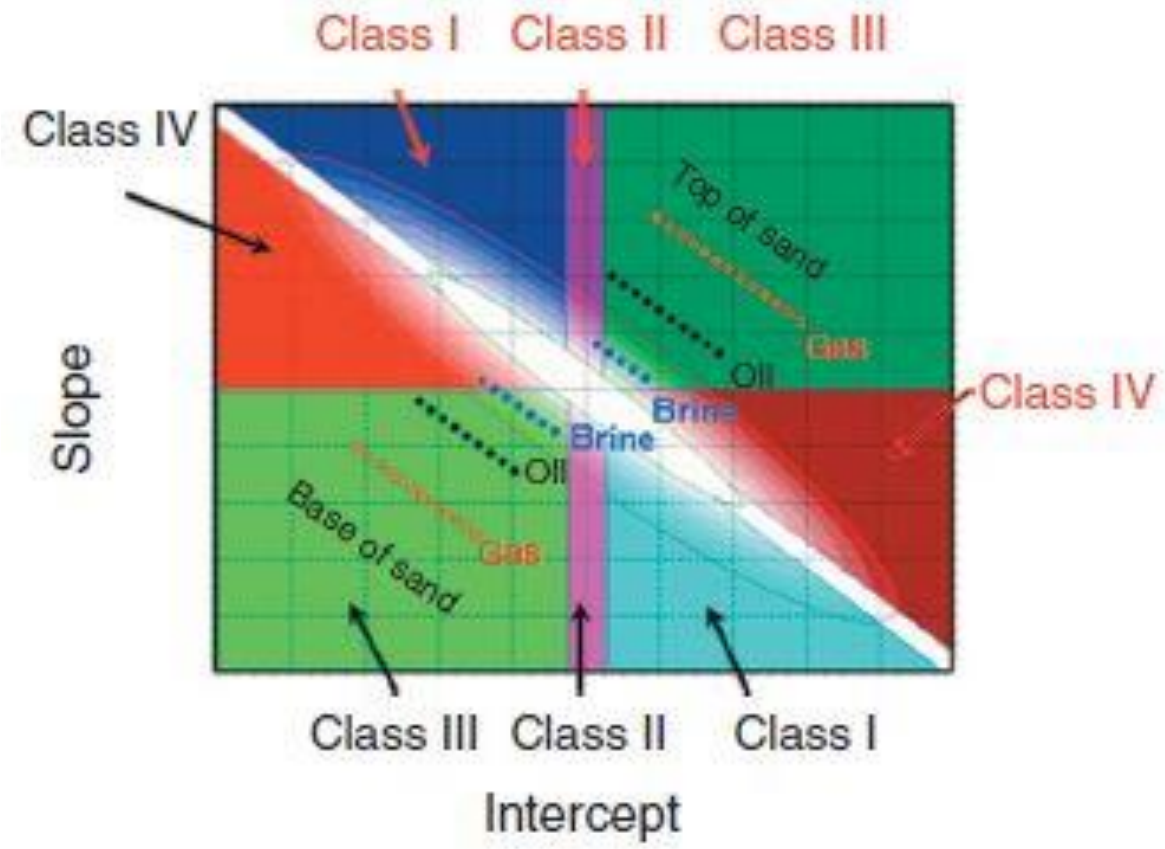

Figure 1.9: AVO intercept and gradient (Foster et al., 2010)

1.4.4 Joint Inversion of the P-wave velocity and Impedance

Ali & Al-Shuhail (2017) characterized the reservoir pore fluids by joint inversion of the P-wave velocity and P-wave impedance calculated from post-stacked seismic data without requiring well log data. The workflow of this research was tested on a 3-layer geological anticline model. In the model, the first layer extends from the surface to the top of the second layer, the second layer is a shale that acts as a cap rock, and the third layer is a sandstone that is the reservoir in this model. The top part of the reservoir is

saturated with hydrocarbon and the remaining part is fully saturated with water (Figure 1.10).

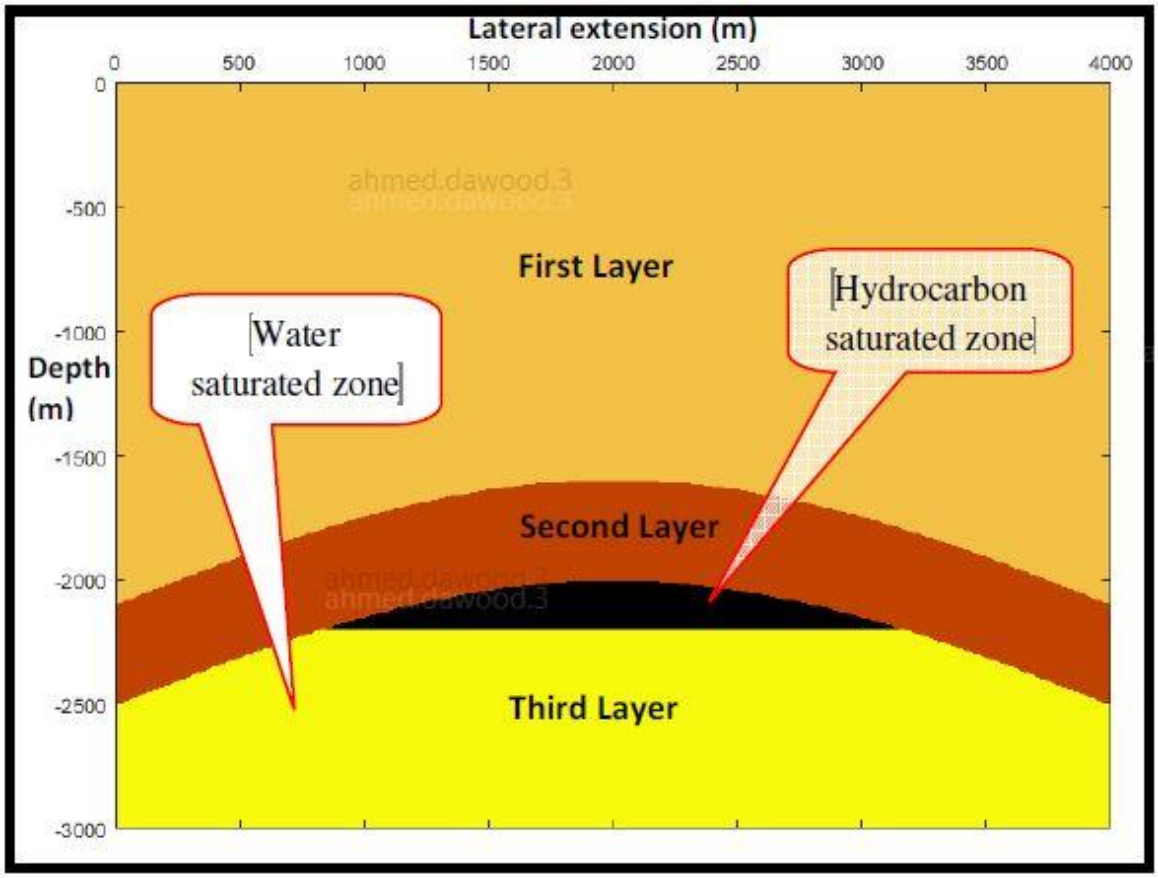

Figure 1.10: A 3-layer geological anticline model (Ali & Al-Shuhail, 2017)

Three different fluids (gas, oil, and water) have been used to compute elastic and seismic properties of the reservoir fluid. Gassmann's equation was used to observe the pore fluid effects on seismic properties. Acoustic impedance was computed by assuming the density and velocity of each layer. Reflection coefficient was computed and convolved with a minimum phase wavelet to generate synthetic seismic data (Figure 1.11). Acoustic

impedance (AI) was calculated from the seismic data using the recursive inversion method. Interval velocities were calculated using Dix equation.

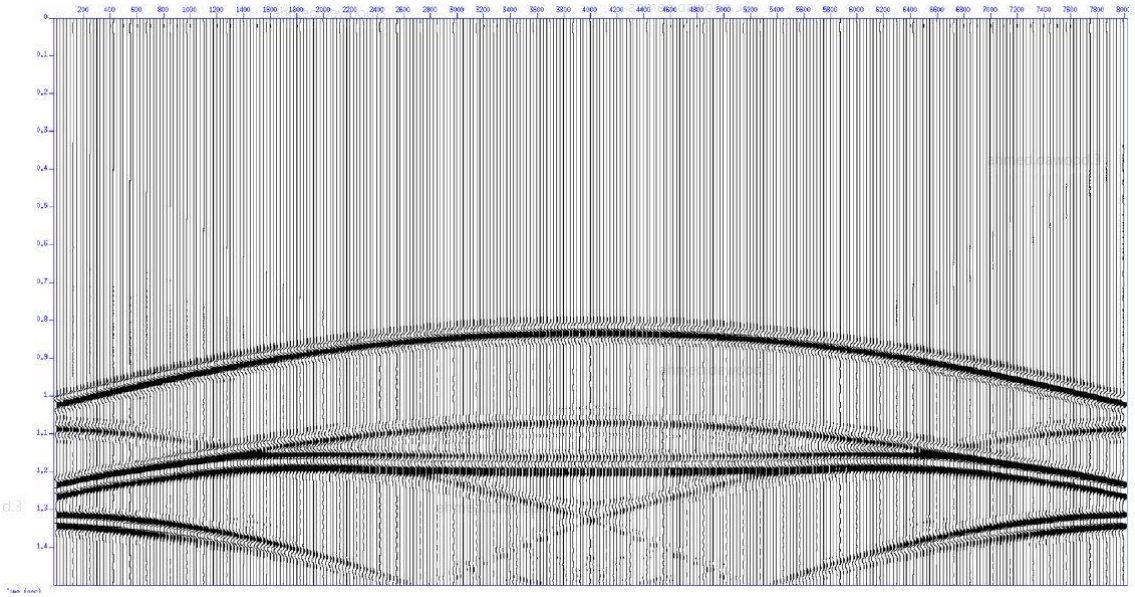

Figure 1.11: Synthetic seismic data (Ali & Al-Shuhail, 2017)

Three different cases were studied in this research. In the first case; the top part of the reservoir is fully saturated with gas, which is followed by brine water (Figure 1.12). In the second case, the top part is saturated with oil, which is followed by brine water. Porosity is assumed to be 20% in these two cases. In the third case, this method was applied to a reservoir in Saudi Arabia, with variable porosity, where the top part is saturated with oil, which is followed by brine water. For all three cases, AI, fluid density, and fluid velocity inversion have been used to identify the pore fluid in the reservoir. All inversions gave good evidence of the presence of two different pore fluids in the reservoir. The inversion of all cases resulted in a small error between the inverted and true fluid properties.

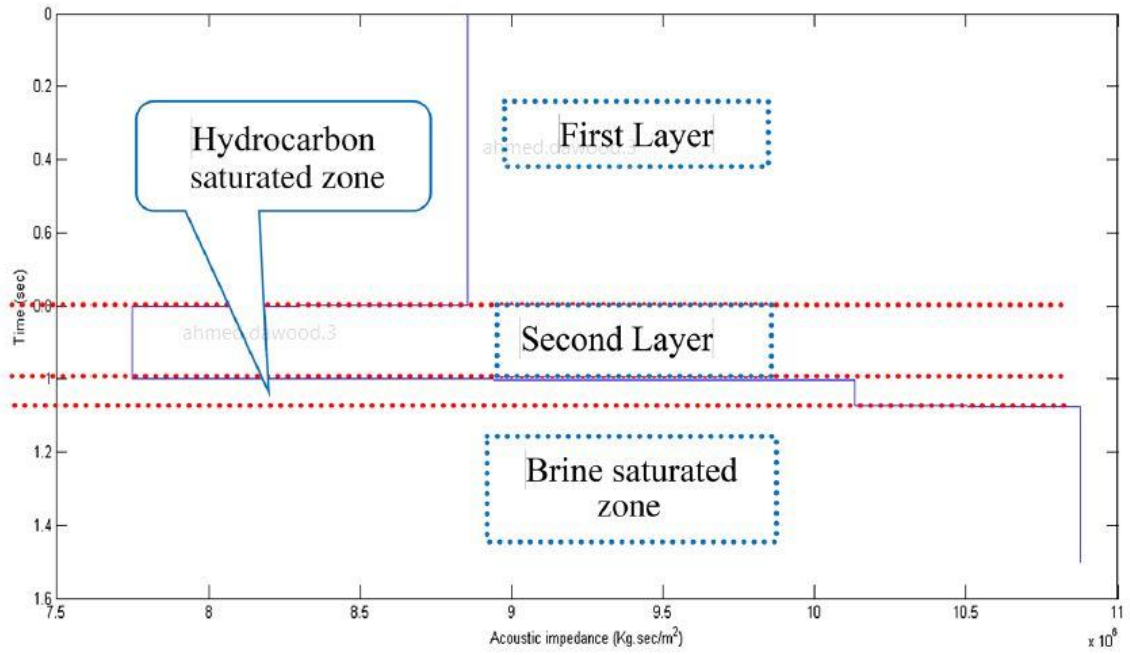

Figure 1.12: Fluid inversion from seismic data (Ali & Al-Shuhail, 2017)

CHAPTER 2

METHODOLOGY

This research is divided into two parts. The first part is using the well logs cross plots for rock physics modeling to get the feasibility study and pay zone through gas fluid substitution utilizing Gassmann's fluid substitution equation followed by inversion analysis to predict properties such as porosity and gas saturation zones. The second part is to assume we have no wells in our seismic block and the wells we have are future planned wells and we would like to know if the reservoir is porous and gas saturated. I create a synthetic seismogram that matches the seismic response at the location of interest by forward modeling of P-wave interval velocity and density. Inversion analysis is run on the synthetic wells. Property prediction is done by a feasibility study and pay zone calculation by rock physics modeling of the nearest well to our seismic block which is about 60 km away from the block. The results from the two inversion results are compared with each other. The workflow of model-based Inversion is indicated in Figure 2.1

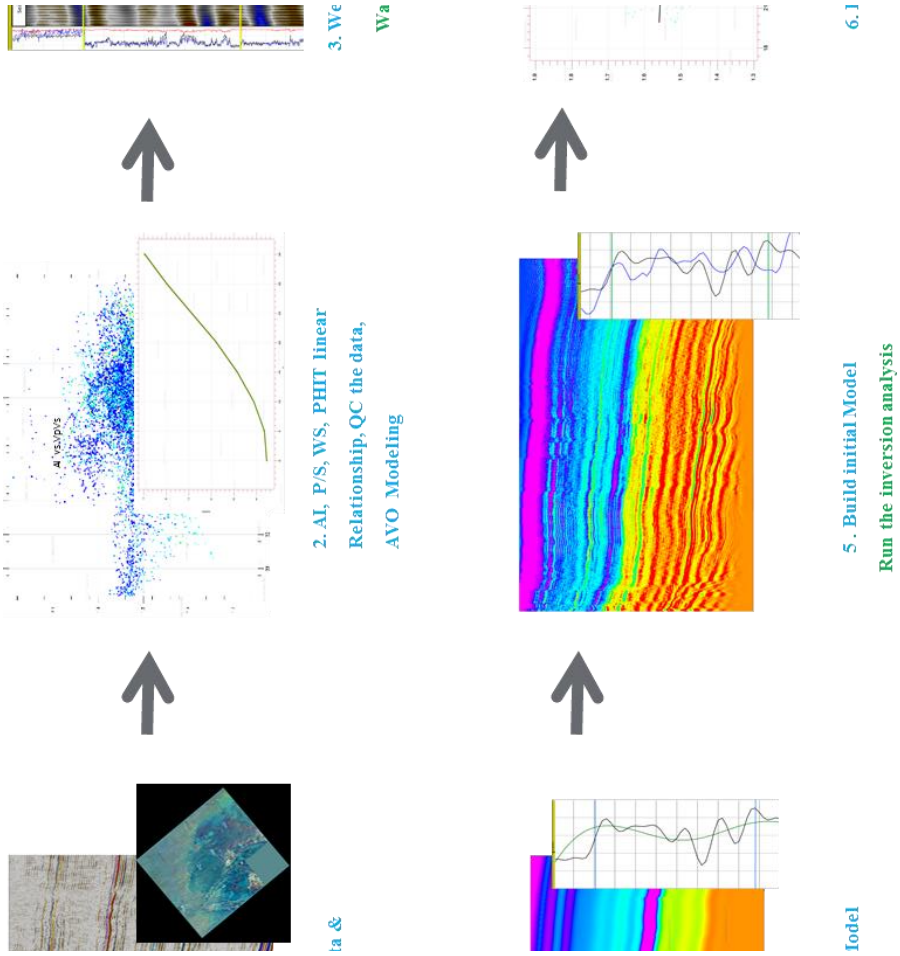

Figure 2.1: Model-based inversion workflow

2.1 Seismic and Wells Data

The 3D seismic volume used in this study covers an area of approximately 3400 km^2. Interpretation was done on post-stack data. Inversion was run on five angle stacks, which go from 0° to 50° at an increment of 10°. Six exploration wells' measured and calculated logs data such as sonic, density, and their mineral contents are used in this study. Five of those exploration wells are located in the seismic block (Figure 2.2).

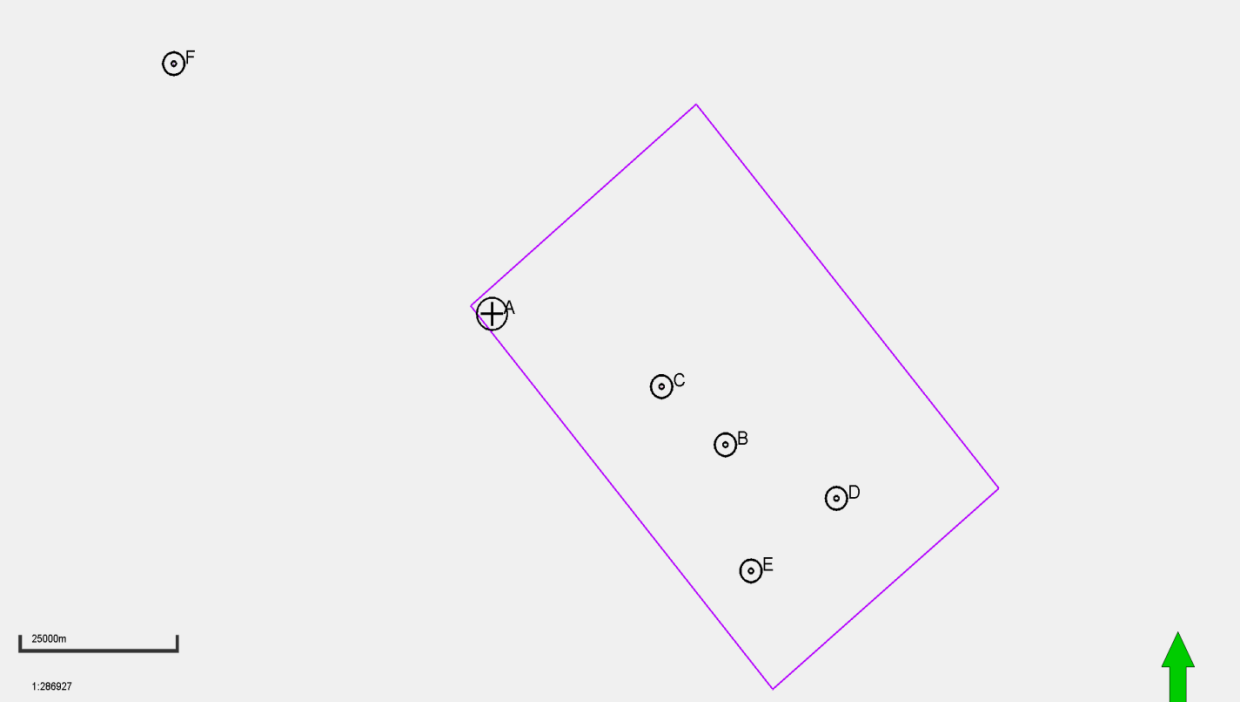

Figure 2.2: Base map showing the wells and the seismic block

2.2 Seismic Interpretation

Five horizons are picked on seismic data ranging from shallow to deep (Figure 2.3). They are used in building the low frequency model to constrain the inversion.

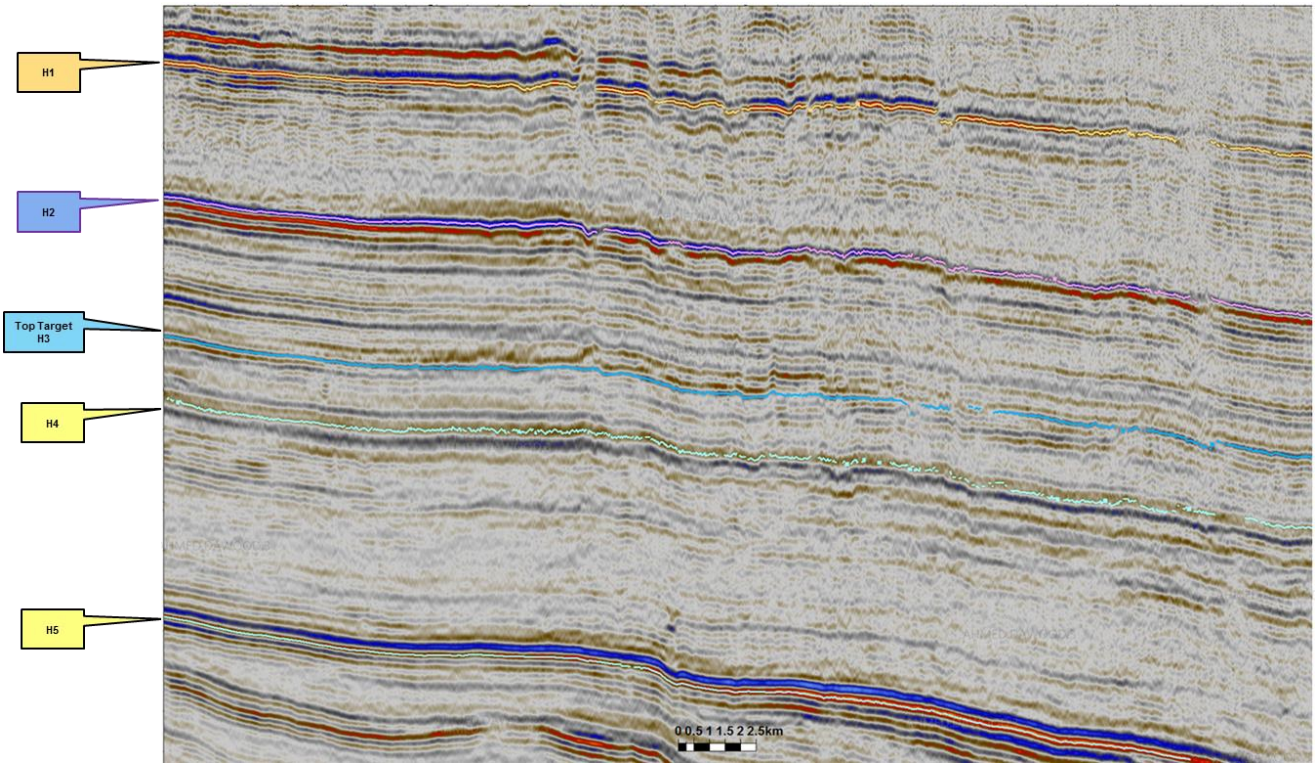

Figure 2.3: Seismic section showing picked horizons

After picking horizons, seismic data is flattened at Top target (H3) and spectral decomposition attributes are generated at 15, 20, and 25 Hz. These three attributes are blended together to form a Red-Green-Blue (RGB) color blended map where each color corresponds to a specific frequency range (Figure 2.4).

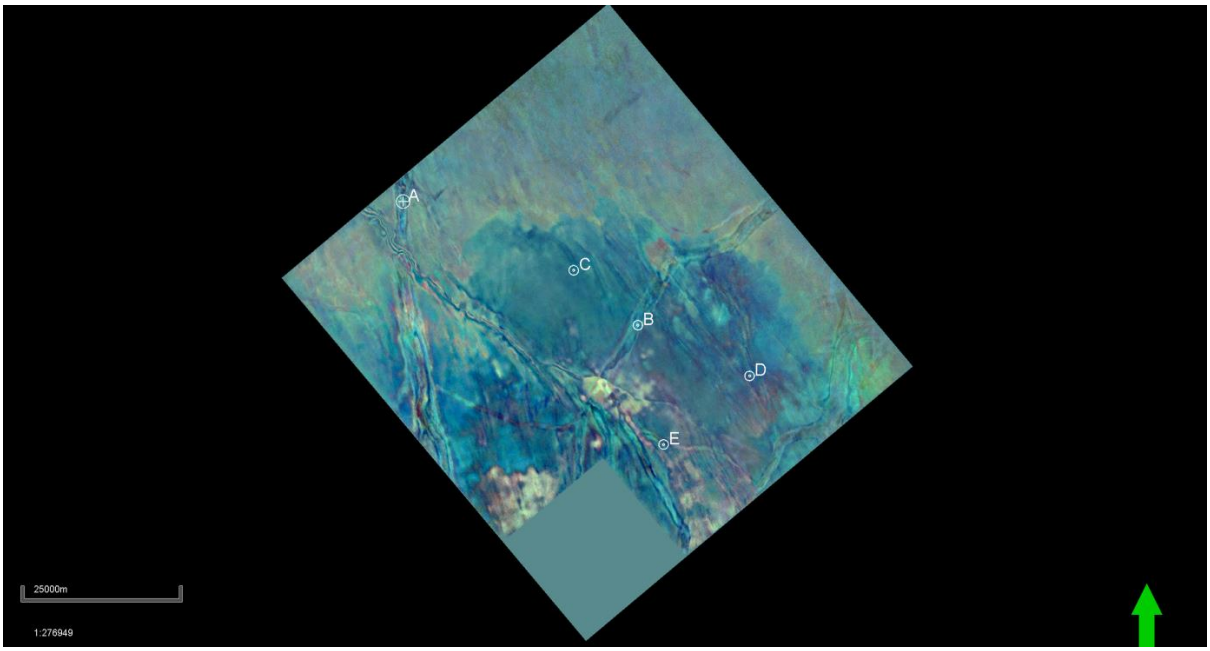

Figure 2.4: Spectral decomposition attribute (15, 20, 25 Hz)

RGB color blended map is used to view the channels geometry. Channels extent and shape are clear on this map. Channels polygons are drawn from this attribute map (Figure 2.5).

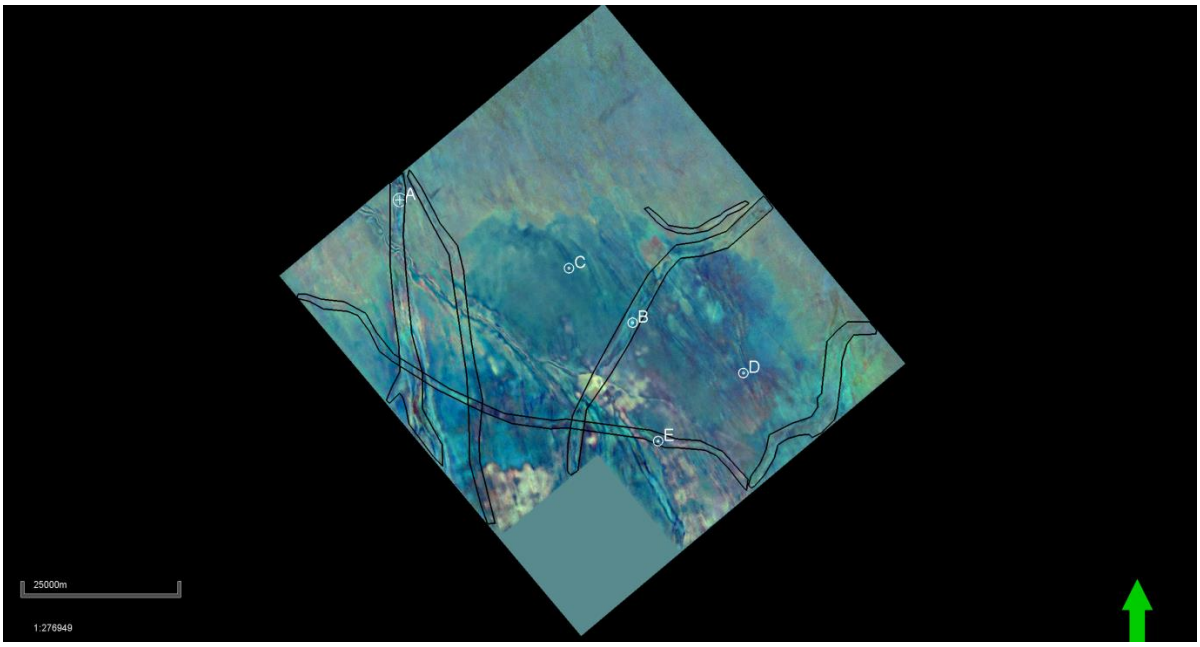

Figure 2.5: Spectral decomposition attribute map with channels polygons

2.3 Feasibility Study

The first step in feasibility study is to cross plot all the log data. Since the target formation is clastic, the best data distribution is to cross plot acoustic impedance and Vp/Vs color coded with water saturation (Figure 2.6). When cross plotting acoustic impedance and porosity, there is a direct relationship between them (Figure 2.7).

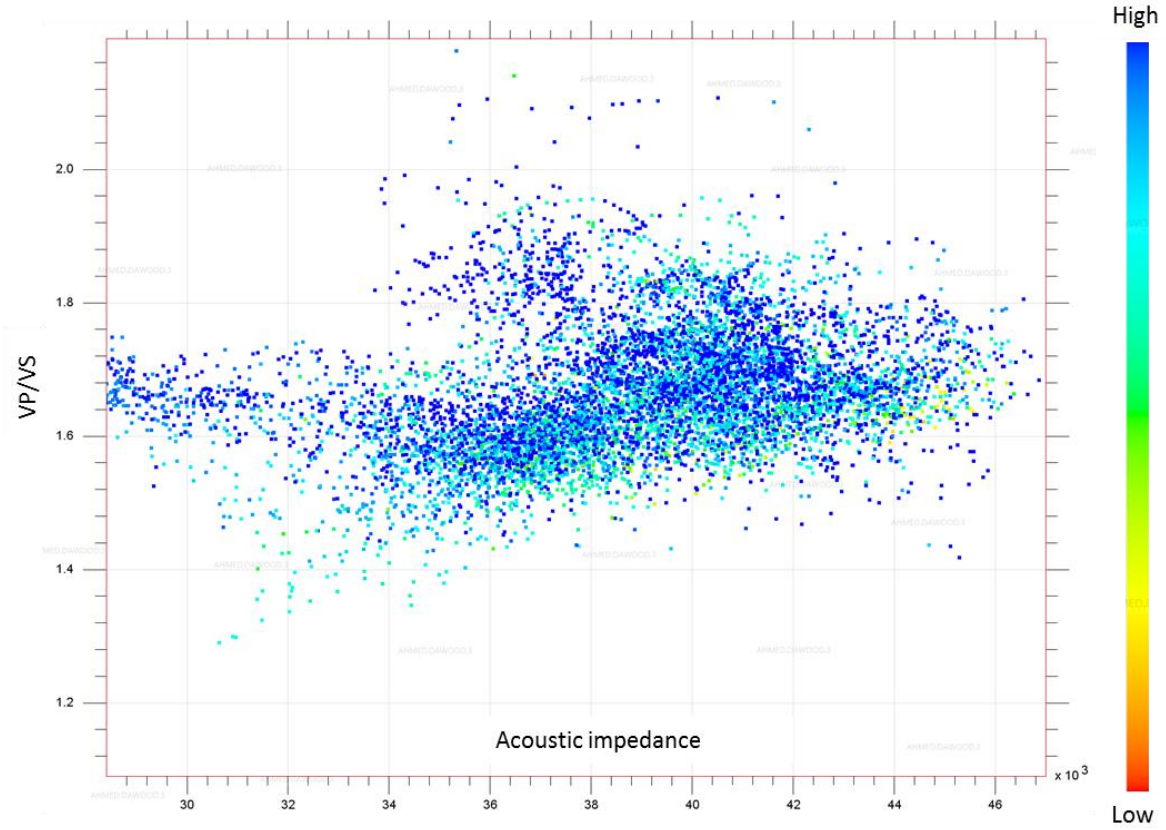

Figure 2.6: Crossplot of Acoustic Impedance and Vp/Vs

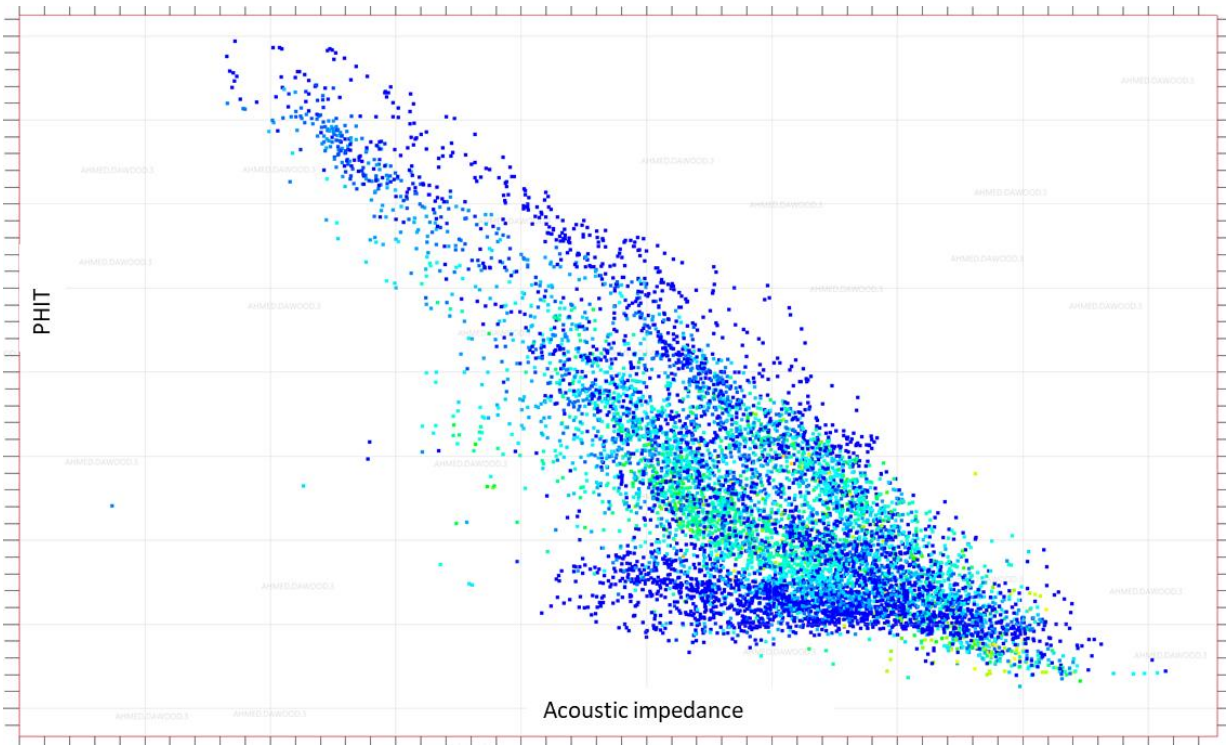

Figure 2.7: Crossplot of Acoustic Impedance and porosity

From these two graphs, AI inversion differentiates between porous and tight zones. It does not indicate the rock's fluid type. Vp/Vs inversion needs to be performed along with AI inversion to determine the rock's fluid type.

Three rock types were classified from AI and Vp/Vs crossplot, which are gas, water, and tight. Rock types are verified when gas zones are detected on the well logs (Figure 2.8).

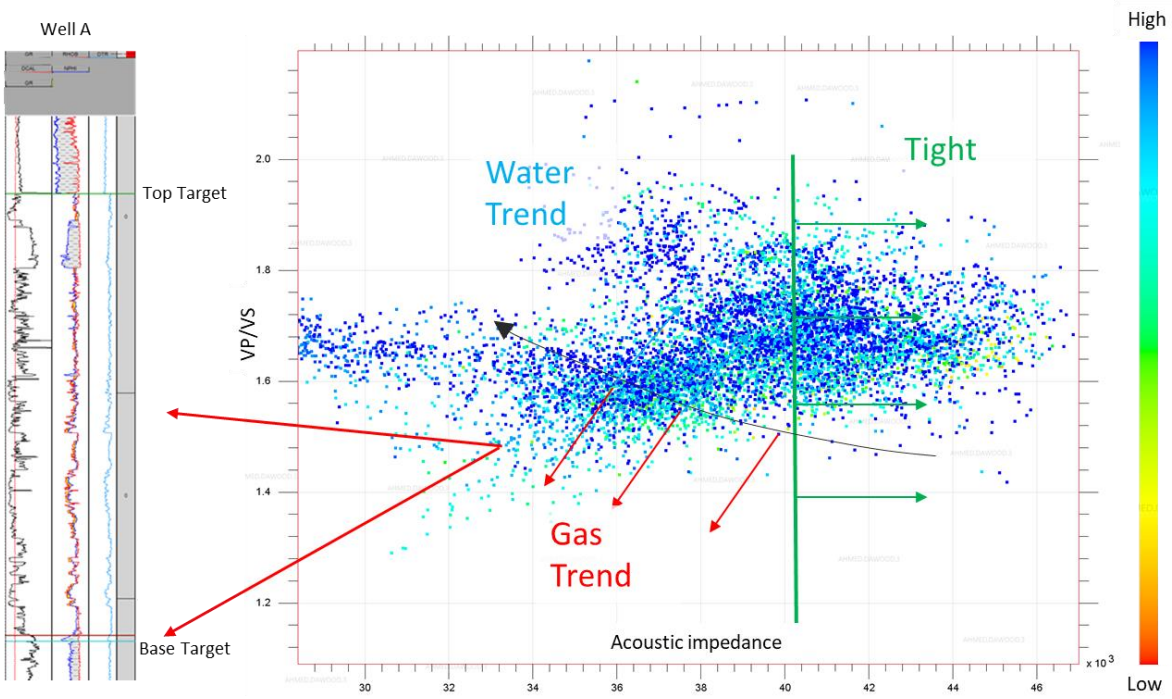

Figure 2.8: Rock type classification from crossplots

The target formation frequency spectrum range is between 7-42 Hz (Figure 2.9). Well logs were filtered to 30 Hz, which is even lower than the maximum frequency for the target formation, to see if rock types can be detected at seismic bandwidth. Rock types are verified when the lower gas zone is detected on the well logs (Figure 2.10).

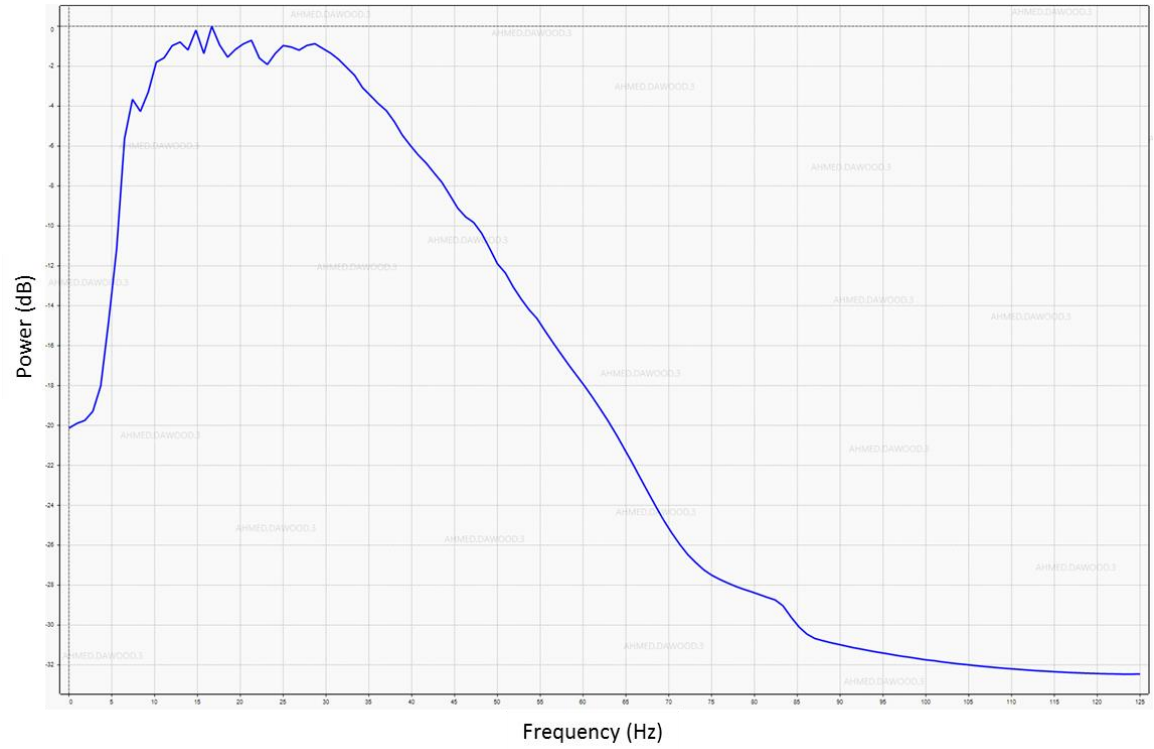

Figure 2.9: Target formation frequency spectrum

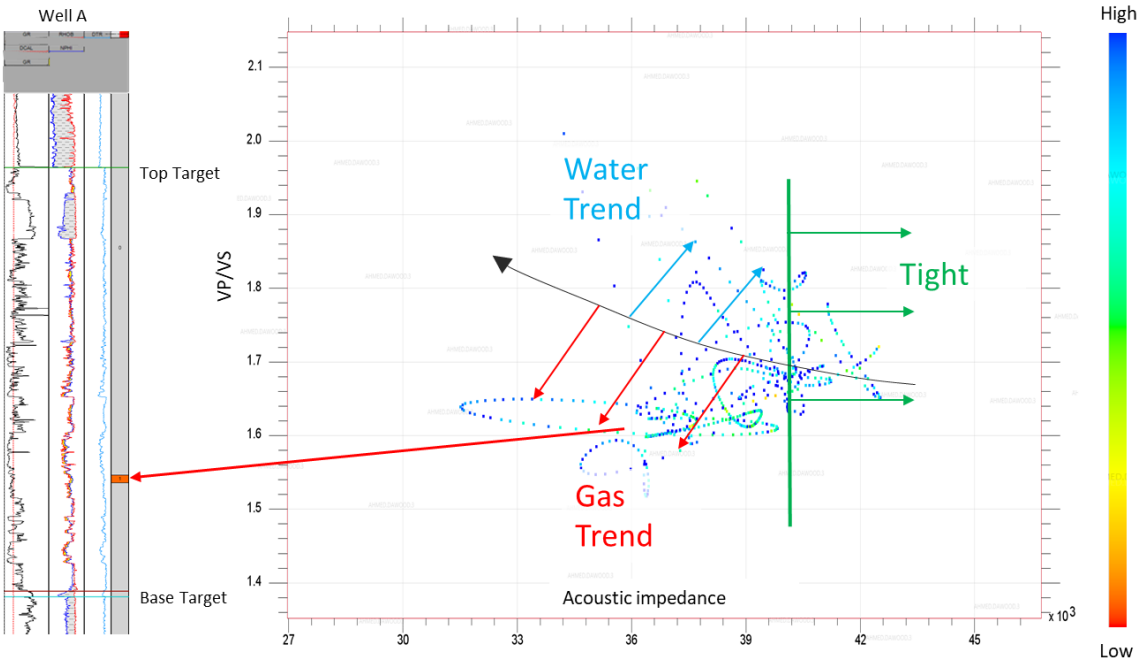

Figure 2.10: Rock types classification with 30 Hz logs filter

To define the pay zone, well logs were fluid substituted to 100% gas since most of the original fluid content is water. Fluid substitution aims to estimate changes in elastic properties due to changes in pore fluids. Based on the cross plot derived from fluid substitution, a regression line equation is calculated to define the pay zone (Figure 2.11).

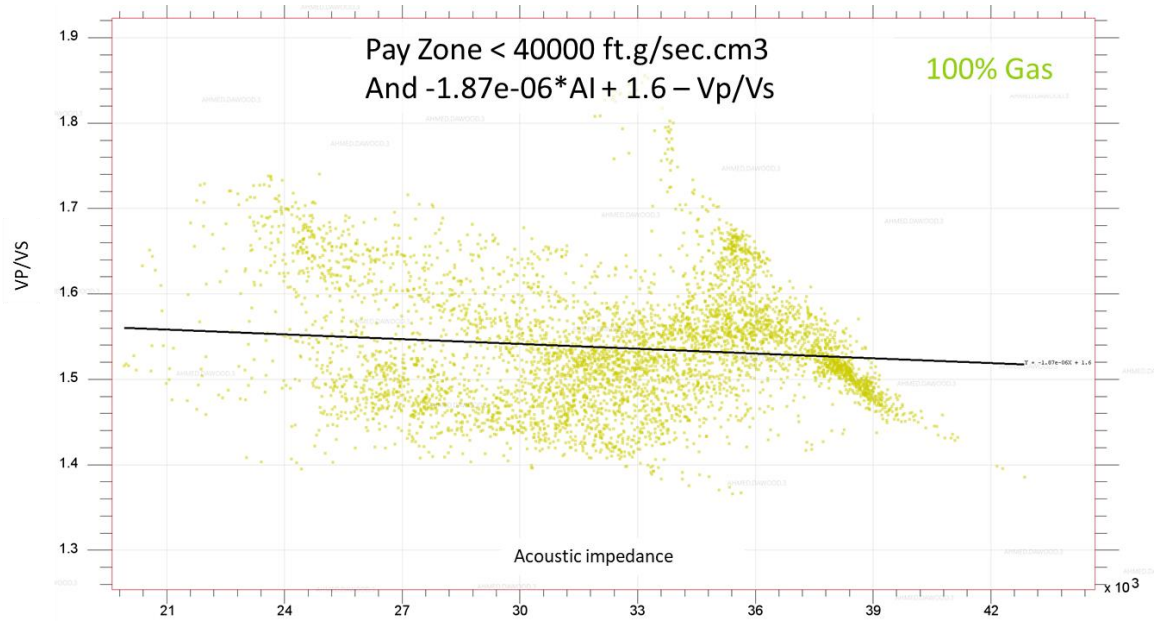

Figure 2.11: Pay zone classification by fluid substitution

2.4 AVO Modeling

A synthetic gather is generated at the top of the gas zone in well C (Figure 2.12).

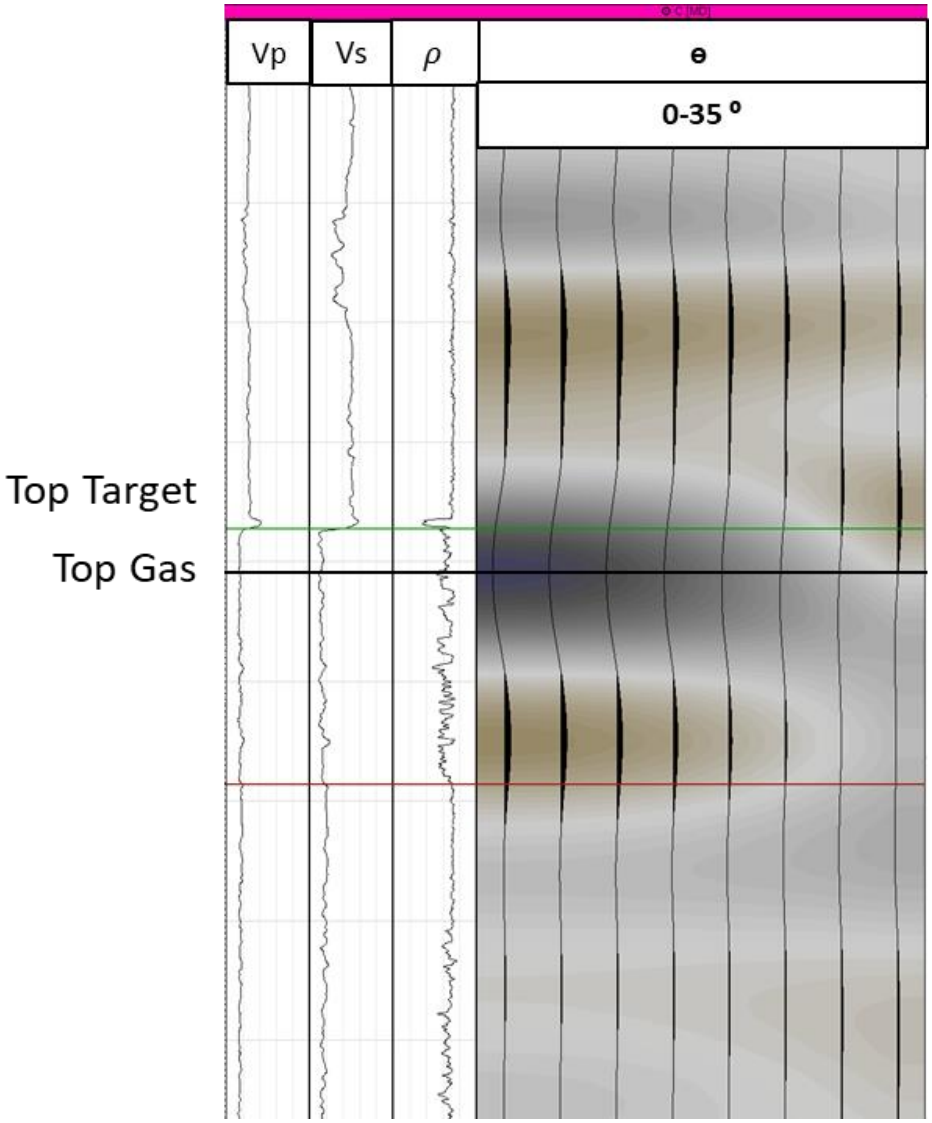

Figure 2.12: Synthetic gather at top of gas zone in well C

An AVA analysis is then run at the same zone on both the observed (Figure 2.13) and synthetic gathers (Figure 2.14).

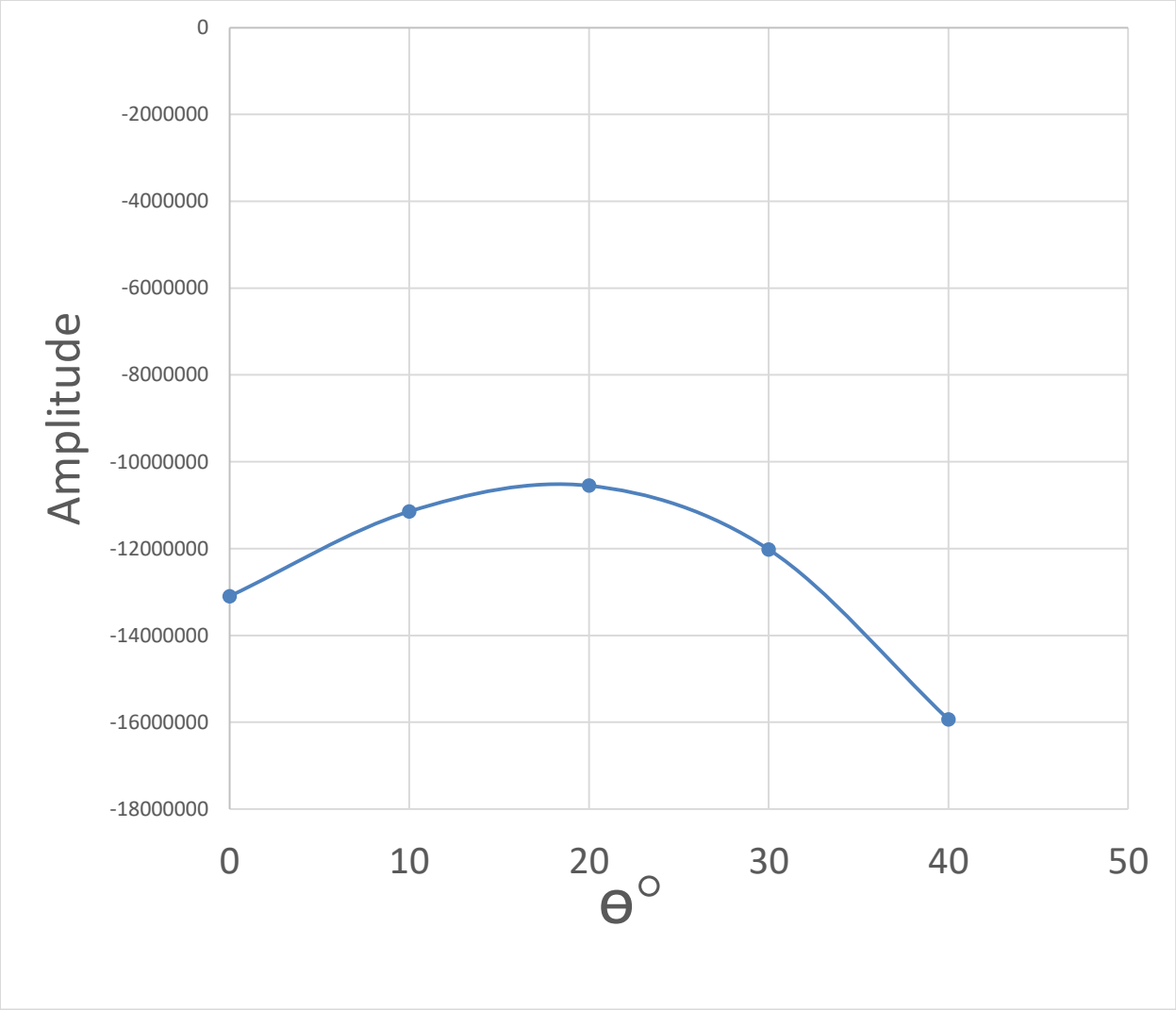

Figure 2.13: Observed AVA analysis curve on top gas zone in well C

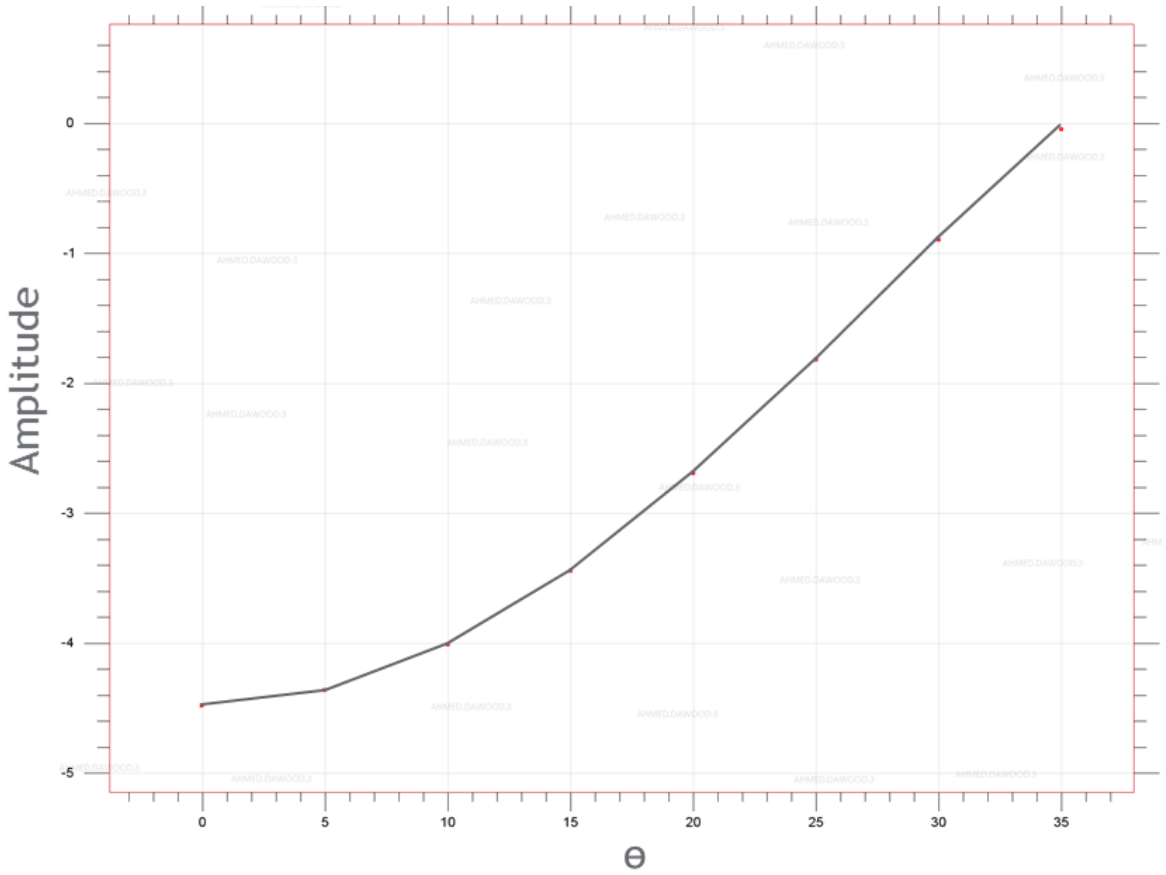

Figure 2.14: Synthetics AVA analysis curve on top gas zone in well C

When comparing these two AVA curves, both curves decrease in the near offset. In the mid offset when reaching angle 20^0, the observed AVA curve starts to increase while it decreases in synthetics AVA curve. Synthetics AVA curve is classified as Class IV where amplitude decreases with offset in a low shear impedance reservoir. Intercept and gradient were calculated from synthetics AVA curve and plotted (Figure 2.15).

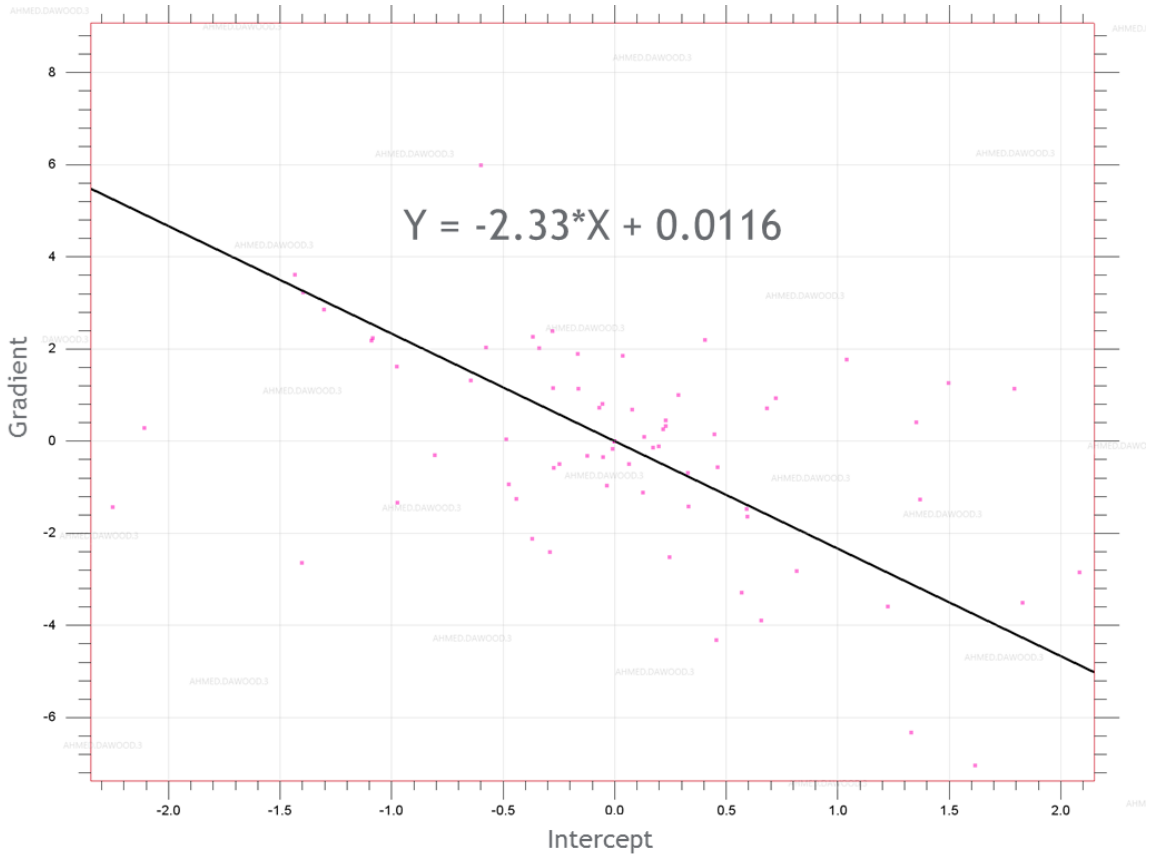

Figure 2.15: Intercept vs. gradient for synthetics AVA curve in well C

After plotting the intercept and gradient for synthetics AVA curve, a best-fit line of the data is plotted. Using this line, the angle of this trend line is calculated which is about -67º.

In Well A, a synthetic gather is generated at top of porosity zone. Another synthetic gather is also generated where well logs are fluid substituted to 100% gas, since most of the original fluid content is water, to observe changes in the gathers when they have different pore fluids (Figure 2.16).

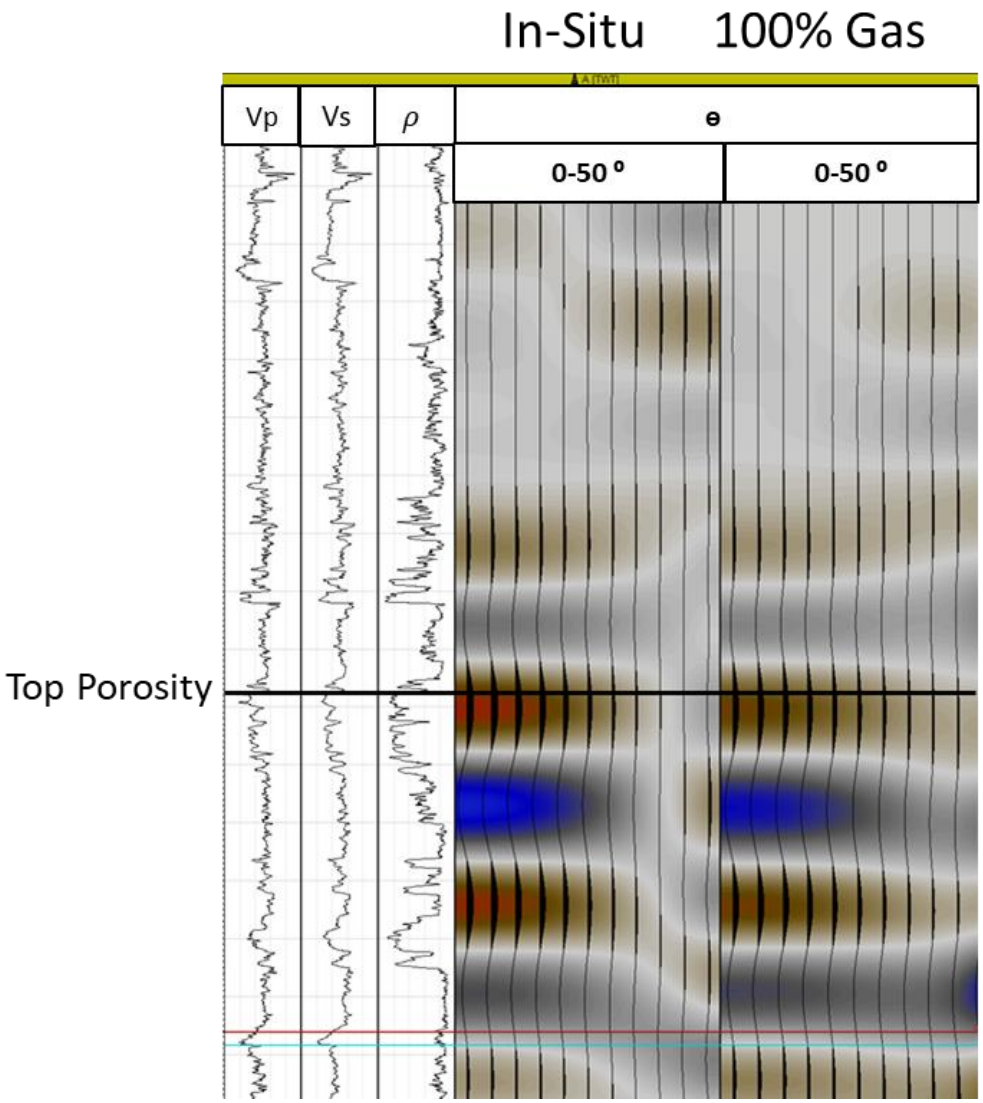

Figure 2.16: Comparison between in-situ and 100% gas in well A synthetic gathers

When analyzing these two AVA curves, both curves decrease with offset. In the far offset, gas AVA curve decreases slightly more than the in-situ AVA curve (Figure 2.17).

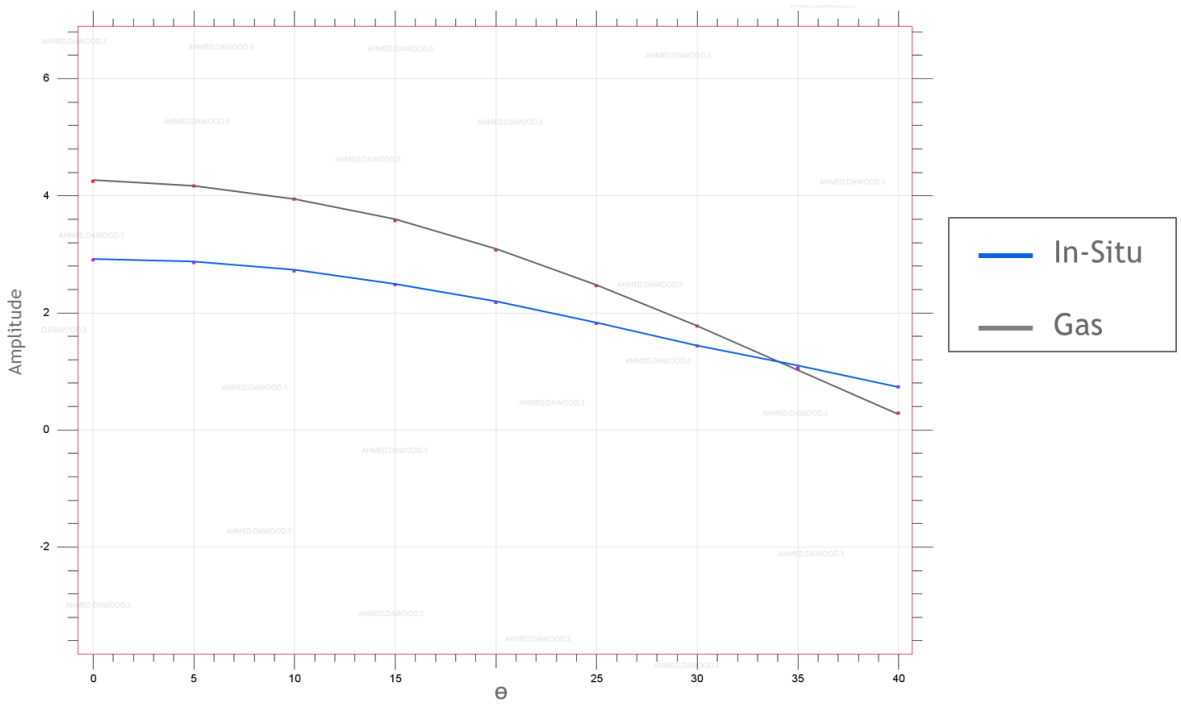

Figure 2.17: AVA curves for in-situ and 100% gas in well A synthetic gathers

Synthetics AVA gas curve is classified as Class I where amplitude decreases with offset in a low higher impedance reservoir and a dim-out is present on seismic. Intercept and gradient were calculated from both AVA curves. In-situ AVA curve is plotted in Figure 2.18 and 100% gas AVA curve in Figure 2.19.

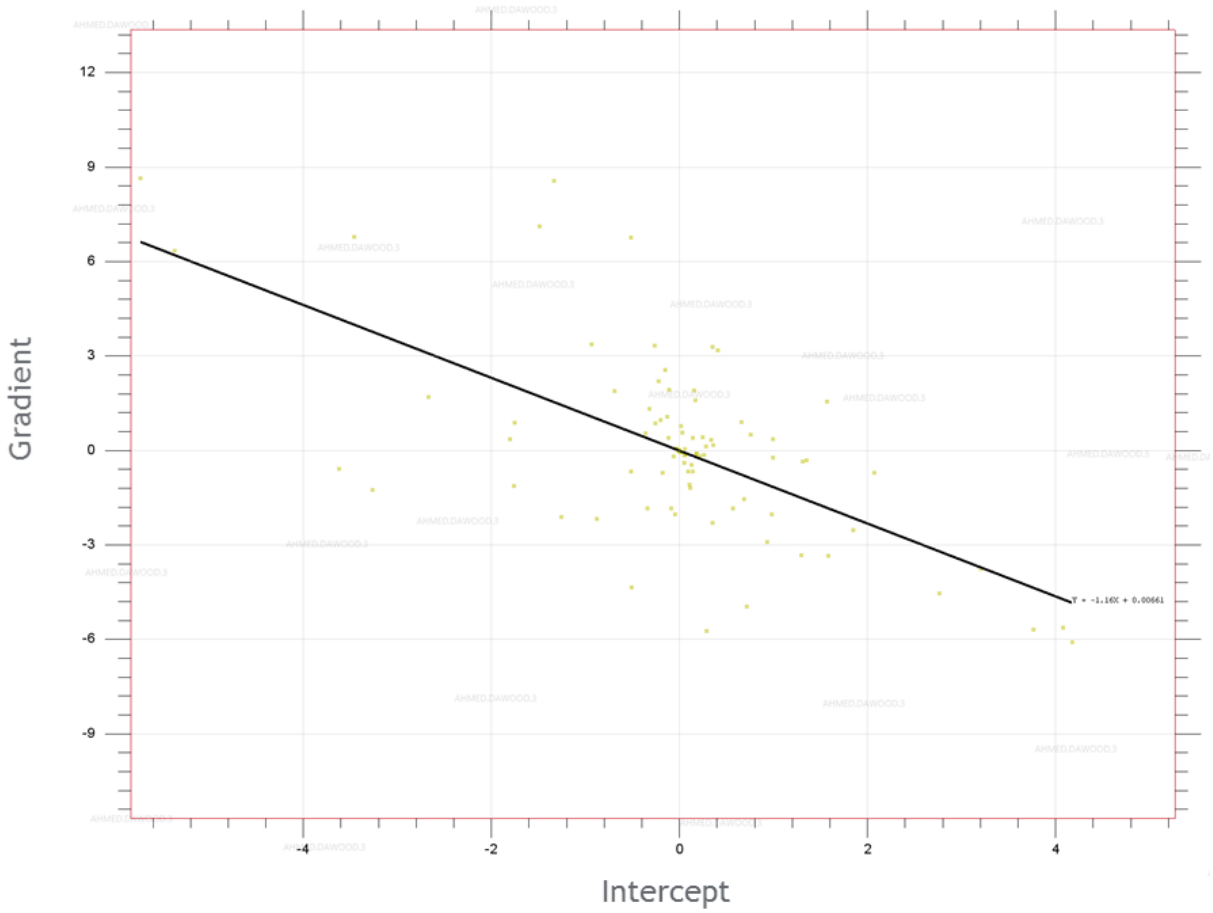

Figure 2.18: Intercept vs. gradient for in-situ synthetics AVA curve in well A

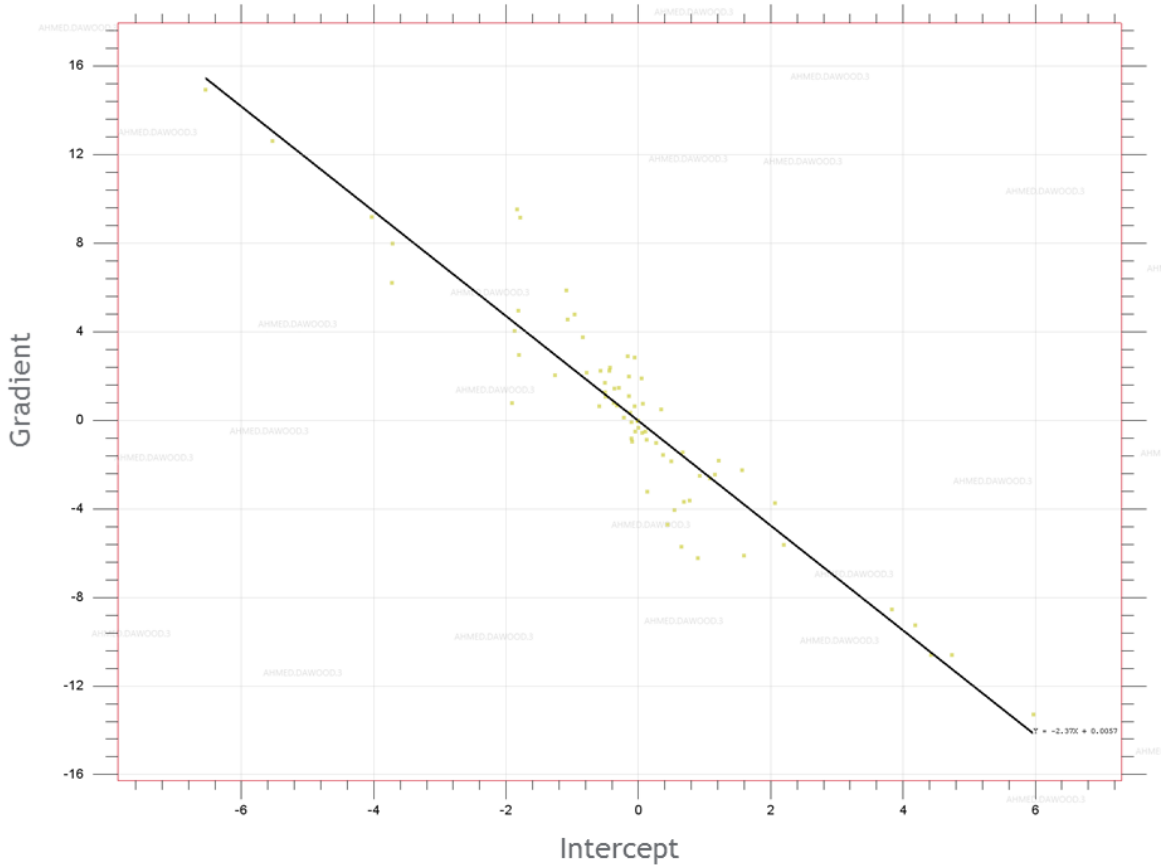

Figure 2.19: Intercept vs. gradient for 100% gas synthetics AVA curve in well A

After plotting the intercept and gradient for both synthetics AVA curves, a best-fit line of the data is plotted. Using this line, the angle of this trend line is calculated to be about -49^0 for the in-situ case and -67^0 for the 100% gas case, which is similar to the trend line angle of the gas zone in well C.

A linearized line across the seismic within the target window was approximated to calculate intercept and gradient from two-term approximation of Zoeppritz equations:

$R(\theta) = A + B\sin^2\theta.$ (5)

Intercept and gradient from angle stacks are plotted. From this plot, trend line of the seismic data at target level is approximated. Water trend line from well A synthetics is

also plotted as well as the gas trend line from well C synthetics and the gas substituted synthetics from well A (Figure 2.20).

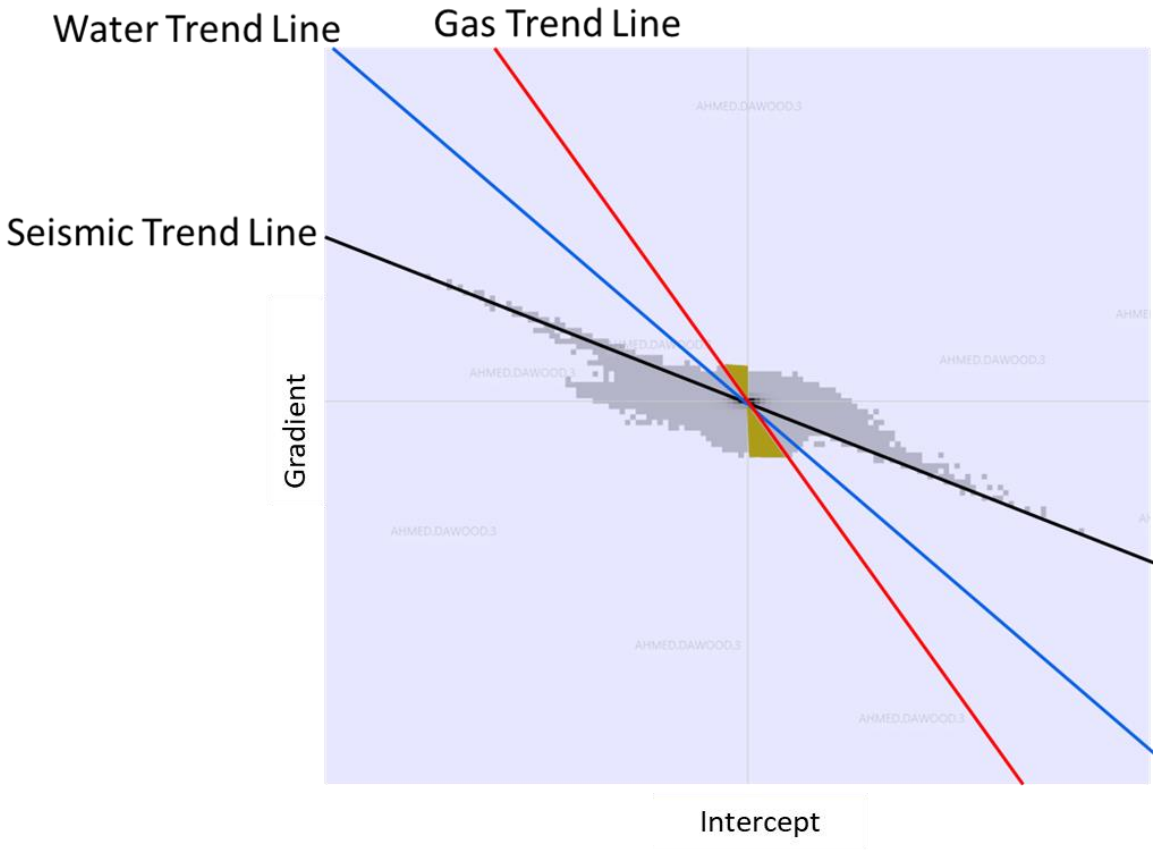

Figure 2.20: Intercept vs. gradient for angle stacks

The area of interest is the area that falls at an angle that is lower than the gas trend angle and it is highlighted in the figure above. The area of interested is displayed on a map view with the channels polygons that were drawn from the spectral decomposition attribute (Figure 2.21).

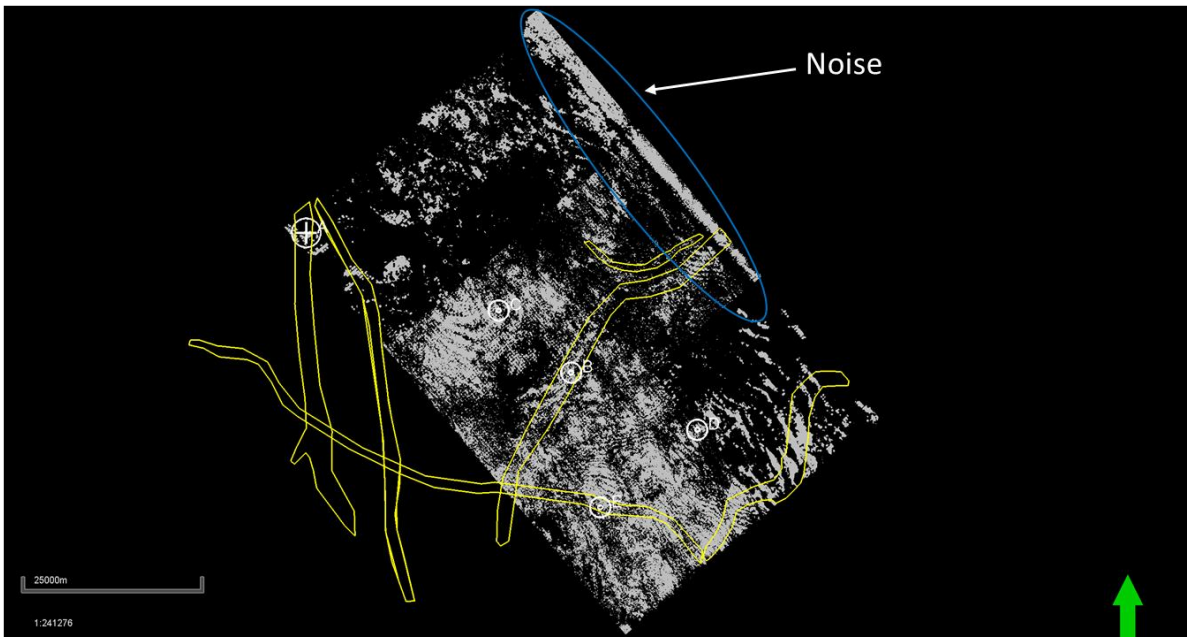

Figure 2.21: Area of interest from Intercept vs. gradient plotting of angle stacks

There is a clear noise in the map especially at the top right corner, which is probably due to edge effects.

A dominant frequency attribute was generated at top target formation displaying the data only inside the channels (Figure 2.22). The average dominant frequency is around 25 Hz. The dominant frequency at the channels south of the block is high, which is probably due to noise as the data in this part is noisy.

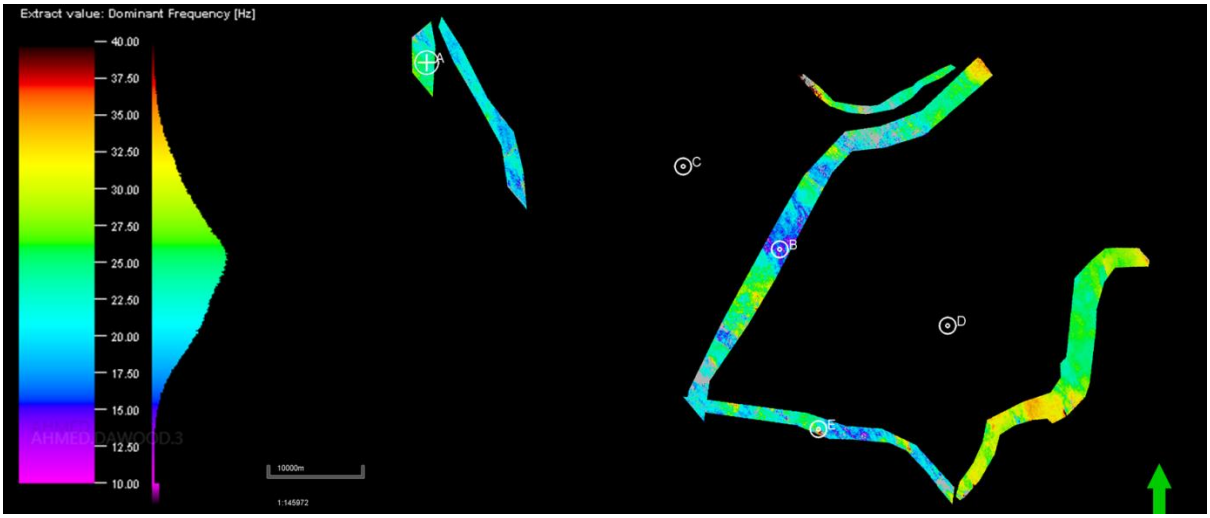

Figure 2.22: Dominant frequency attribute inside channels

Utilizing the dominant frequency map and the average velocity of the three channel wells, a tuning thickness map is generated inside the channels (Figure 2.23). The average tuning thickness is around 140 ft.

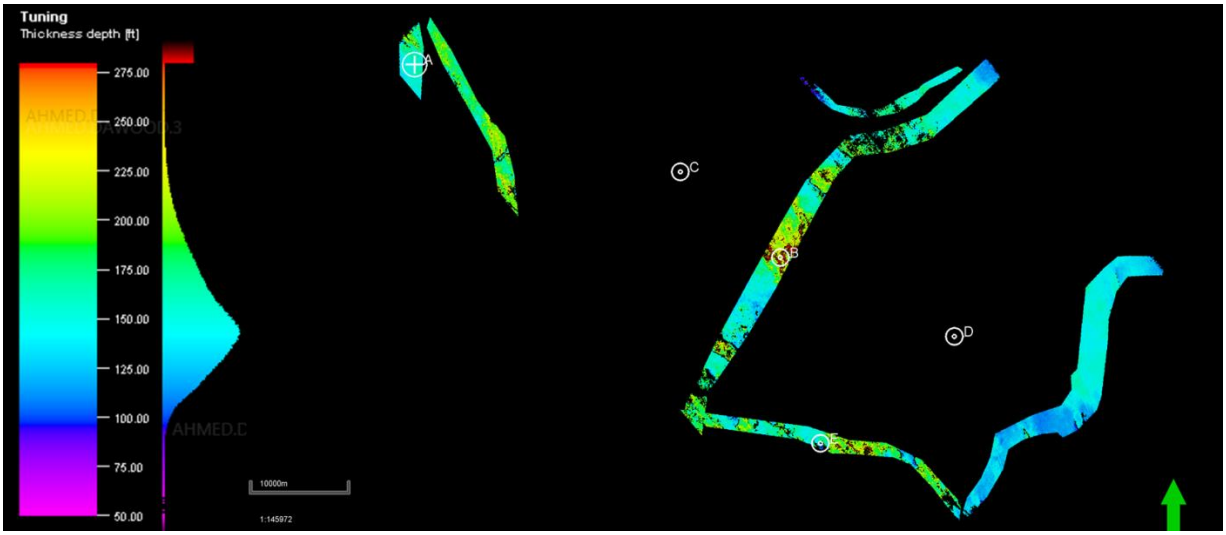

Figure 2.23: Tuning thickness attribute inside channels

2.5 Wavelet Extraction and Well to Seismic Tie

A very important step in building the inversion model is wavelet extraction. The wavelet suitability in running the inversion is measured by its predictability percentage, which measures the similarity or repeatability between the seismic and the synthetics generated using this wavelet.

Different kinds of wavelets have been tested on inversion such as different multiwell wavelets, wavelet extraction from filtered seismic, phase shifted wavelets to correct for inconsistent phase within the seismic, and statistical wavelets which are extracted from the seismic alone without the use of well logs.

Seismic data in this block is noisy (Figure 2.24). Structural smoothing and median filter attributes were run on the volume to reduce the noise and improve the seismic quality (Figure 2.25). Structural smoothing is used to increase the seismic reflectors continuity while honoring the local structure. Local structure is detected by computing azimuth and principle component dip. Then, parallel to the structure orientation, a Gaussian smoothing is applied. Median filter removes random noise high amplitudes.

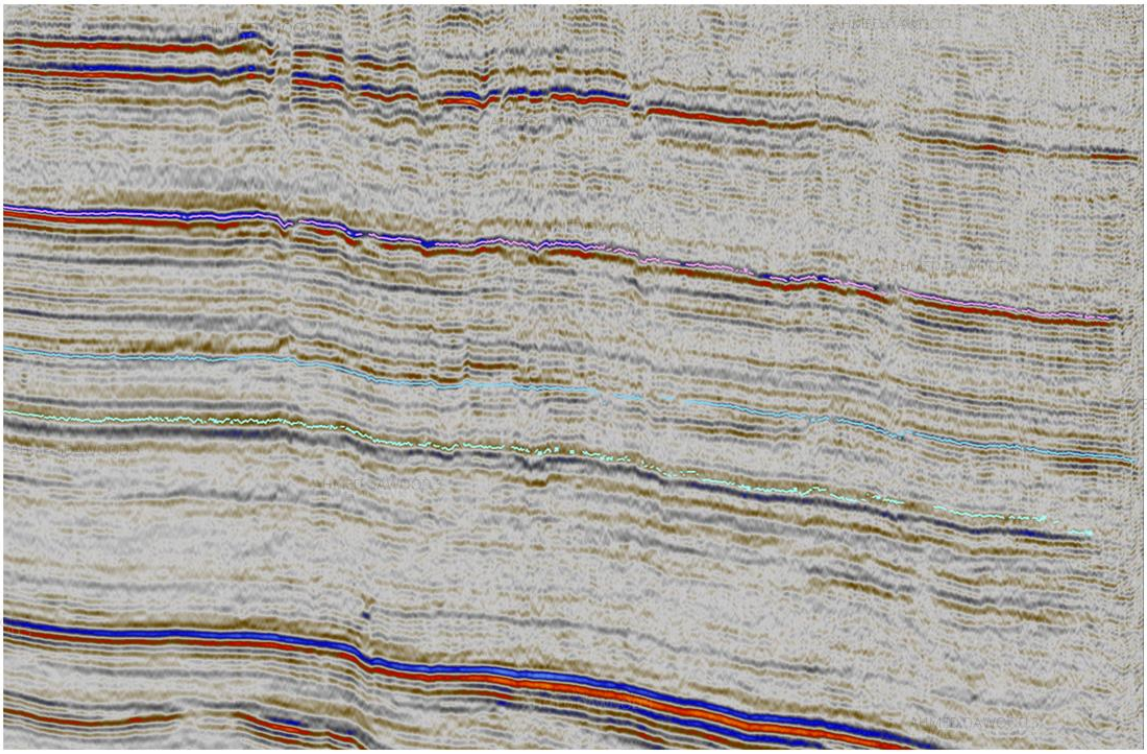

Figure 2.24: Noisy seismic cross section

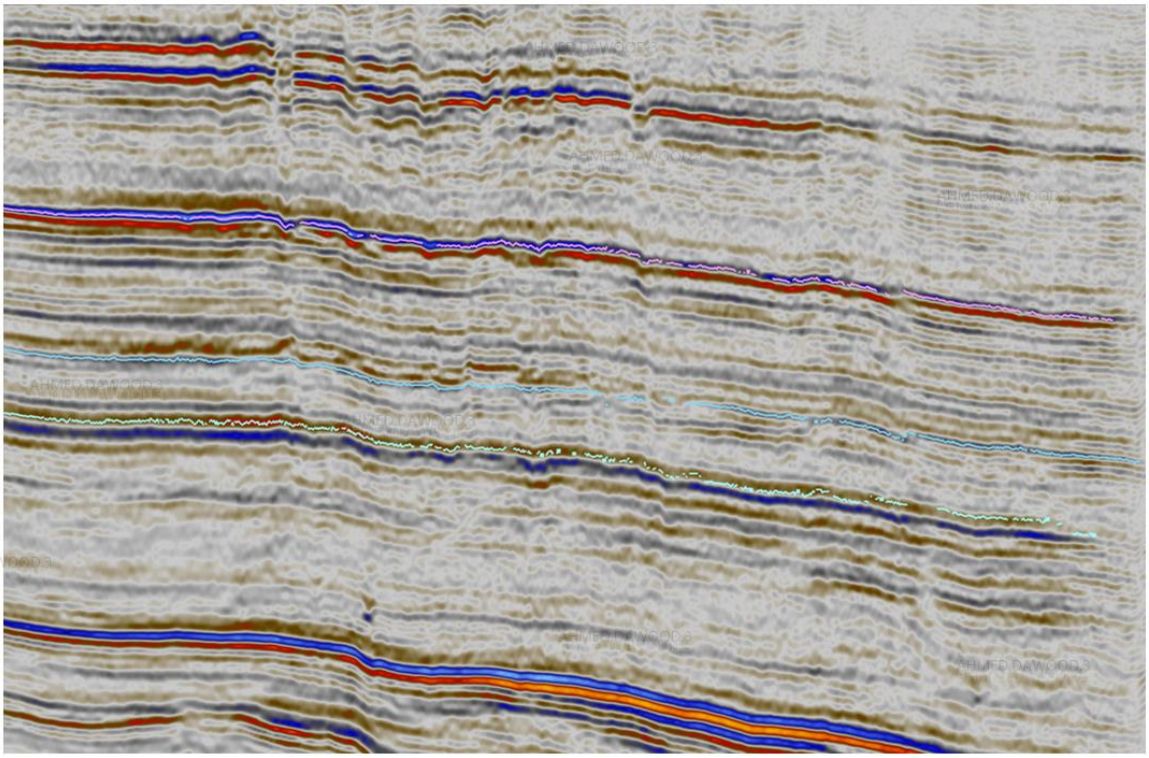

Figure 2.25: Seismic cross section in previous figure after applying structural smoothing and median filter attributes

Wavelets were extracted from original seismic volumes. An example of well A wavelet extraction is shown in Figure 2.26, from well B in Figure 2.27, and a multiwell wavelet that gave a predictability value of 5.6%, which is very low in Figure 2.28.

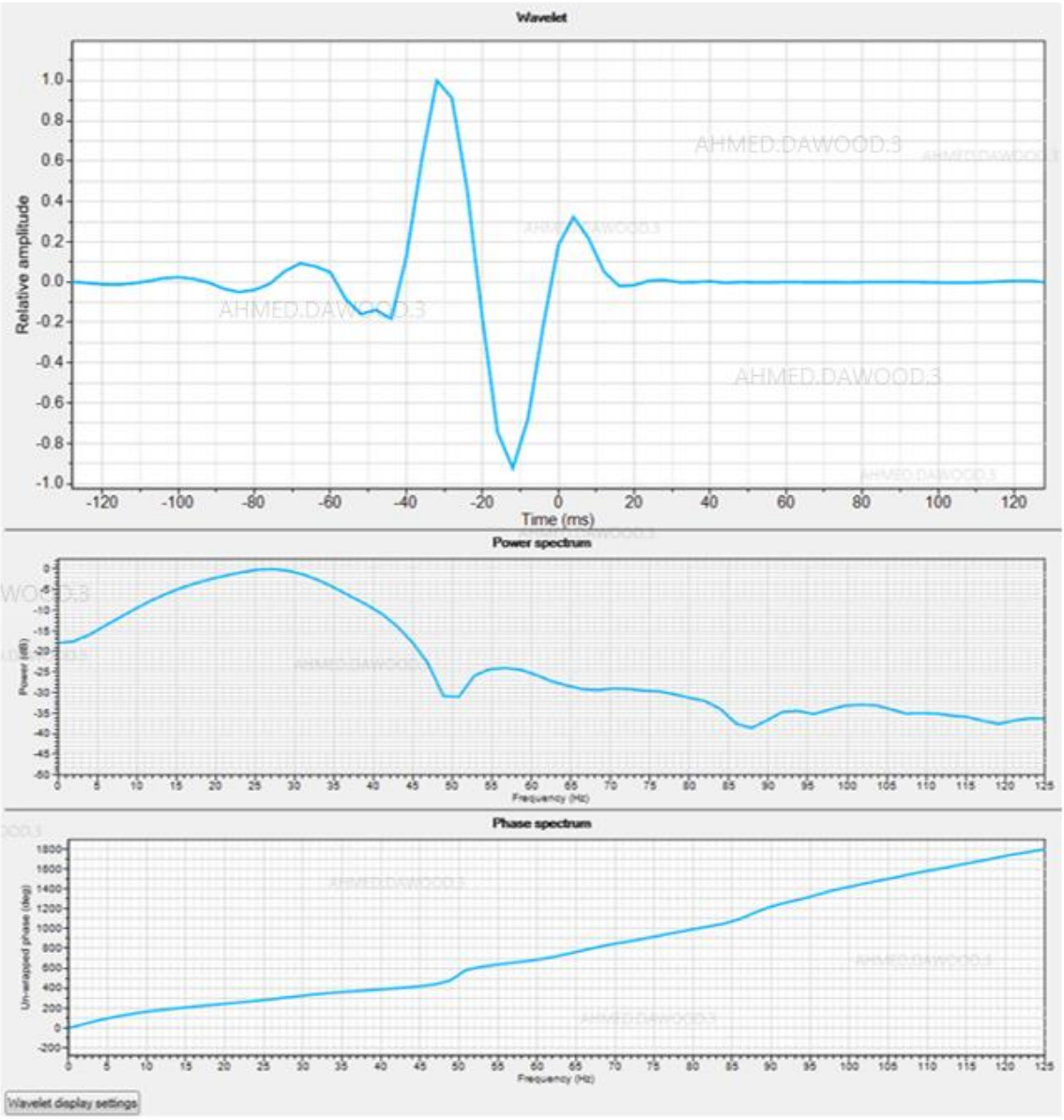

Figure 2.26: Well A wavelet extraction from original volume

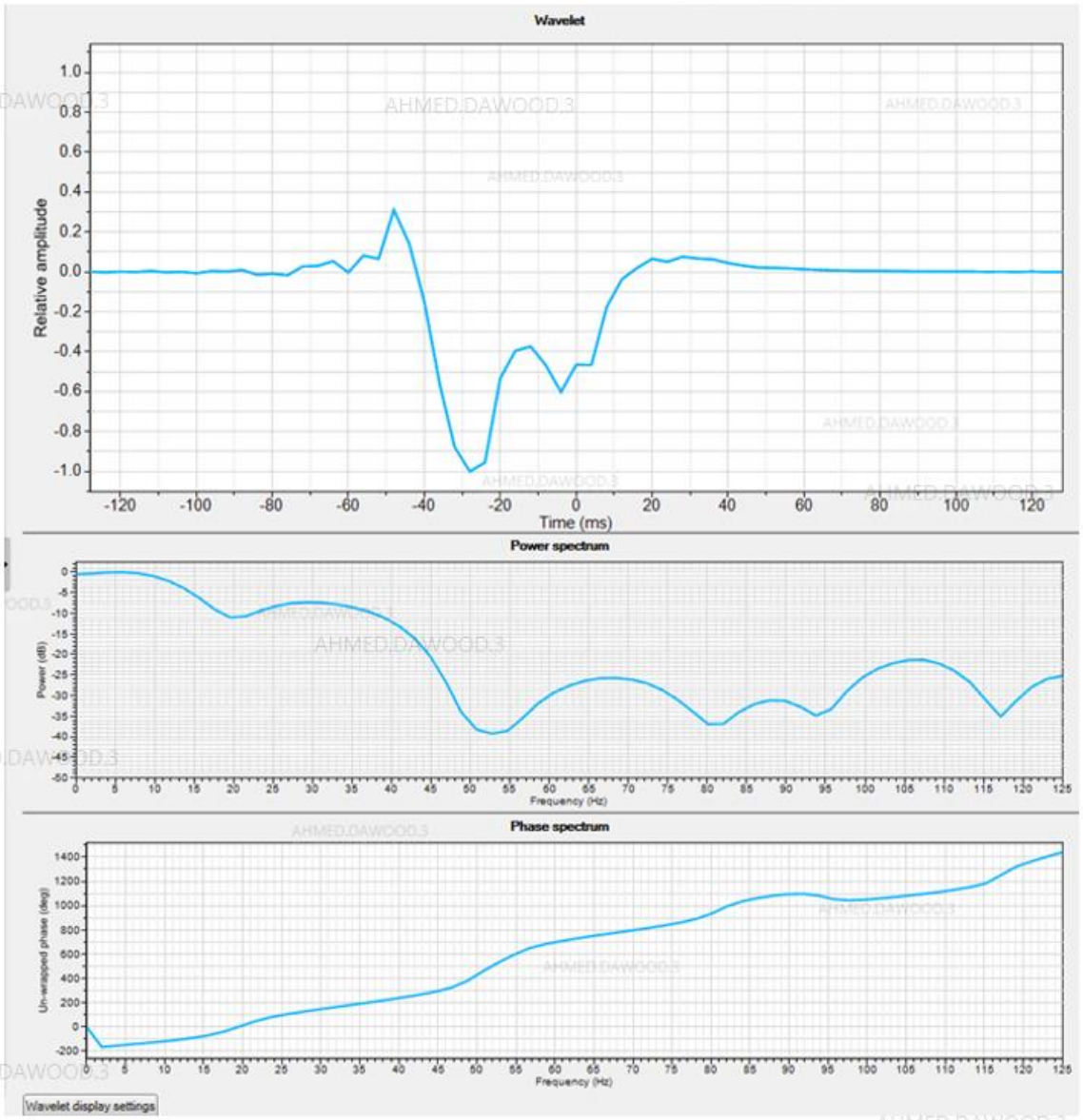

Figure 2.27: Well B wavelet extraction from original volume

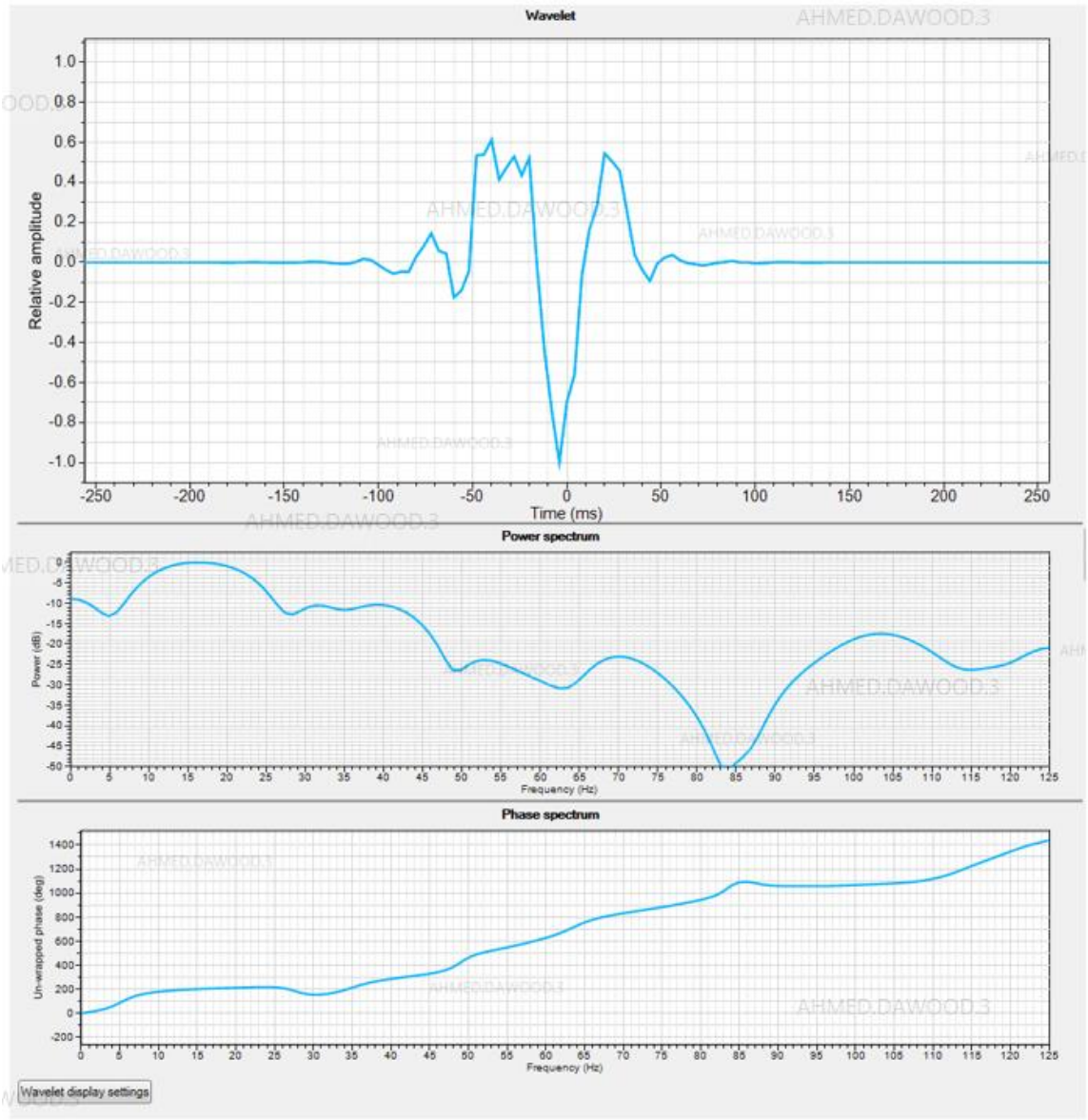

Figure 2.28: Multiwell wavelet extraction from original volume

Then wavelets were extracted from filtered seismic to compare with the original volume wavelets. An example of well A wavelet extraction is in Figure 2.29, from well B in Figure 2.30, and a multi-well wavelet that gave a predictability value of 6.5% in Figure 2.31. This predictability value is slightly higher than the multi-well wavelet from the original volume. It is still lower than the acceptable range.

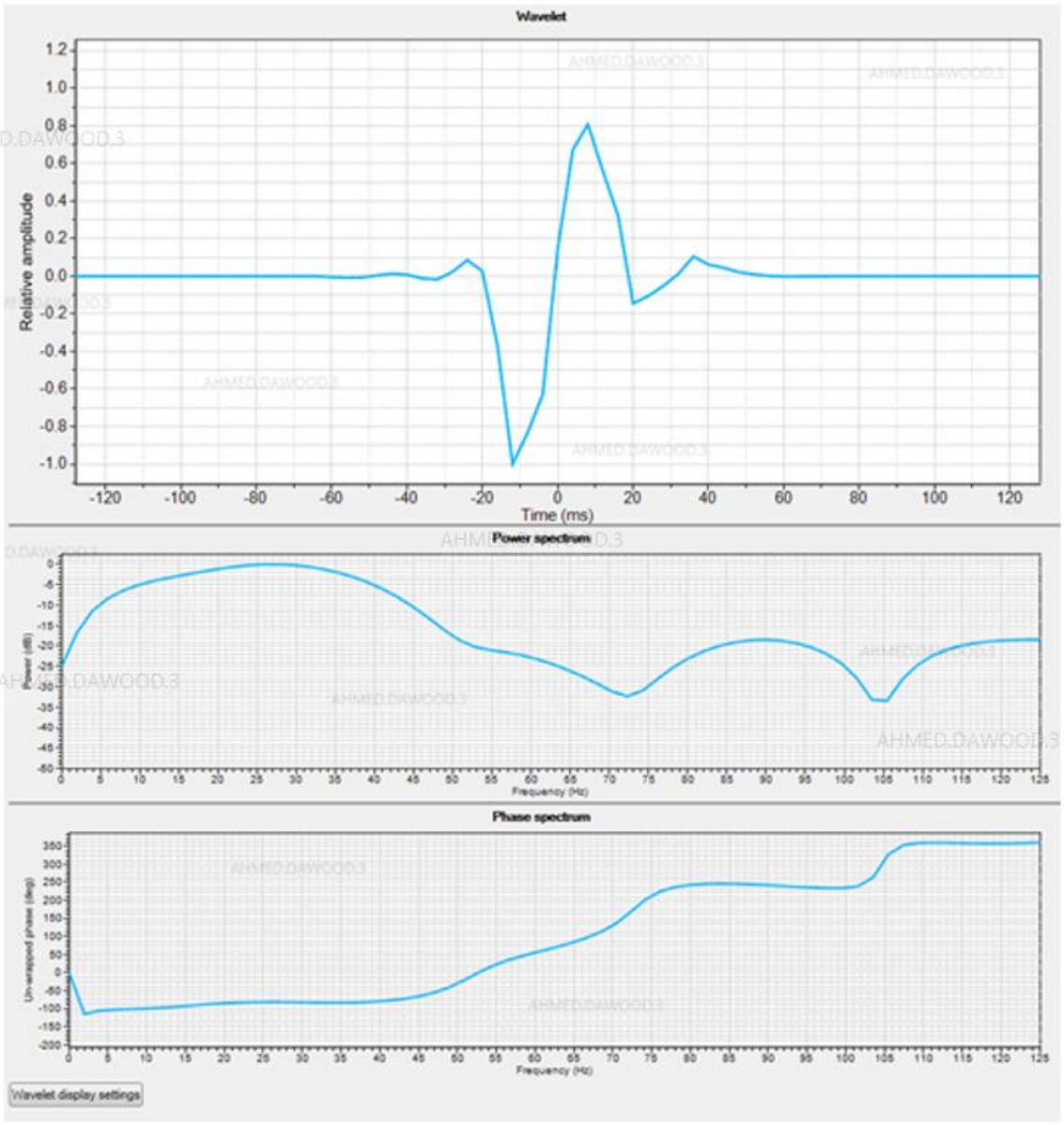

Figure 2.29: Well A wavelet extraction from filtered volume

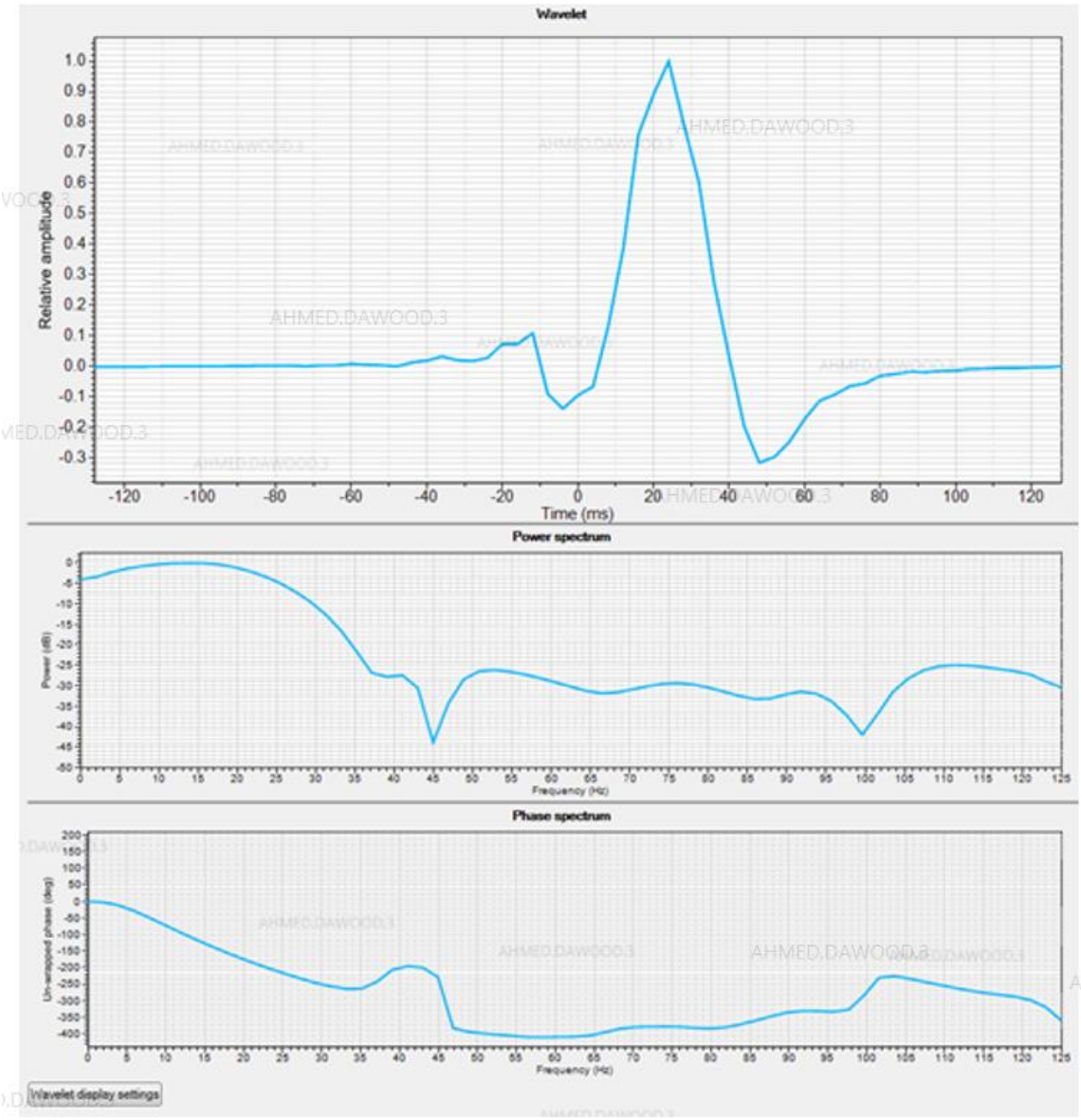

Figure 2.30: Well B wavelet extraction from filtered volume

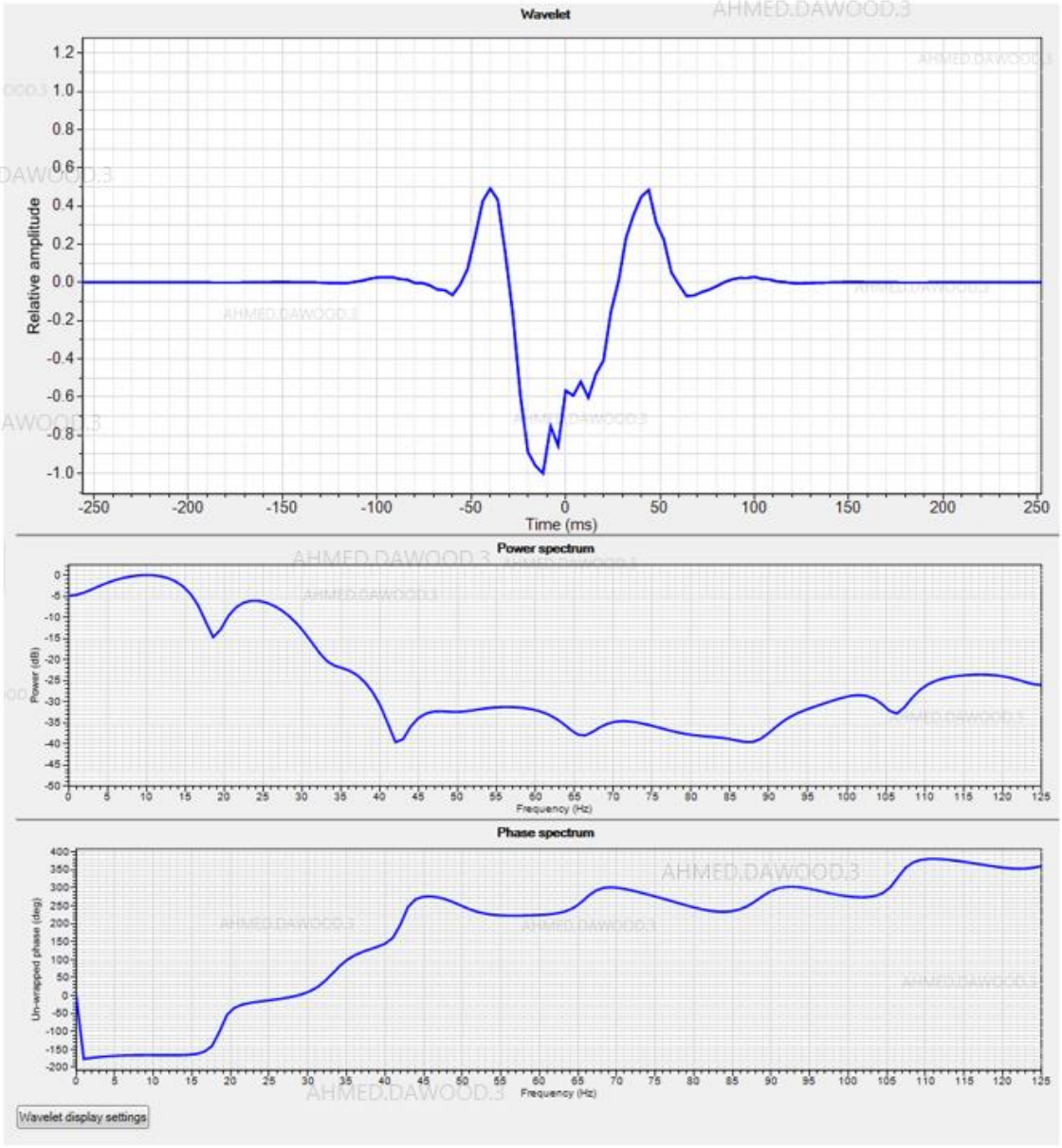

Figure 2.31: Multiwell wavelet extraction from filtered volume

The best wavelet extraction was from the original volume and it gave a predictability value of 52% (Figure 2.32). This wavelet has a larger right-side lobe than normal which is due to noise effects. The key to increase the predictability value is to make the reflectivity window scan starts from top target to base target.

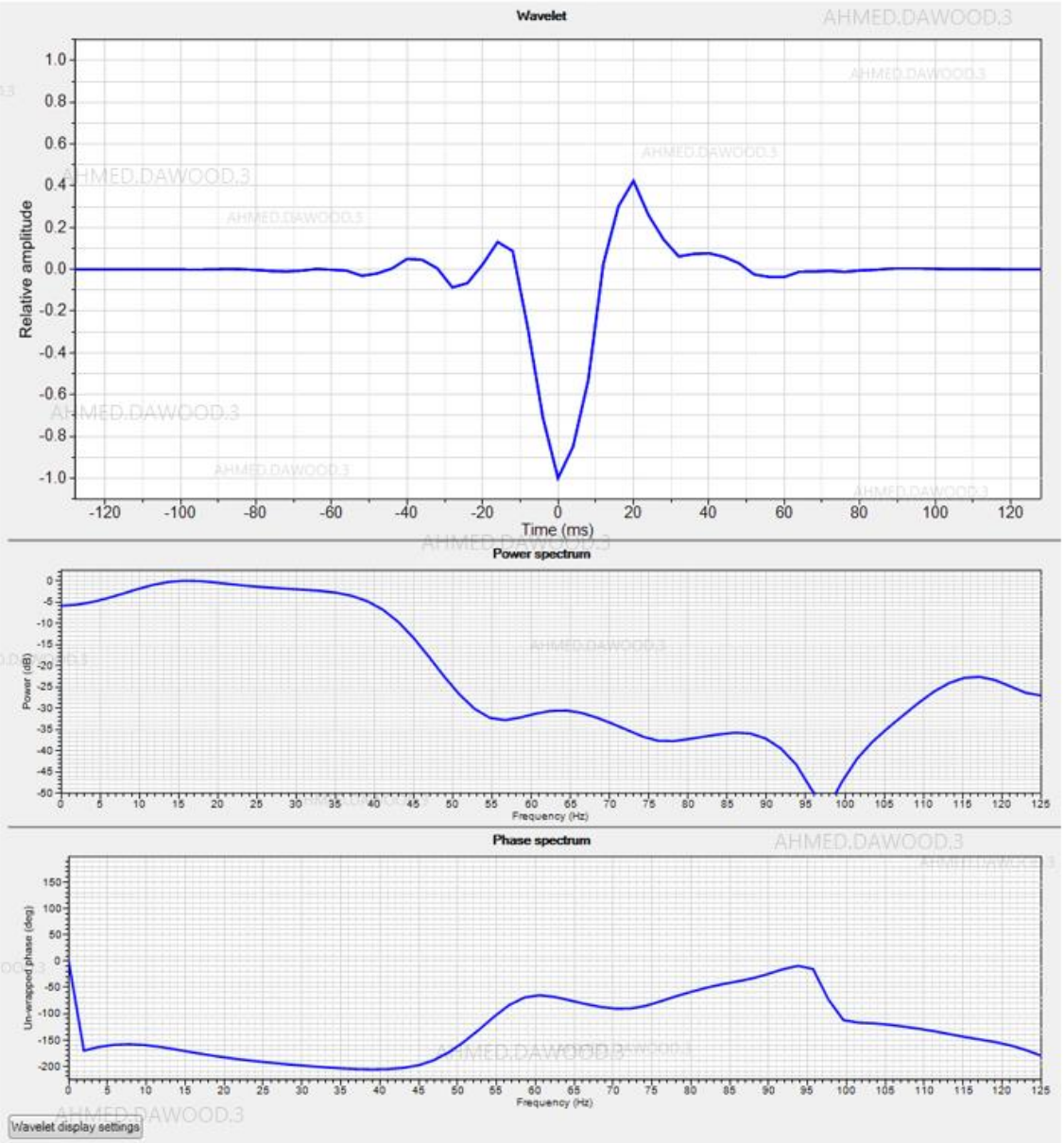

Figure 2.32: Best extracted wavelet from original volume

Evaluating well A tie to seismic (Figure 2.33), there is a slight miss-tie at the top target but it ties well toward the base.

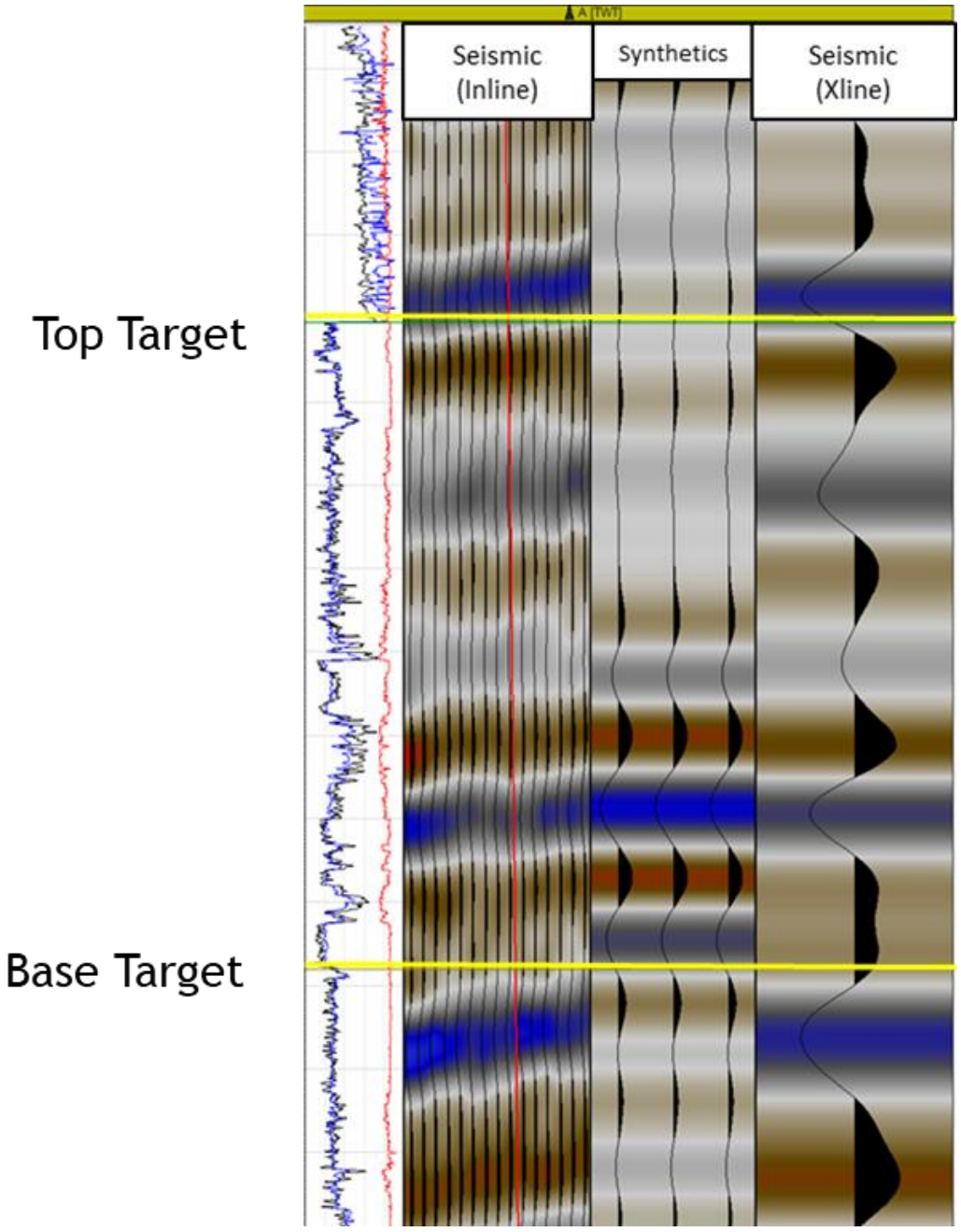

Figure 2.33: Well A tie to seismic

In well B, the tie to seismic is not that good due to noise in that part of the block (Figure 2.34).

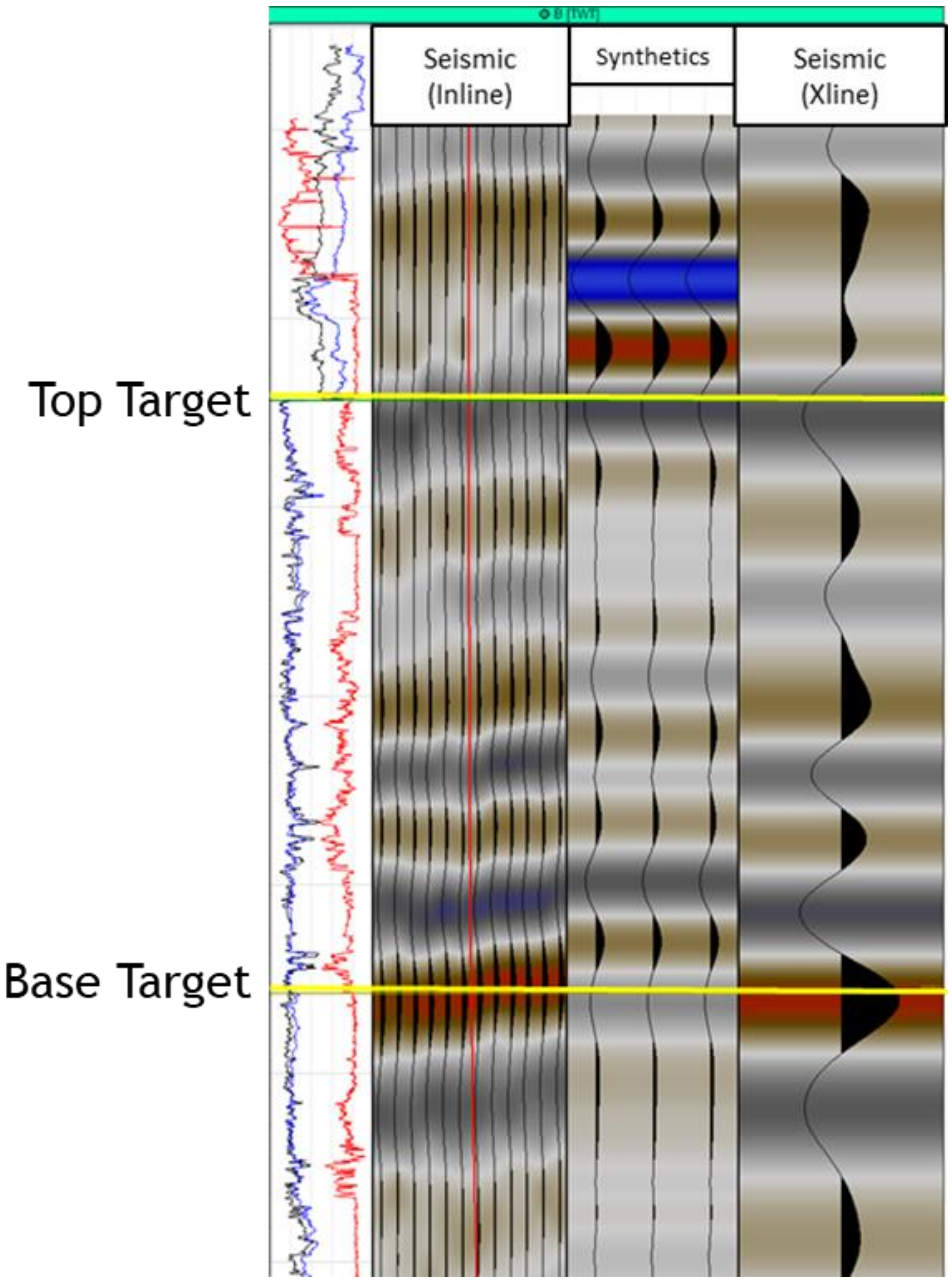

Figure 2.34: Well B tie to seismic

In evaluating the frequency spectrum of angle stacks, far angle stacks have less high frequencies than near angle stacks and they have more low frequencies than near angle stacks (Figure 2.35).

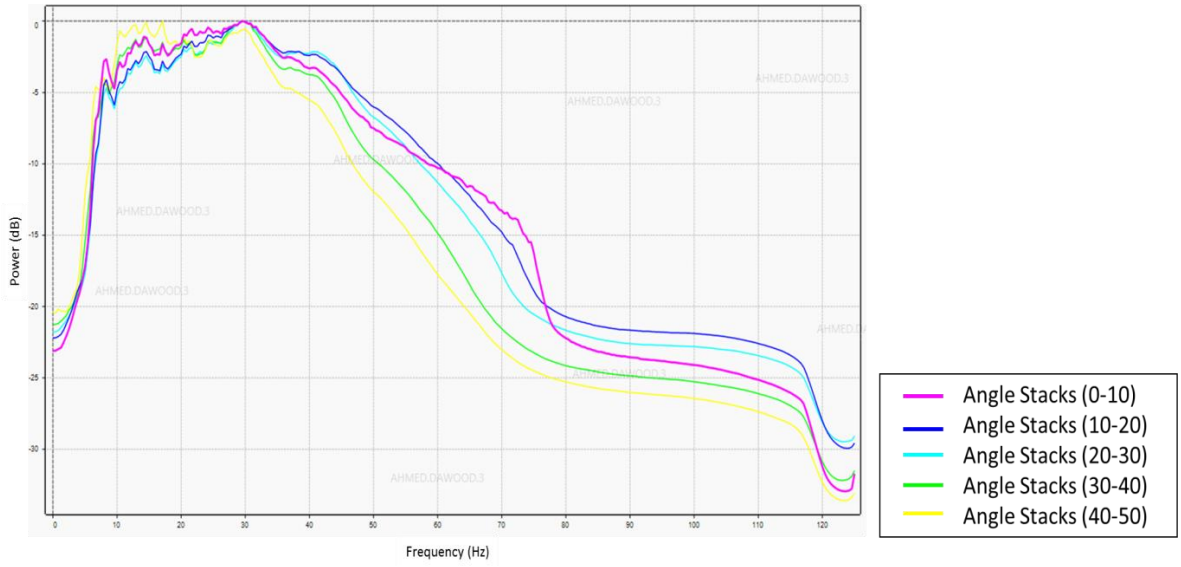

Figure 2.35: Frequency spectrum of angle stacks

The five multiwell angle stacks wavelets that are used in pre-stack inversion are displayed in Figure 2.36.

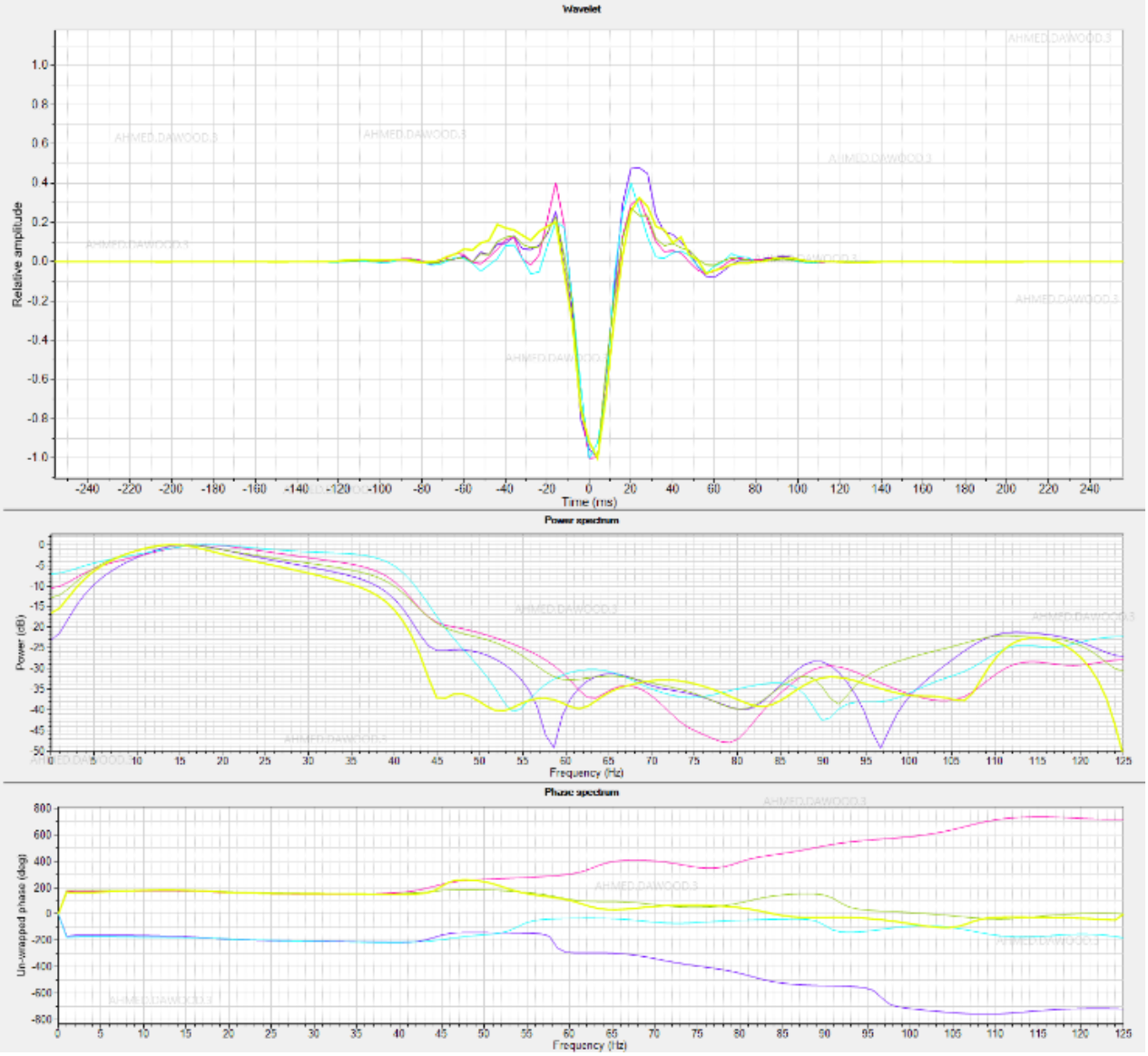

Figure 2.36: Angle stacks wavelets

2.6 Low Frequency Model

Low frequency model is built because seismic is band limited. Seismic only gives relative changes in the values of rock properties. To get the absolute values, low frequency model needs to be added to the seismic data because it makes up for the missing low frequency in the seismic. The low frequency model is built from the well logs added to the seismic for interpolation. It also needs horizons input to constrain the model.

For pre-stack inversion, low frequency models are needed for acoustic impedance, density, Vp/Vs. Figure 2.37 shows an example of a low frequency model for acoustic impedance built from 0-8 Hz. The layering between horizons is clear.

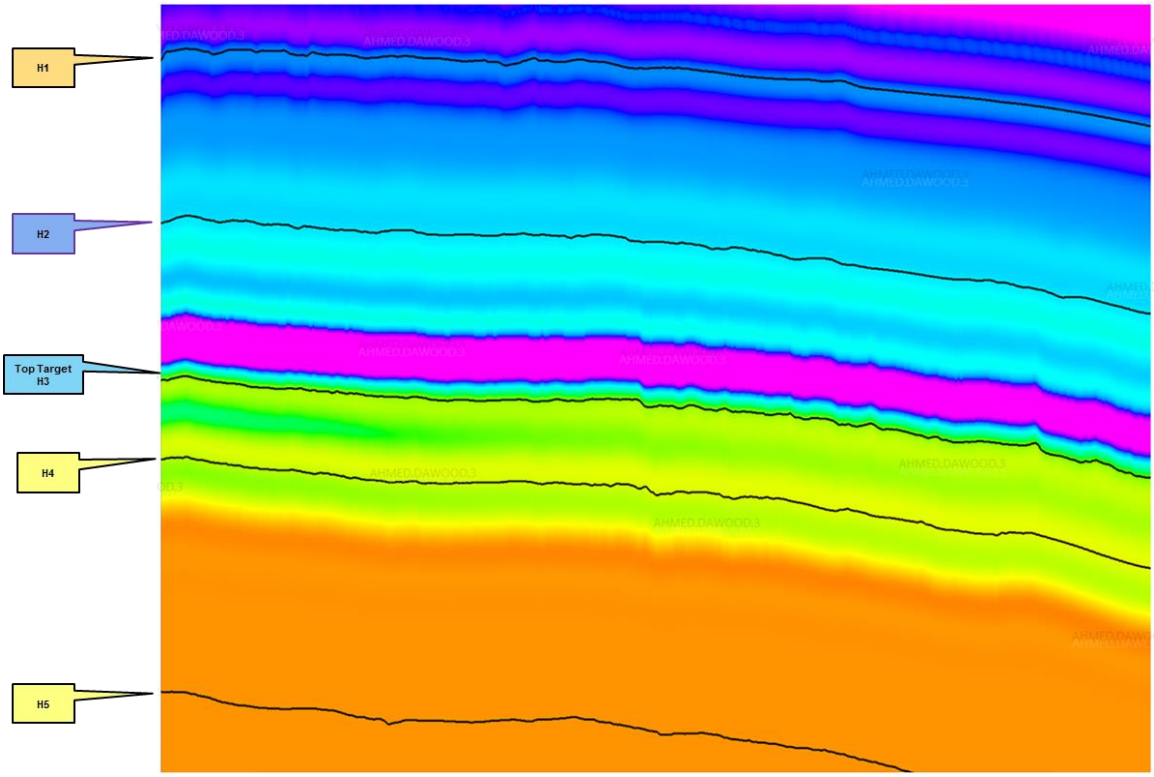

Figure 2.37: Acoustic impedance low frequency model (0-8 Hz)

Another way to QC the low frequency model is to display the log and observe the trend (Figure 2.38).

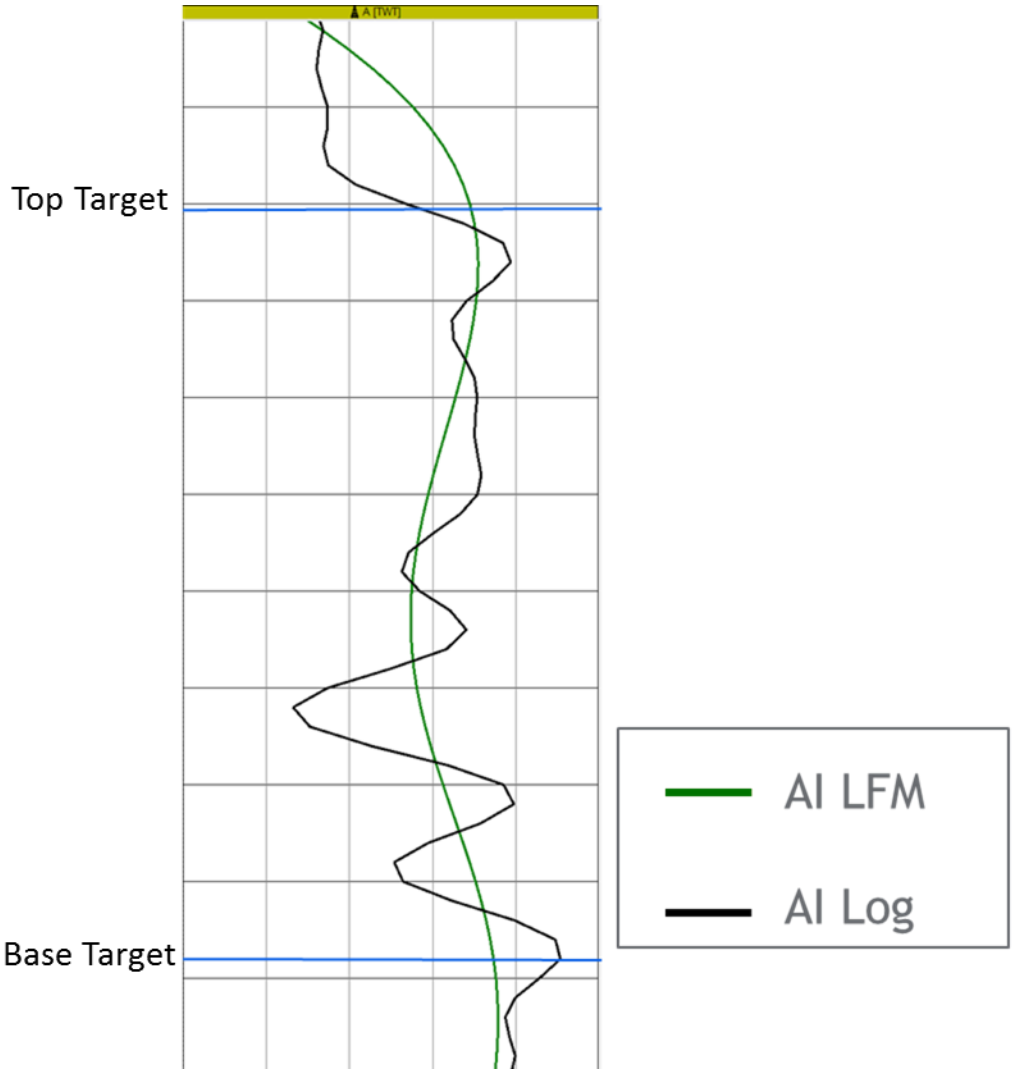

Figure 2.38: Acoustic impedance low frequency model QC with the log in well A

2.7 Synthetics

2.7.1 Forward Modeling

In this part, it is assumed there are no wells in this seismic block and those identified wells on the map are future planned wells and we would like to know if the target is

porous and gas saturated. A synthetic is created to match the seismogram at the location of interest by forward modeling of P-wave interval velocity and density and convolving the resulting acoustic impedance with a statistical wavelet. Figure 2.39 shows an example of well A synthetics forward model with the channel boundary drawn on the seismic section.

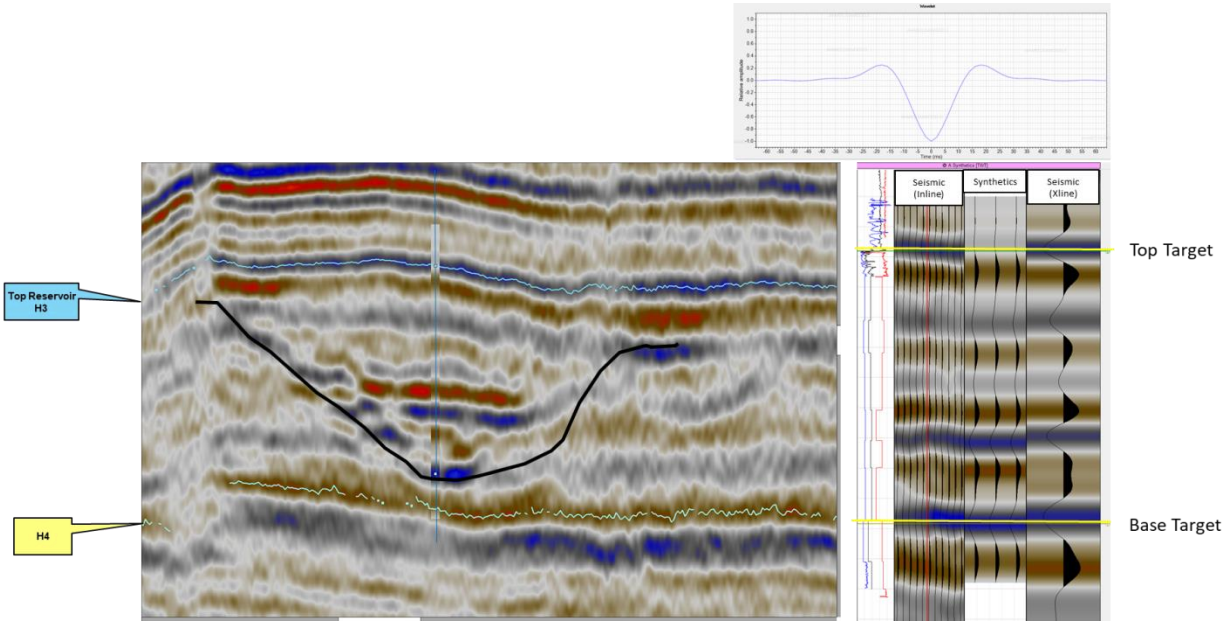

Figure 2.39: Well A synthetics forward model

Another example of well E synthetics forward model which is a channel well is shown in Figure 2.40.

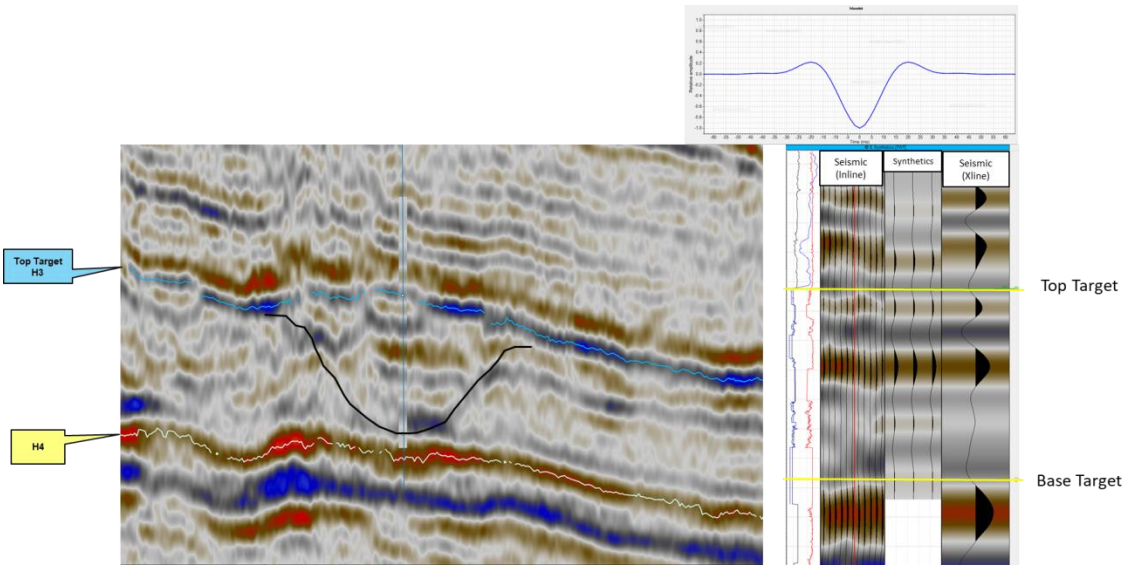

Figure 2.40: Well E synthetics forward model

Vs is estimated from Vp using Vs relationship in Well F (Figure 2.41).

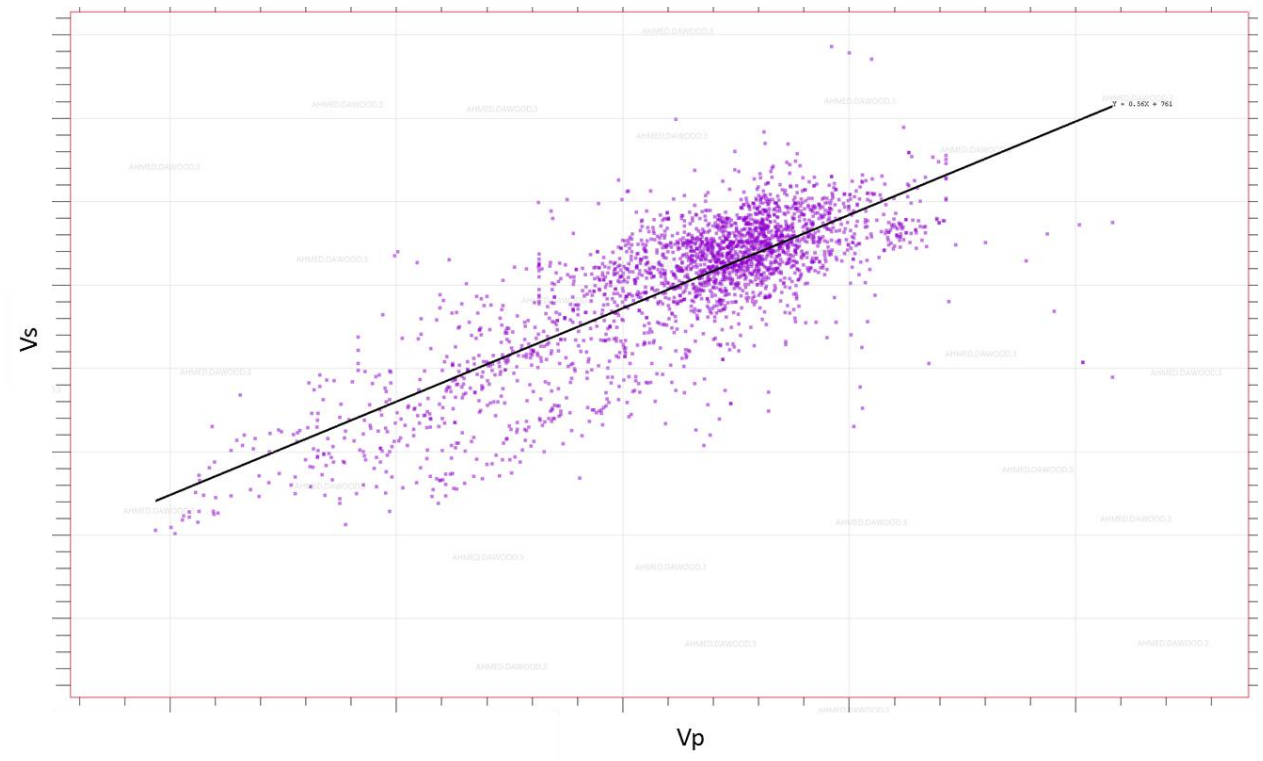

Figure 2.41: Vp and Vs relationship in Well F

2.7.2 Feasibility Study

The feasibility study and pay zone calculation by rock physics modeling was done on the nearest well to the seismic block, which is well F. Acoustic impedance and Vp/Vs color coded with water saturation are cross plotted to show the distribution of the data. Three rock types were classified from AI and Vp/Vs crossplot, which are gas, water, and tight (Figure 2.42). Acoustic impedance and porosity are crossplotted to find a relationship between them (Figure 2.43).

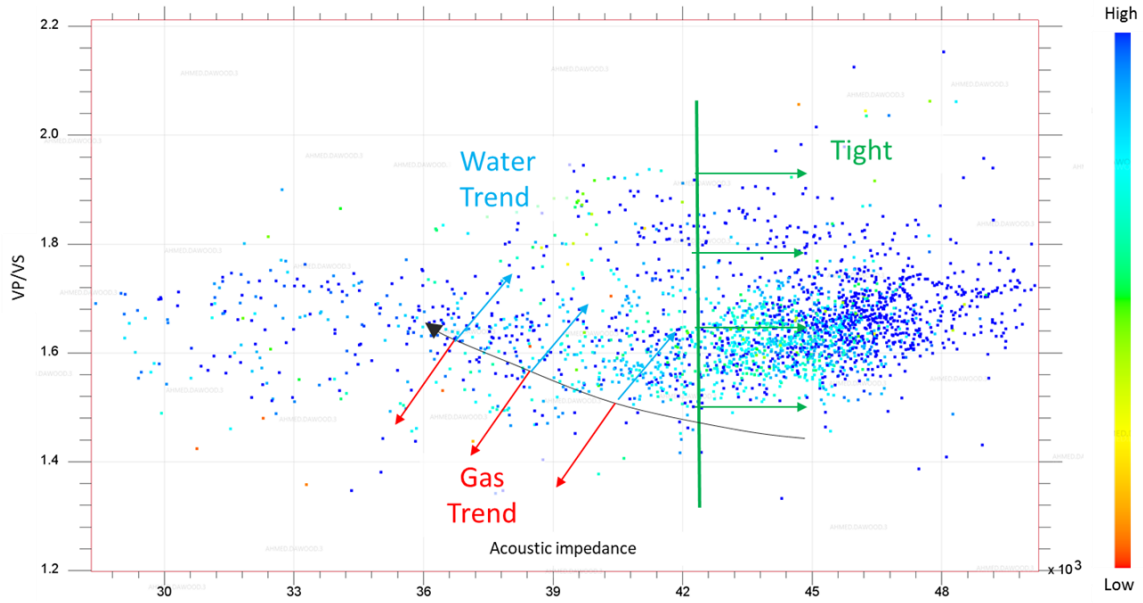

Figure 2.42: Crossplot of AI and Vp/Vs in Well F

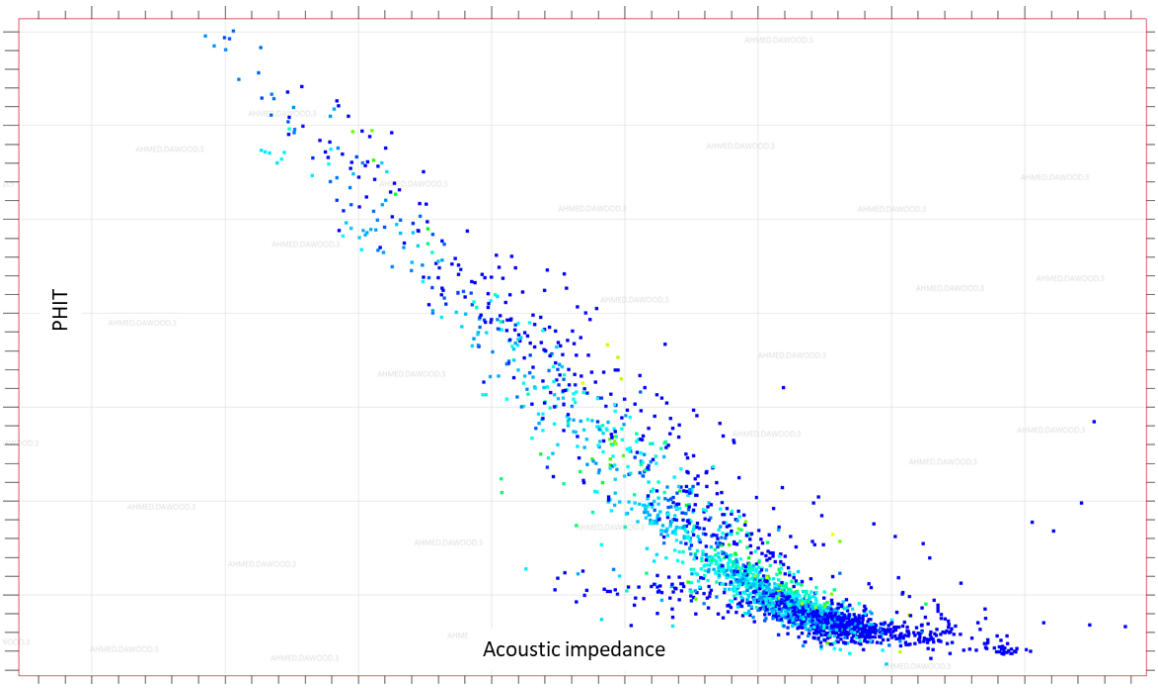

Figure 2.43: Cross plot of AI and porosity in Well F

To define the pay zone, well F logs were fluid substituted to 100% gas since most of the original fluid content is water. Based on the cross plot derived from fluid substitution, a regression line equation is calculated to define the pay zone (Figure 2.44).

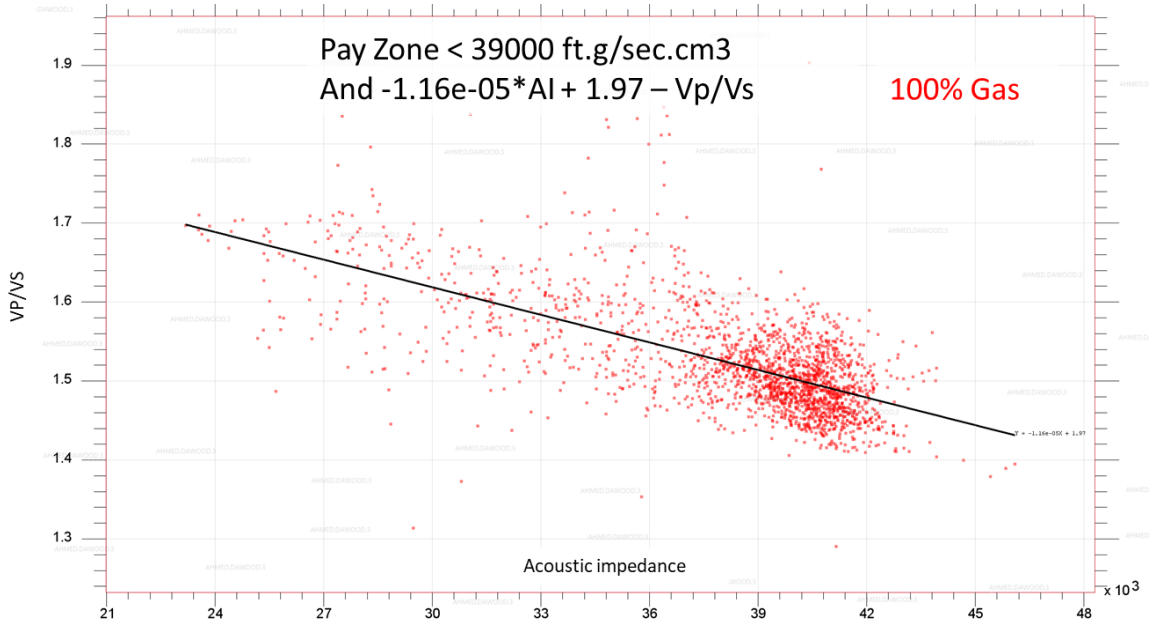

Figure 2.44: Pay zone classification by fluid substitution of Well F

2.7.3 Wavelet Extraction and Well to Seismic Tie

A deterministic wavelet was extracted from each of the three synthetic channel wells and they were combined together to form a multiwell wavelet. This multiwell synthetics wavelet gave a predictability value of 60% (Figure 2.45).

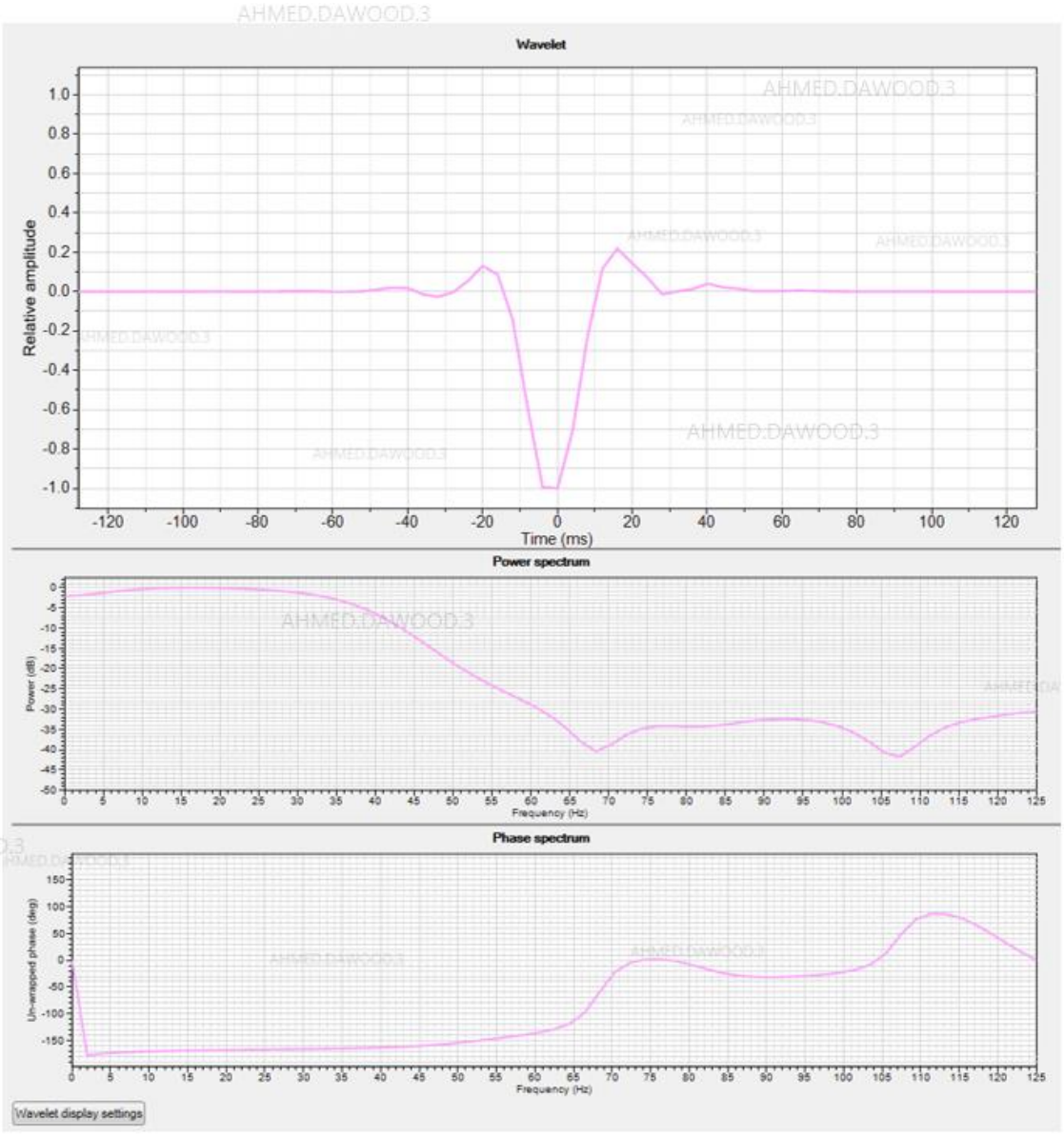

Figure 2.45: Multiwell synthetics wavelet

Multiwell wavelet is used to tie well A synthetics (Figure 2.46) and well B synthetics (Figure 2.47) and the tie is good in both wells.

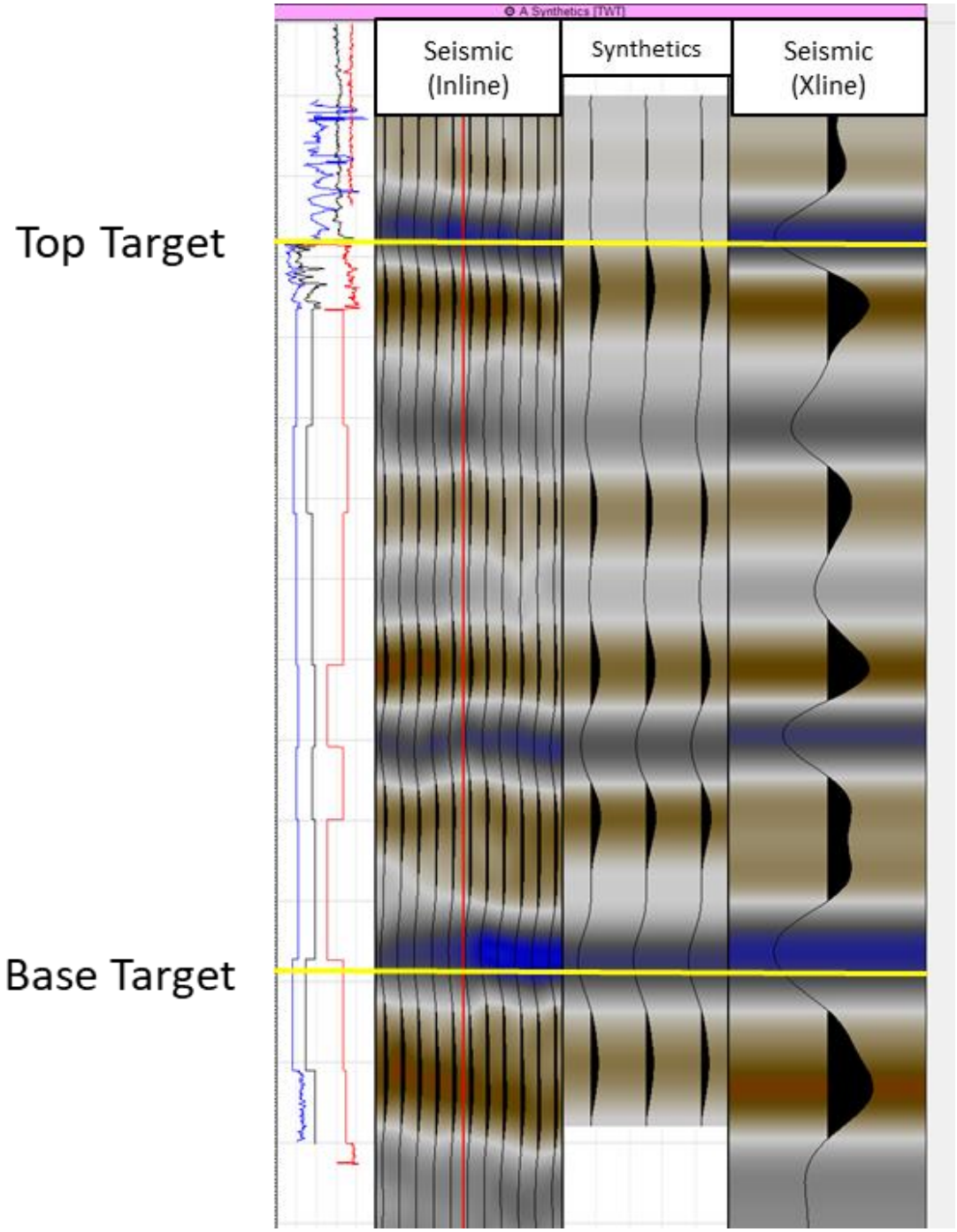

Figure 2.46: Well A synthetics tie to seismic

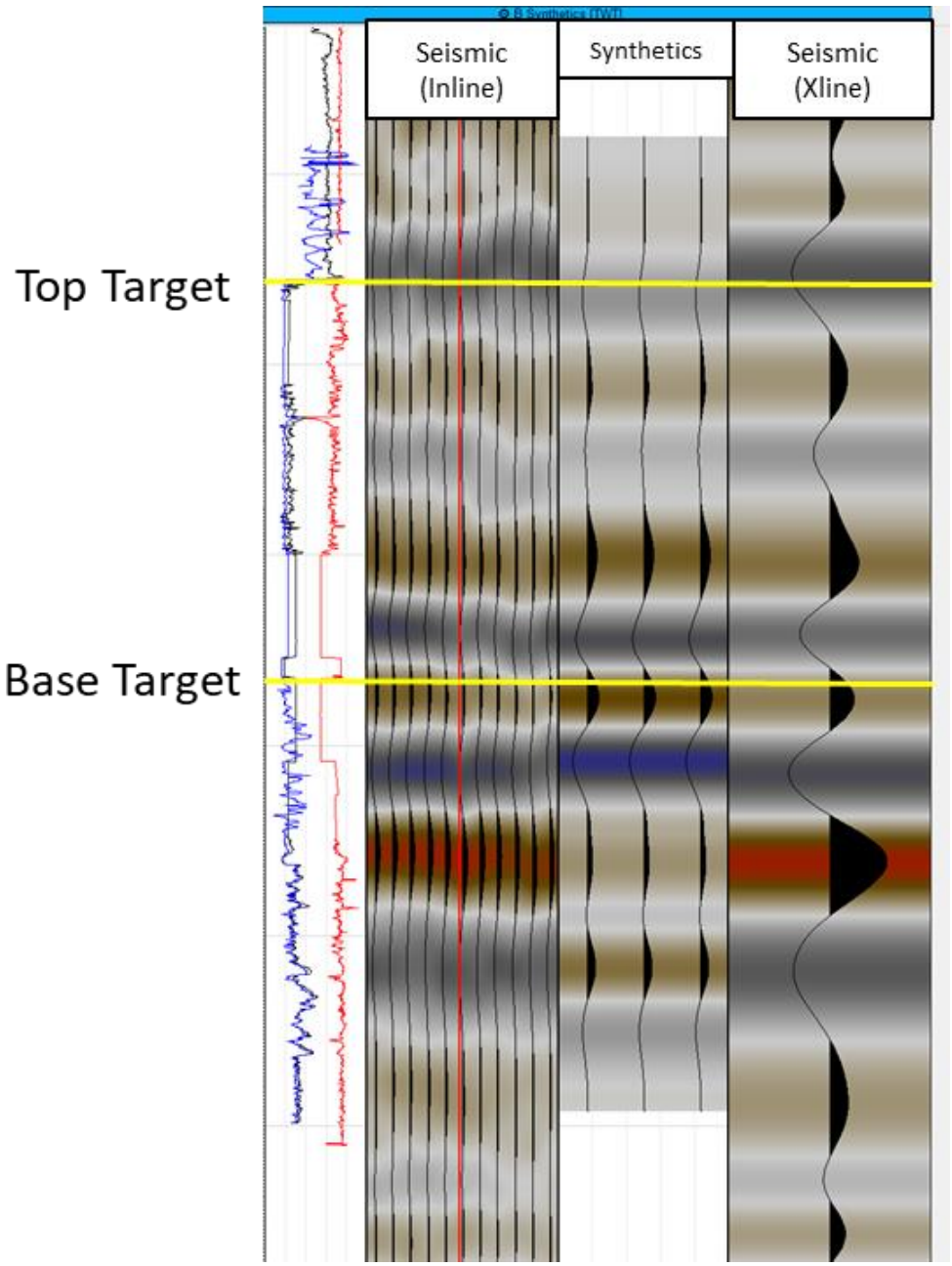

Figure 2.47: Well B synthetics tie to seismic

The five multiwell synthetic angle stacks wavelets that are used in pre-stack inversion are displayed in Figure 2.48.

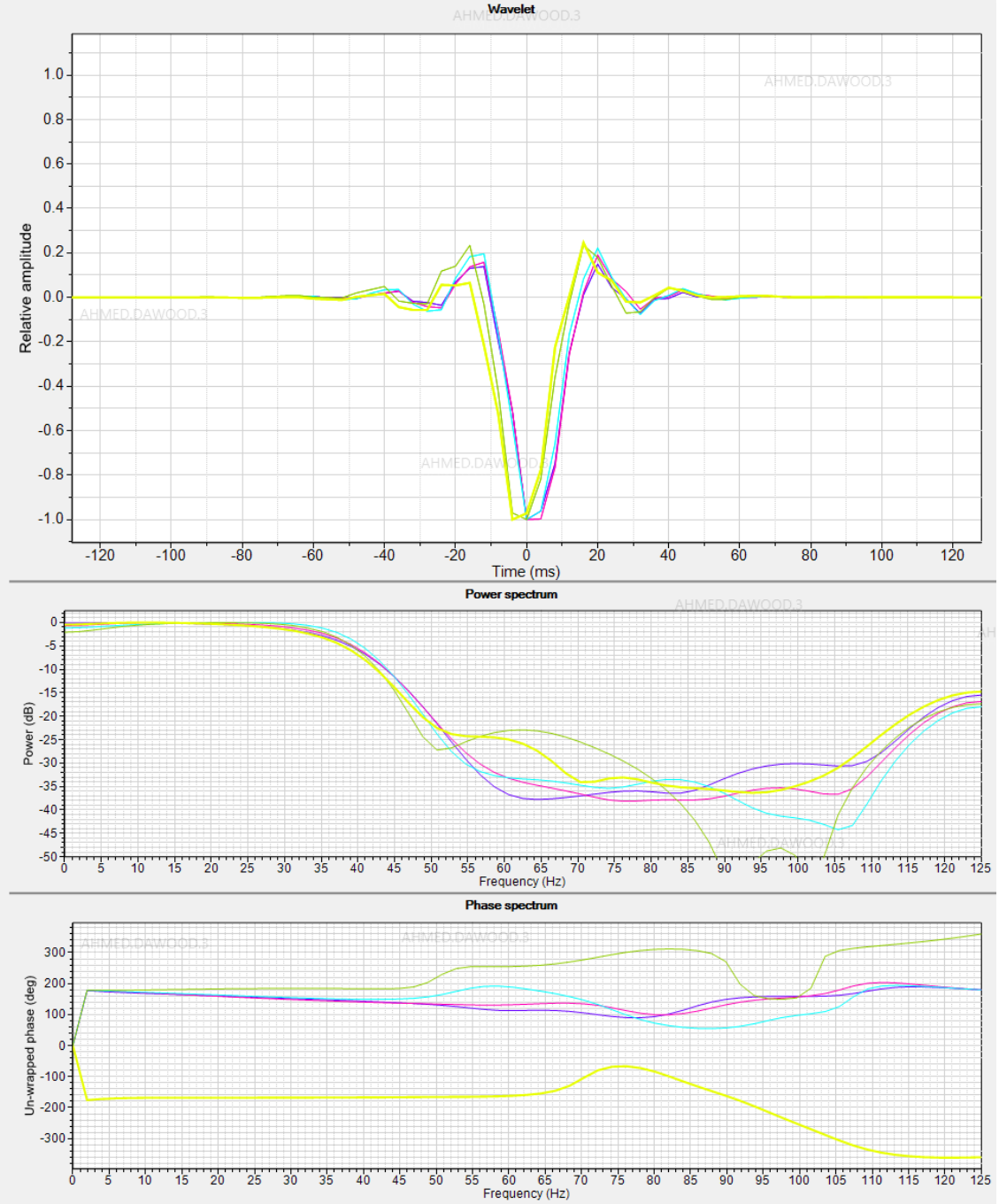

Figure 2.48: Multiwell synthetics angle stacks wavelets

2.7.4 Low Frequency Model

The low frequency model is built from the five synthetic well logs. For pre-stack inversion, low frequency models are needed for acoustic impedance, density, and Vp/Vs. An example of a low frequency model for Acoustic Impedance built from 0-8 Hz is shown in Figure 2.49. The layering between top and base target horizons is clear.

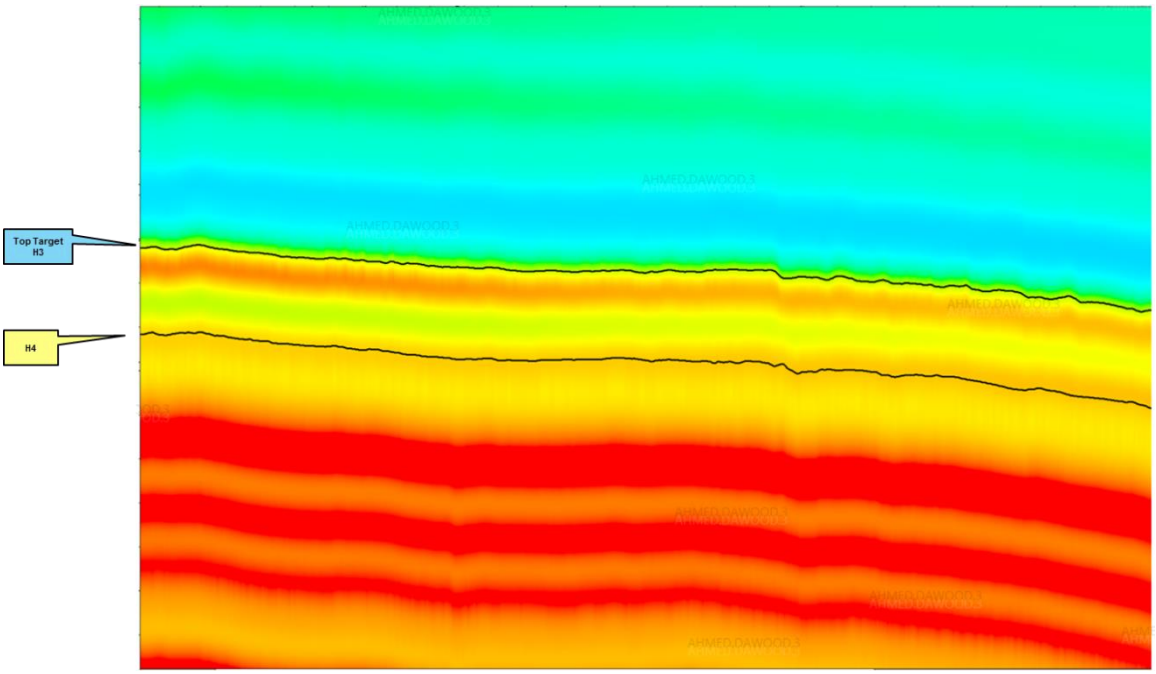

Figure 2.49: Acoustic Impedance low frequency model from synthetic wells (0-8 Hz)

2.8 Pre-stack Inversion

Three low frequency models were created for AI, density, and Vp/Vs. These low frequency models were convolved with the five angle stacks multiwell wavelets for both parts the actual wells and the synthetic wells.

The inversion method being used is a model driven inversion. Aki and Richards approximation of Zoeppritz equations is used to find a relationship between P-wave

reflectivity and the angle of incidence. An initial model of P-wave and S-wave acoustic impedance is convolved with the estimated wavelet to create a synthetic model. The synthetic seismic is subtracted from the real seismic to calculate the residual. The synthetic model is iterated by a simulated annealing technique guided by Monte Carlo approach until the residual is minimized (Ma, 2002).

CHAPTER 3

RESULTS

3.1 Wells Inversion Results

3.1.1 Acoustic Impedance Inversion

In AI inversion result for well A (Figure 3.1), AI inversion and AI log follow the same trend at top target. At the deeper part of the target formation, there is a miss-tie because of the phase.

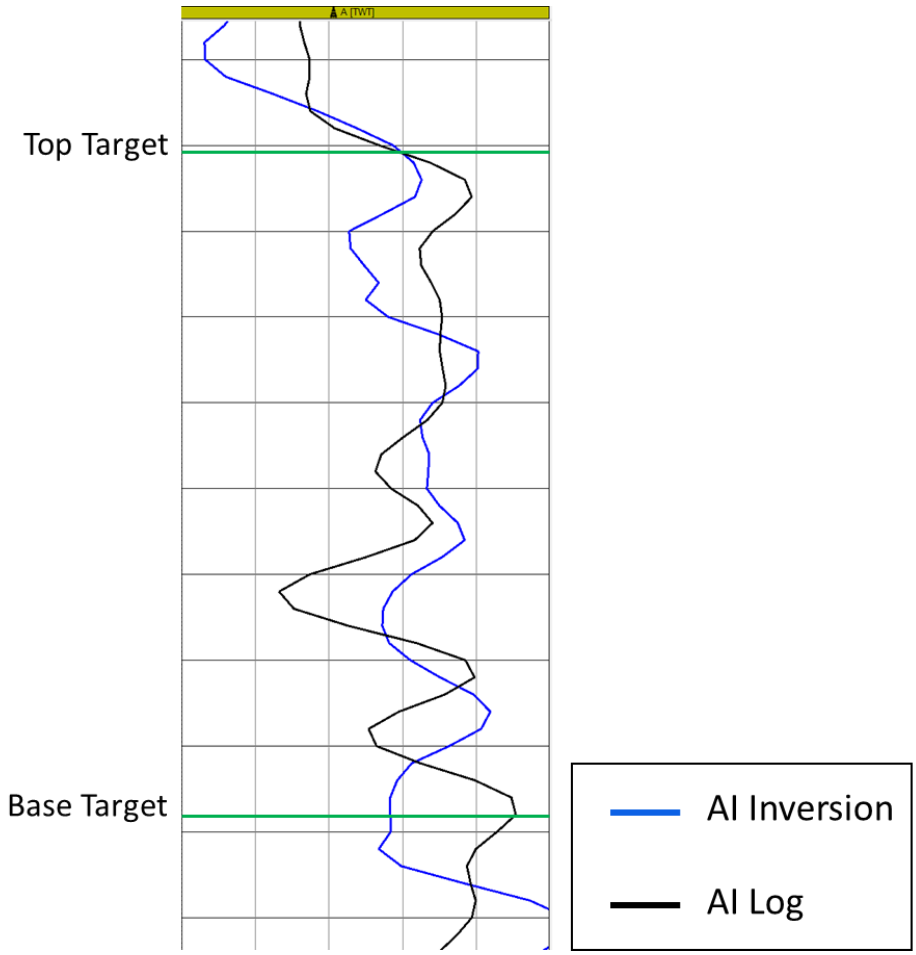

Figure 3.1: AI inversion of well A

In well B (Figure 3.2), AI inversion and AI log are not tying probably because well B is located in the noisy area in seismic block.

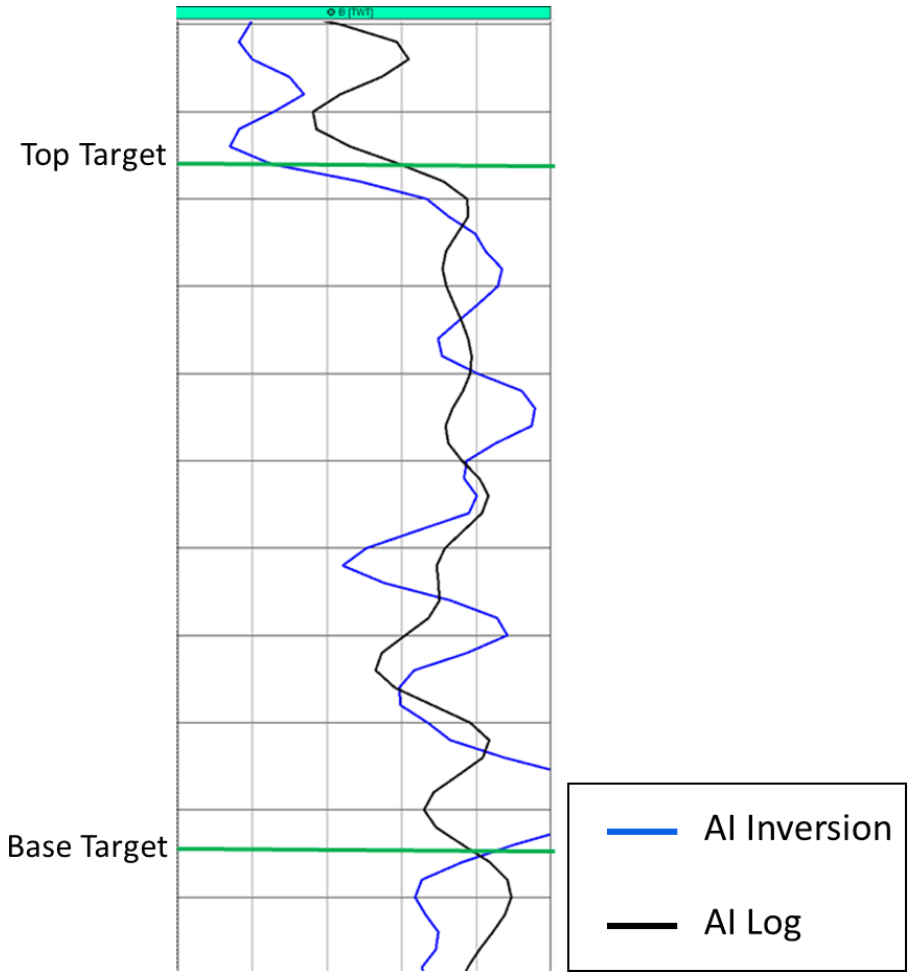

Figure 3.2: AI inversion of well B

3.1.2 Vp/Vs Inversion

In well A (Figure 3.3), Vp/Vs inversion and Vp/Vs log are not tying probably due to noisy angle stacks.

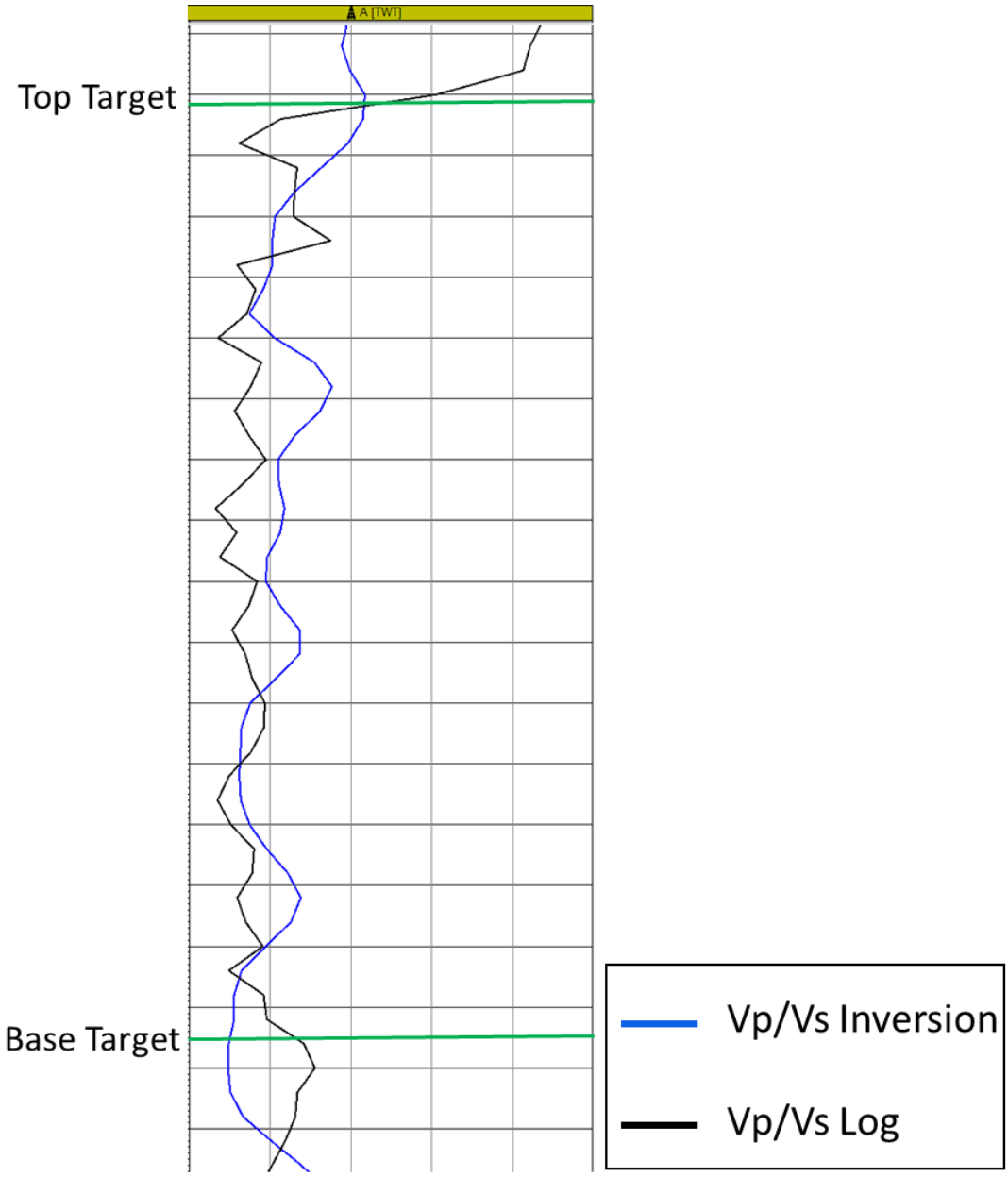

Figure 3.3: Vp/Vs inversion of well A

Well B Vp/Vs inversion is not tying to the log as well (Figure 3.4) probably because well B is located in the noisy area in seismic block.

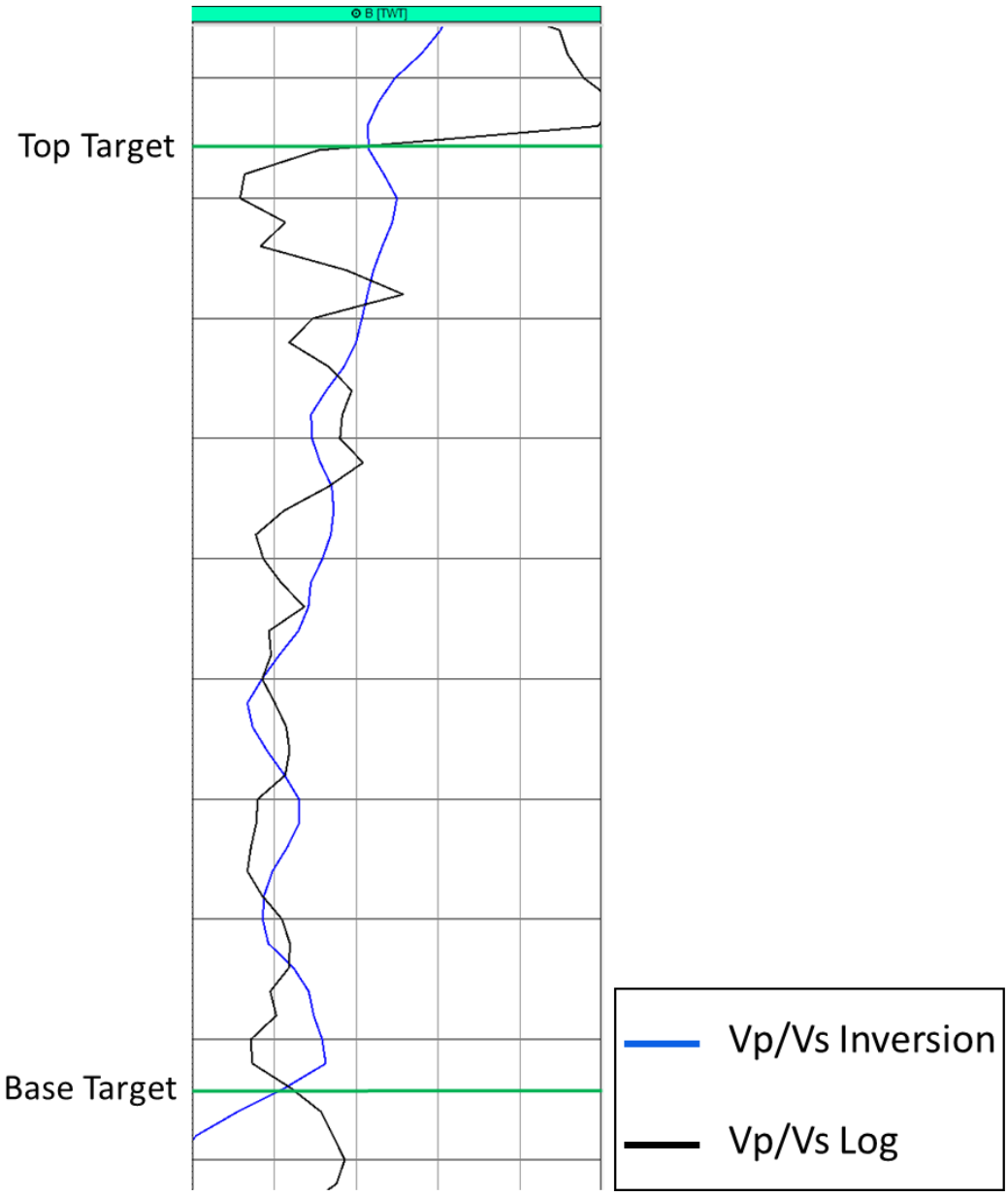

Figure 3.4: Vp/Vs inversion of well B

3.1.3 Density Inversion

In well A (Figure 3.5), density inversion and density log are tying well probably due to the inversion being biased to the low frequency model.

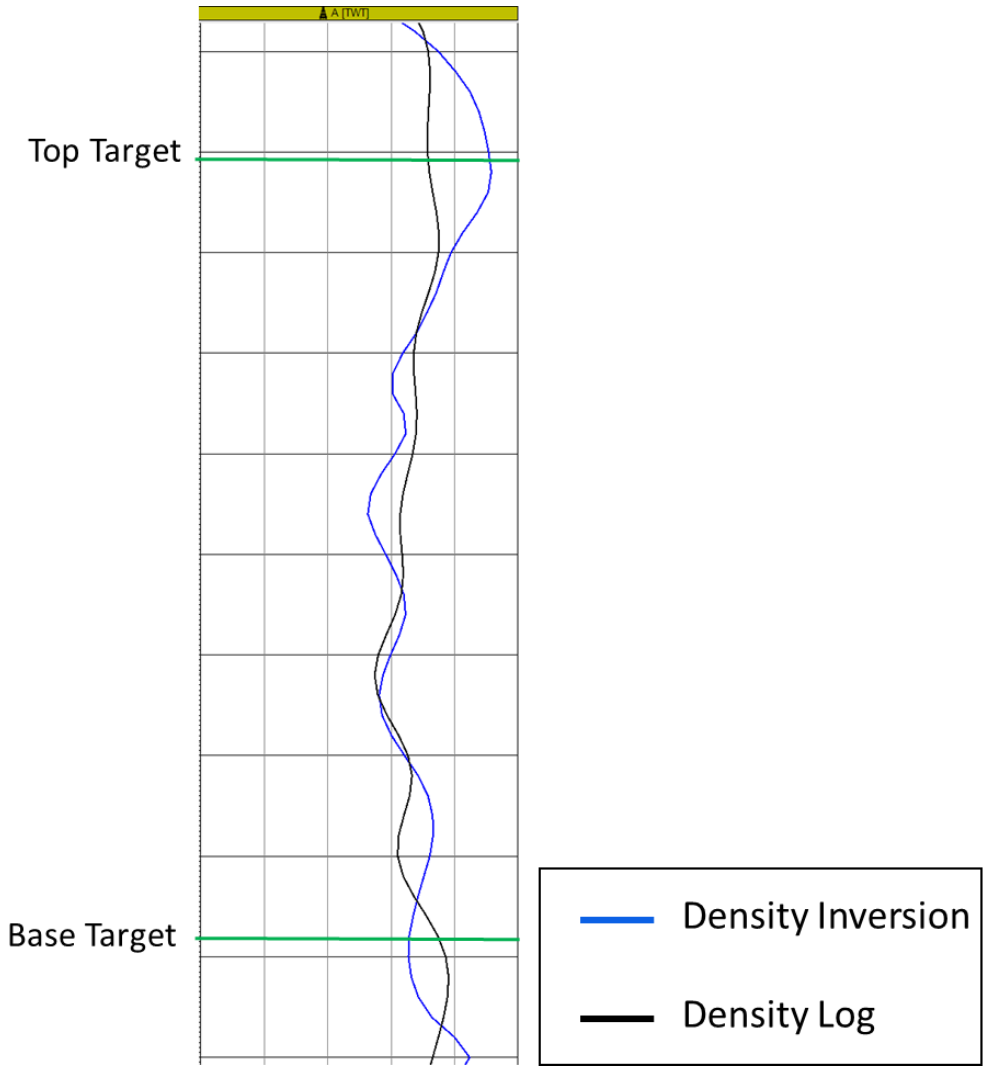

Figure 3.5: Well A density inversion

Similarly, well B density inversion is tying well to the log (Figure 3.6).

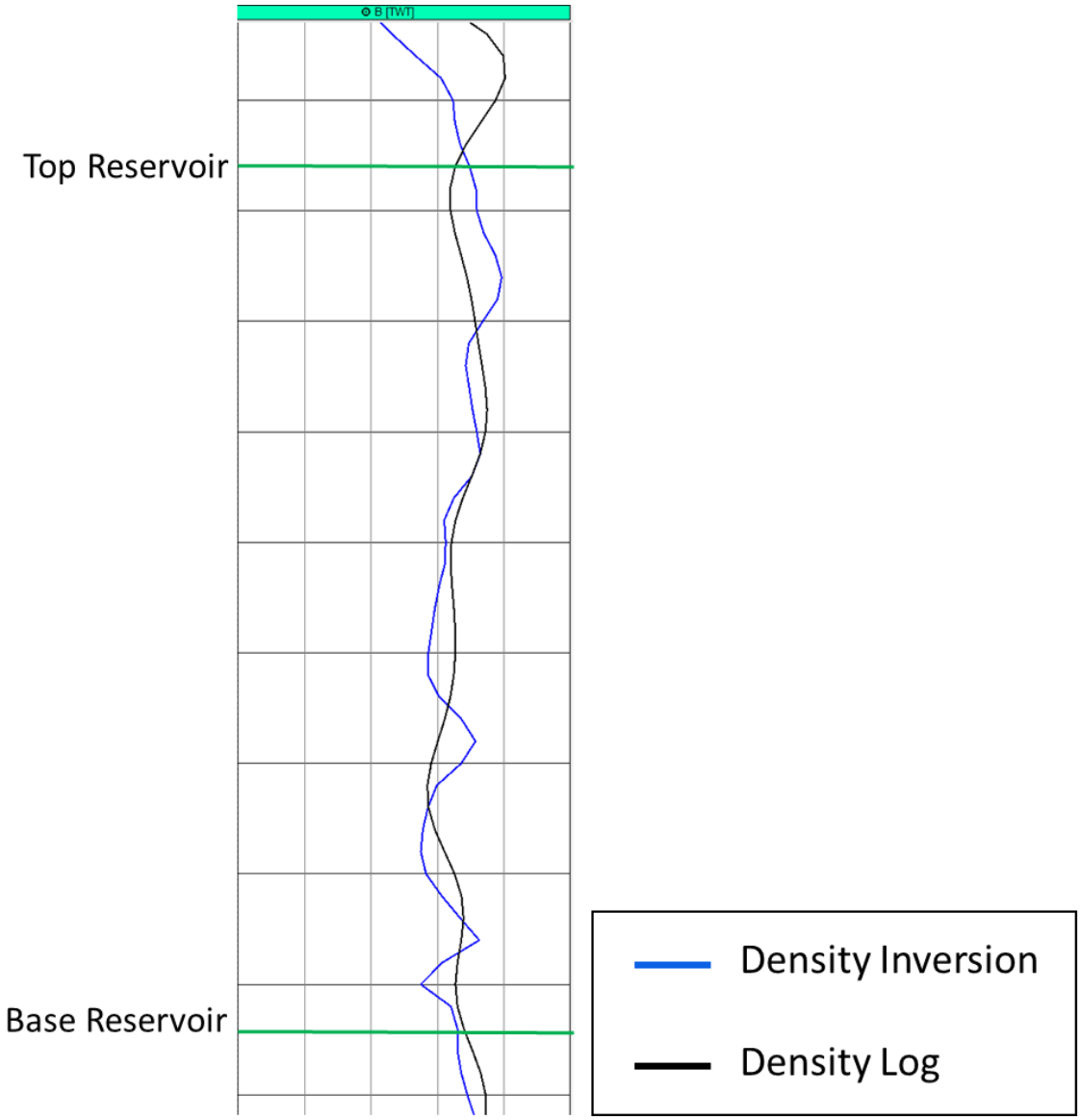

Figure 3.6: Well B density inversion

3.2 Synthetic Wells Inversion Results

3.2.1 Acoustic Impedance Inversion

In AI inversion result for synthetics of well A (Figure 3.7) and well B (Figure 3.8), AI inversion and AI log follow the same trend.

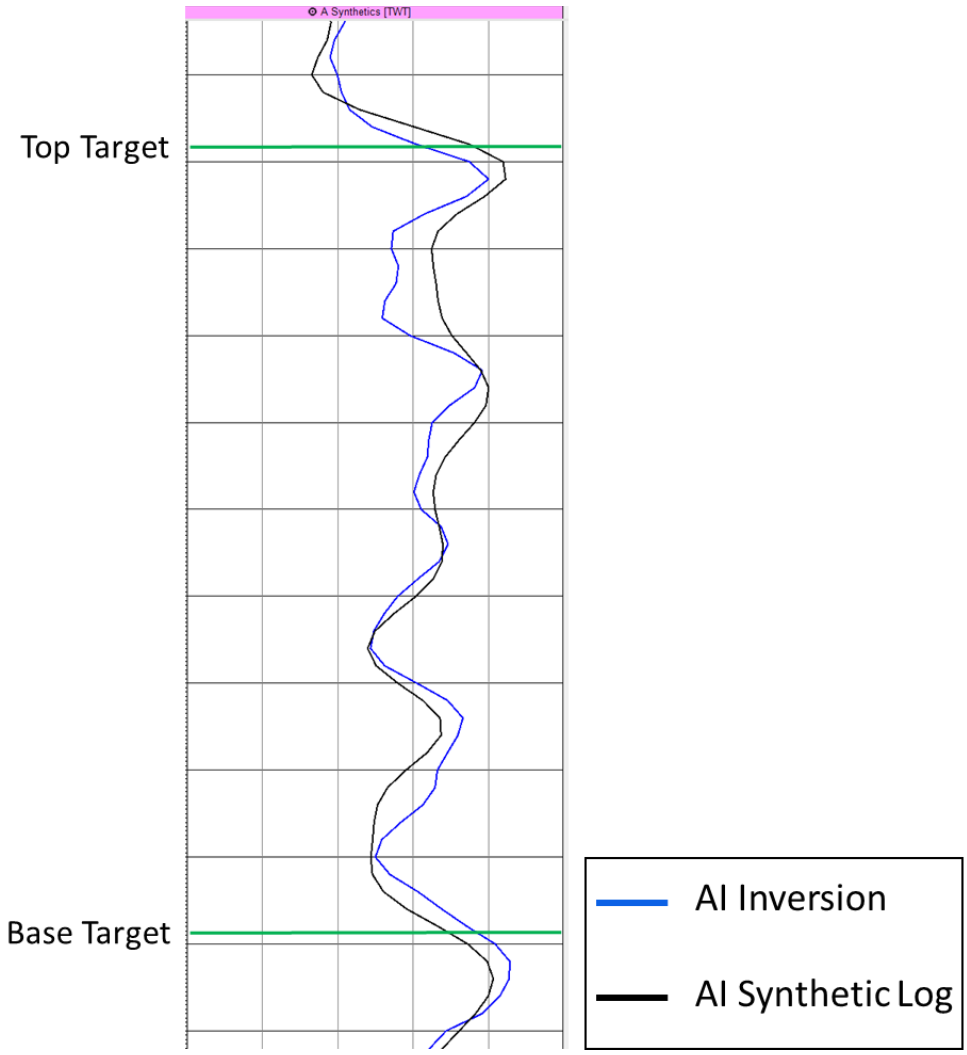

Figure 3.7: Well A synthetics AI inversion

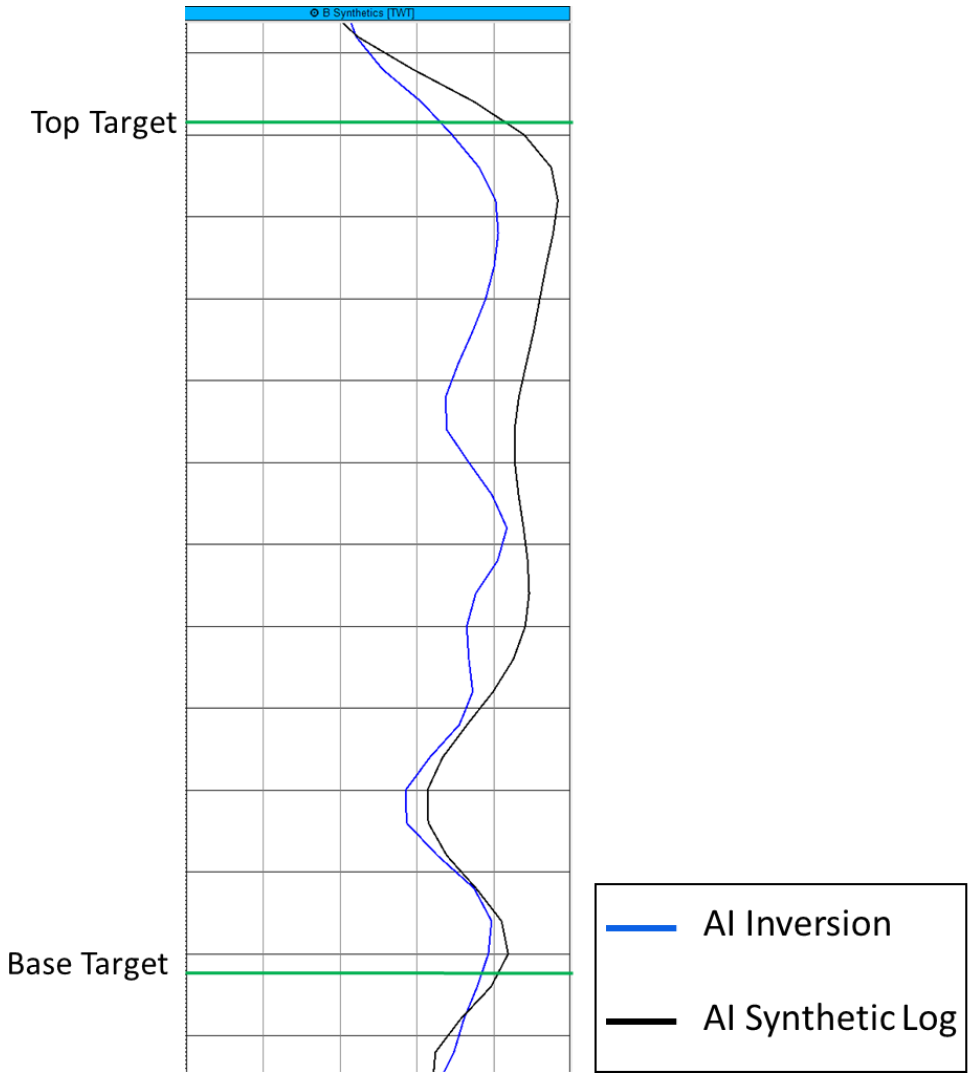

Figure 3.8: Well B synthetics AI inversion

3.2.2 Vp/Vs Inversion

In Vp/Vs inversion result for well A (Figure 3.9) and well B (Figure 3.10), there is a slight miss-tie between Vp/Vs inversion and Vp/Vs log.

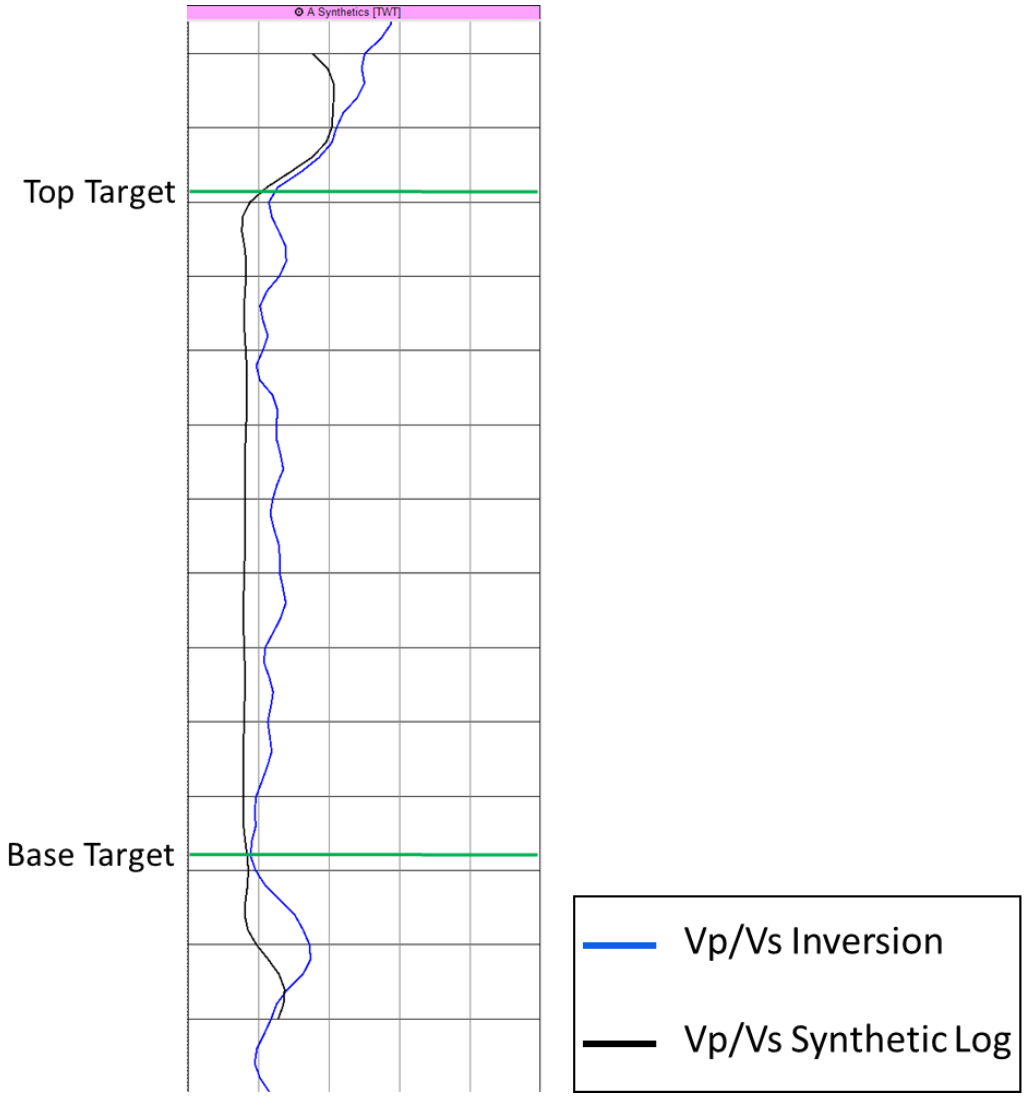

Figure 3.9: Well A synthetics Vp/Vs inversion

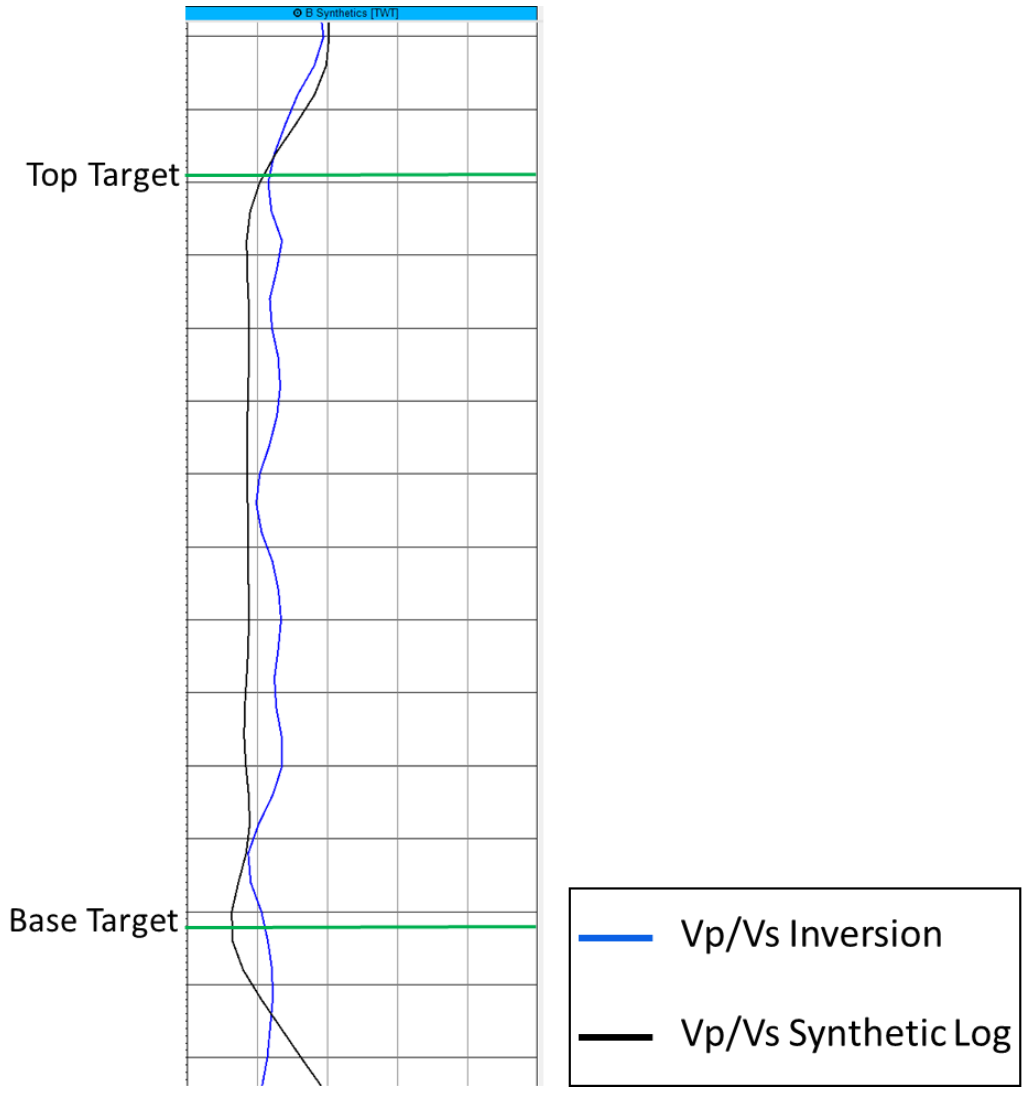

Figure 3.10: Well B synthetics Vp/Vs inversion

3.2.3 Density Inversion

In well A (Figure 3.11) and well B (Figure 3.12) synthetics, density inversion and density log are tying well probably due to the inversion being biased to the low frequency model because the far offset is noisy.

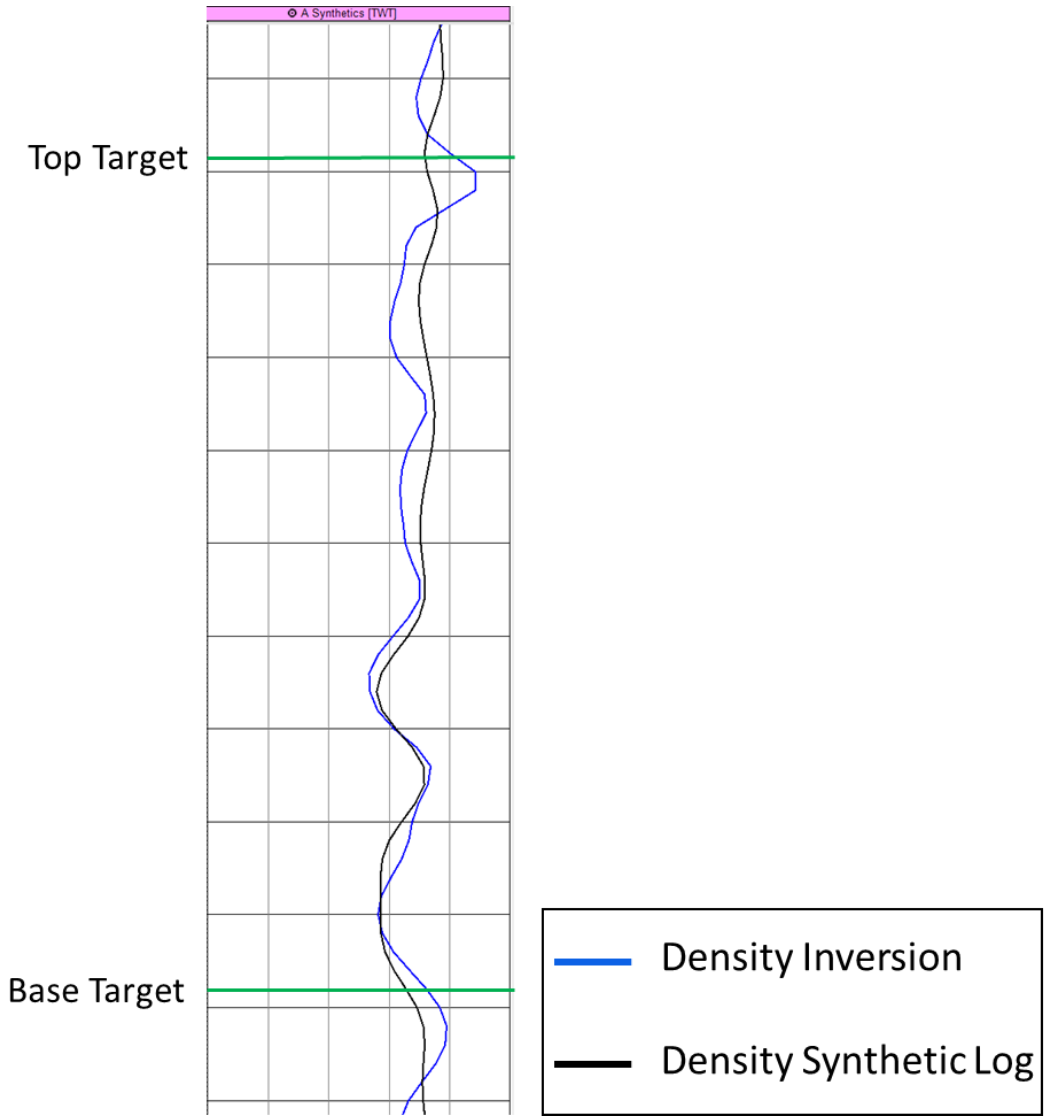

Figure 3.11: Well A synthetics density inversion

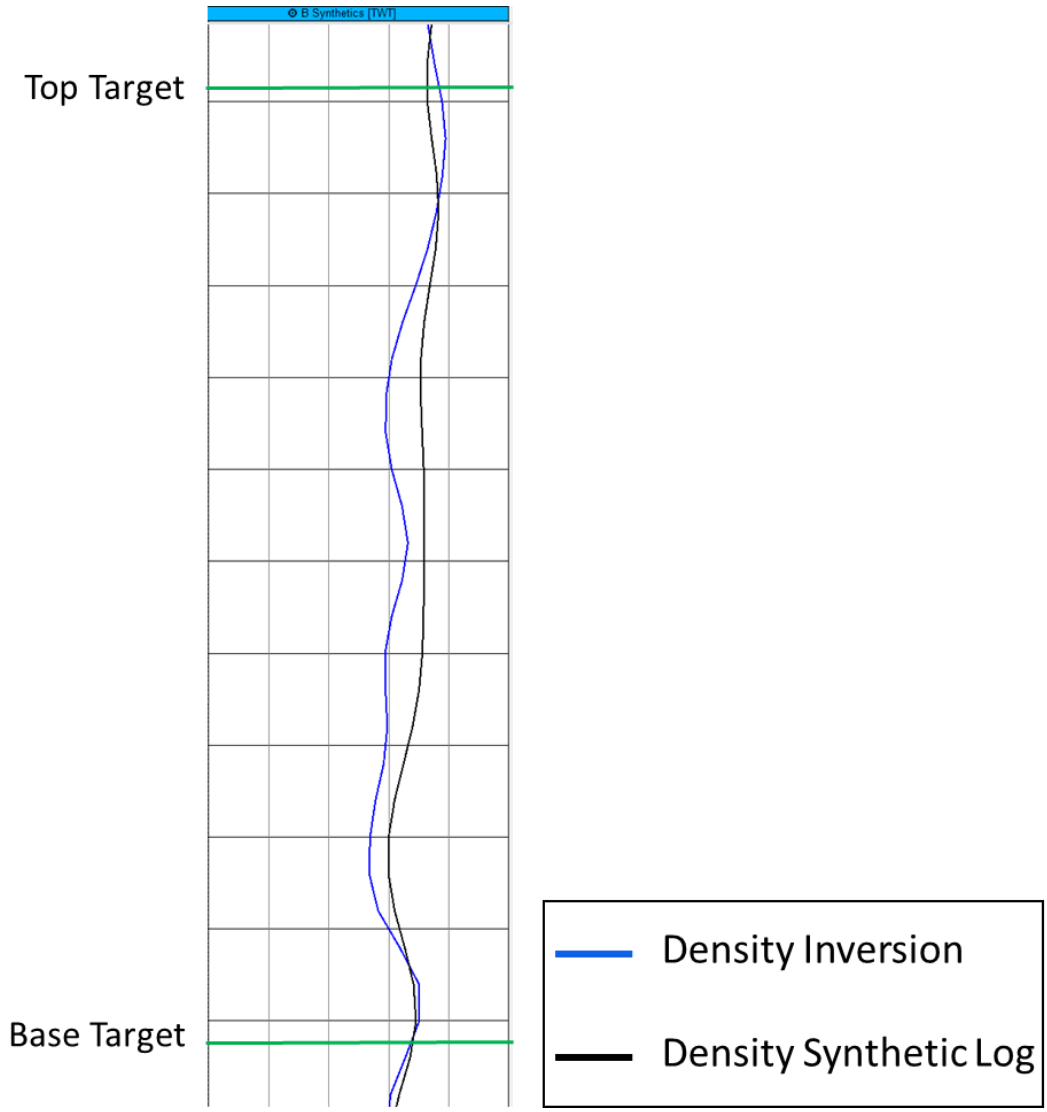

Figure 3.12: Well B synthetics density inversion

CHAPTER 4

PROPERTIES PREDICTION AND DISCUSSION

4.1 Properties Prediction from Actual Wells Inversion

4.1.1 Porosity Volume Estimation

Porosity was estimated using two methods. The first method was done using the direct linear relationship between acoustic impedance and porosity form all the well logs at the target formation level (Figure 4.1). Based on this relationship, AI volume was converted to a porosity volume. Comparing log porosity from well A to the porosity derived from AI inversion gave a matching value of approximately 60%.

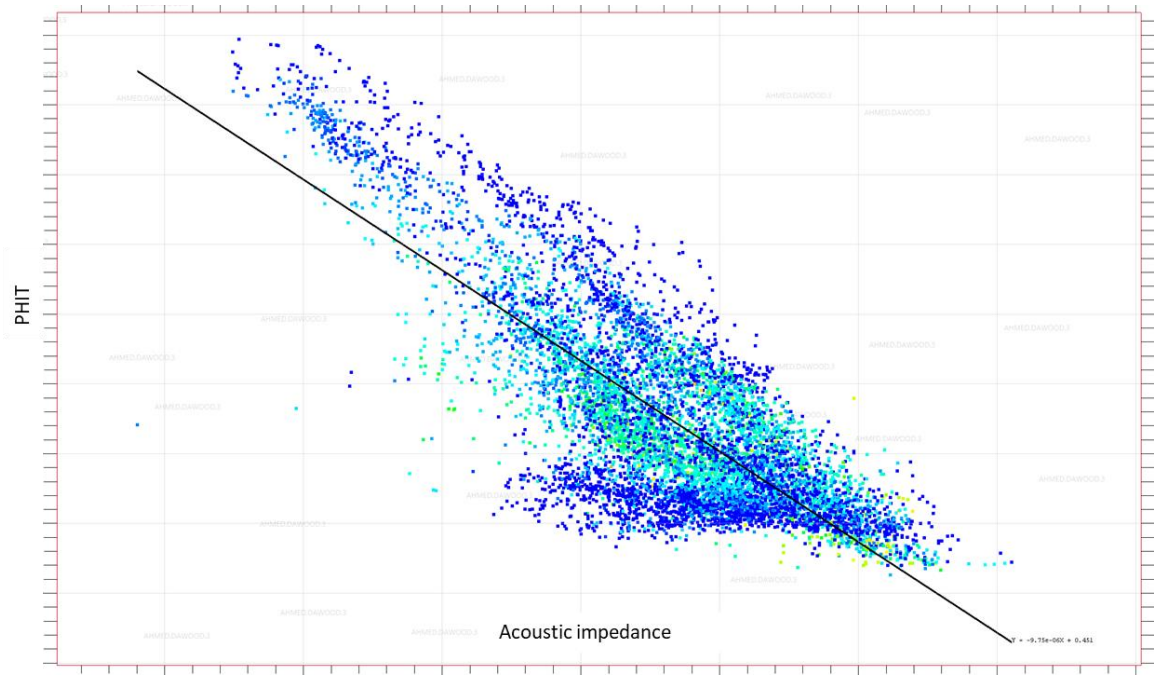

Figure 4.1: Crossplot of acoustic impedance and porosity of all wells

The second method is to estimate porosity using a neural network guided inversion supervised by porosity from well logs. Comparing log porosity from all wells to the porosity derived from neural networks gave a matching value of approximately 78%. At the location of well A, both porosity volumes were converted to well logs using the time depth relationship of well A to compare them to the actual porosity log. The porosity log was sampled to 140 ft, which is the tuning thickness at well A location (Figure 4.2).

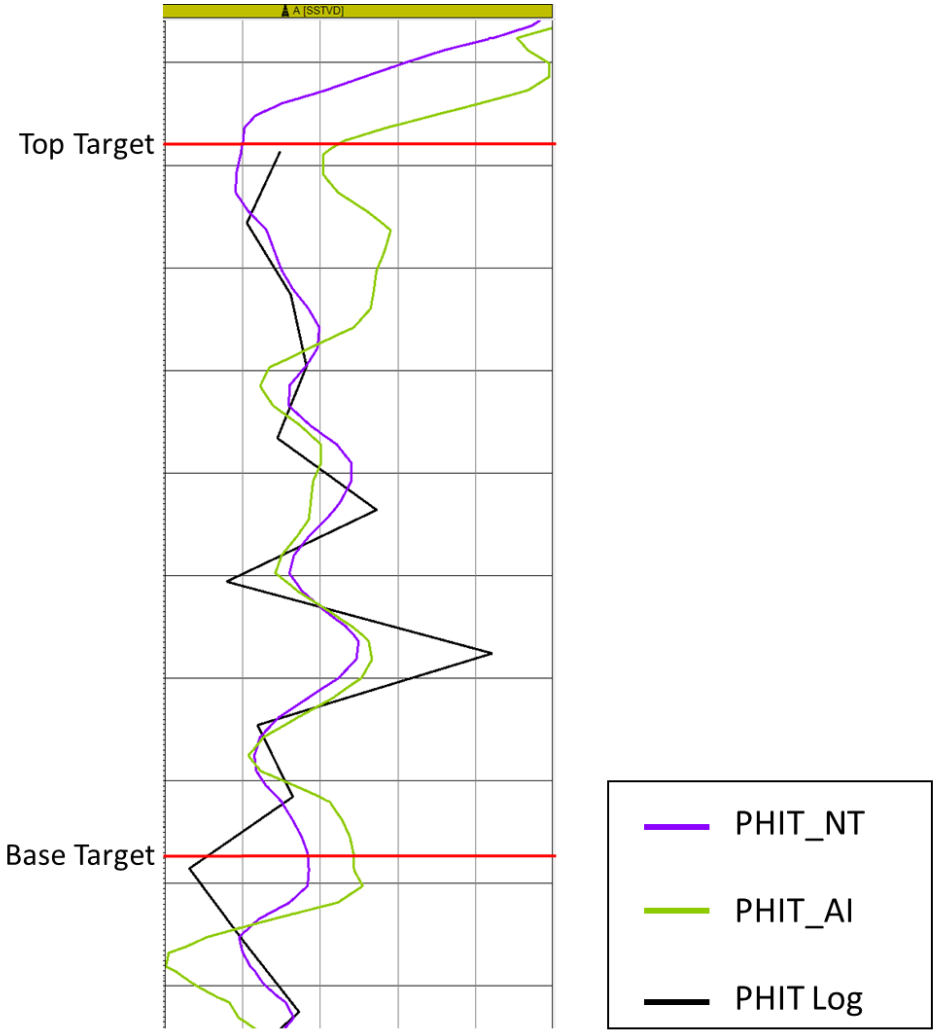

Figure 4.2: Comparison between porosity log and inversion estimated porosities

From the matching percentage and the well logs comparison at well A, porosity derived from neural network is more reliable to be used than AI-derived porosity.

4.1.2 Gas Volume Estimation

Gas saturated volume was estimated using two methods. The first method used the pay zone equation derived from rock physics modeling (Figure 2.11). The second method is to estimate gas saturated volume using a neural network guided inversion supervised by gas saturation from well logs. Comparing log gas saturation from all wells to the gas saturation derived from neural networks gave a matching value of approximately 56%. At the location of well A, both gas volumes were converted to well logs using the time depth relationship of well A to compare them to the actual gas saturation log. The gas saturation log was sampled to 140 ft, which is the tuning thickness at well A location (Figure 4.3).

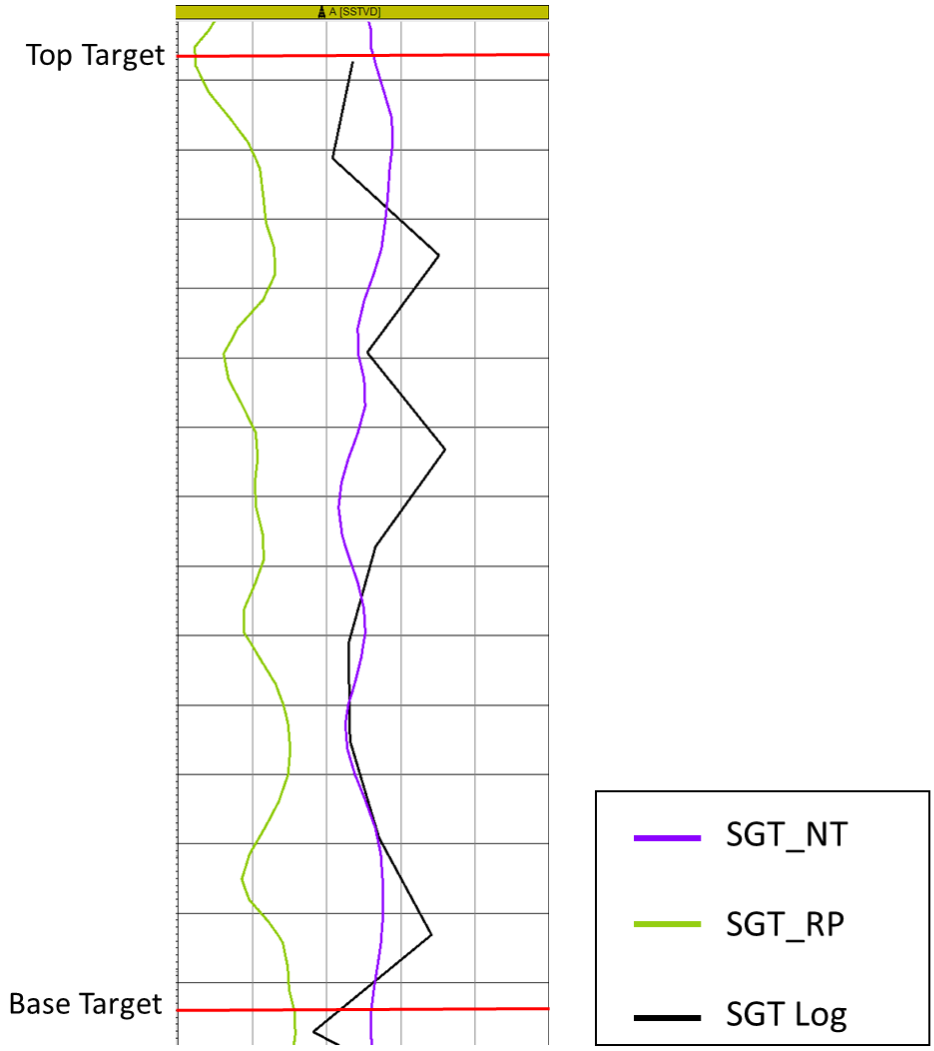

Figure 4.3: Comparison between gas saturation log and inversion estimated gas saturation

From the well logs' comparison at well A, gas saturation derived from neural network is more reliable to be used than rock physics modeling gas saturation.

4.2 Properties Prediction from Synthetic Wells Inversion

4.2.1 Porosity Volume Estimation

Porosity was estimated using the direct linear relationship between acoustic impedance and porosity form well F at the target formation level (Figure 4.4).

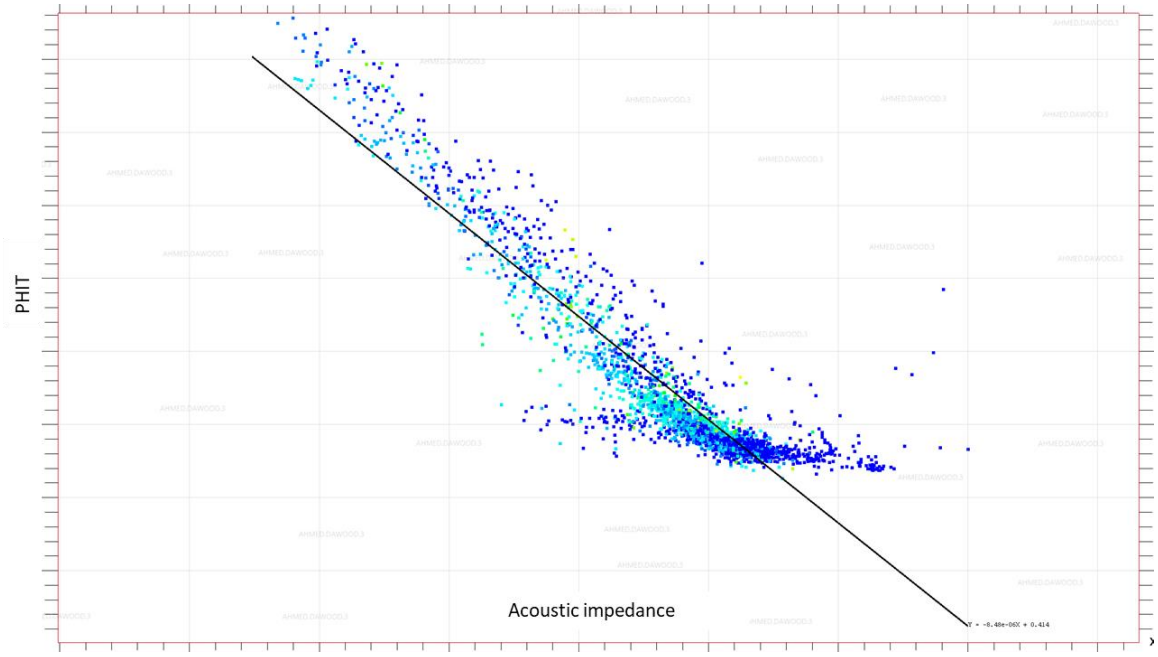

Figure 4.4: Crossplot of acoustic impedance and porosity of well F

Based on this relationship, AI volume was converted to a porosity volume. At the location of well A, the porosity volume was converted to a well log using the time depth relationship of well A to compare it to the actual porosity log as well as the porosity derived for the AI relationship in the actual wells' inversion. The porosity log was sampled to 140 ft which is the tuning thickness at well A location (Figure 4.5).

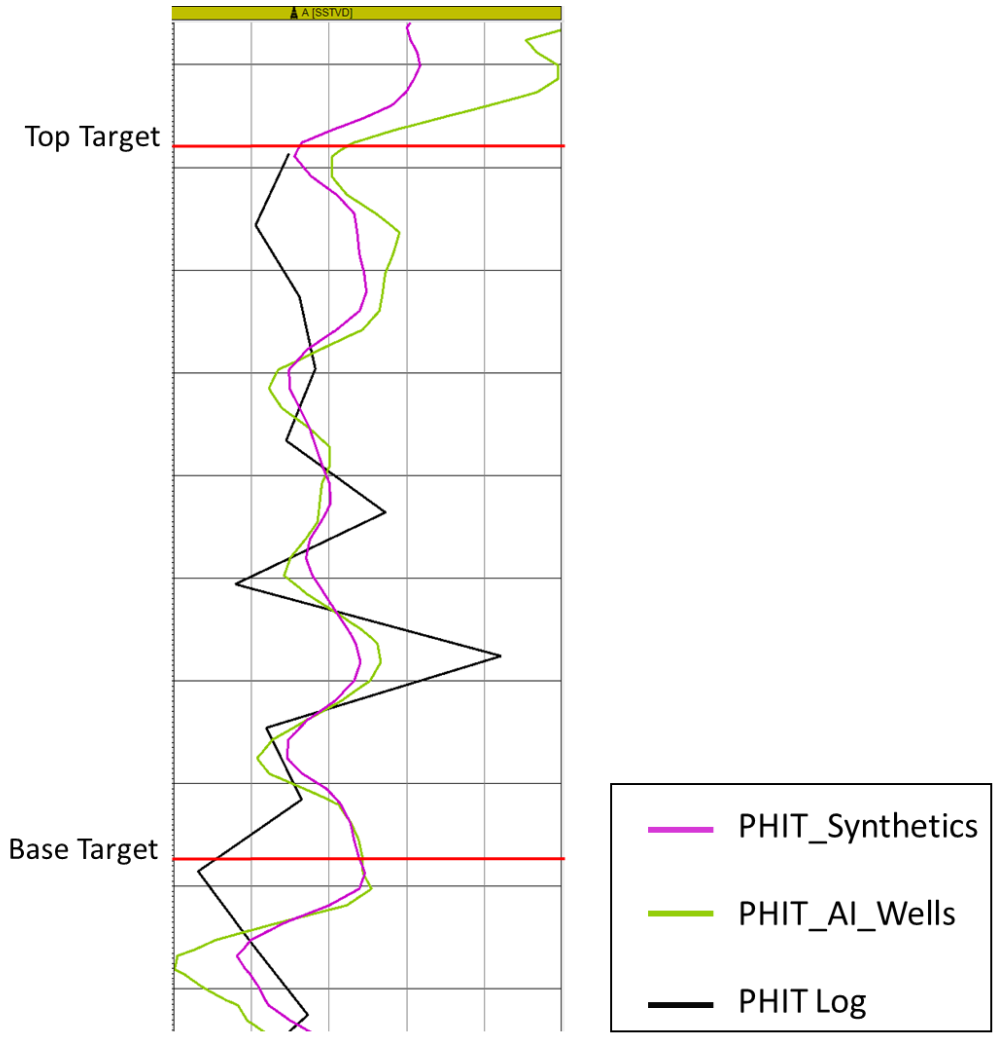

Figure 4.5: Comparison between porosity log and the two different inversion estimated porosities

From the well logs' comparison at well A, porosity derived from synthetics inversion is very similar to the porosity derived from actual wells inversion.

4.2.2 Gas Volume Estimation

Gas saturated volume was estimated using the pay zone equation derived from rock physics modeling (Figure 2.44). At the location of well A, the gas volume was converted to a well log using the time depth relationship of well A to compare it to the actual gas saturated log as well as gas saturation derived from rock physics modeling in the actual

wells' inversion. The gas saturation log was sampled to 140 ft, which is the tuning thickness at the well A location (Figure 4.6).

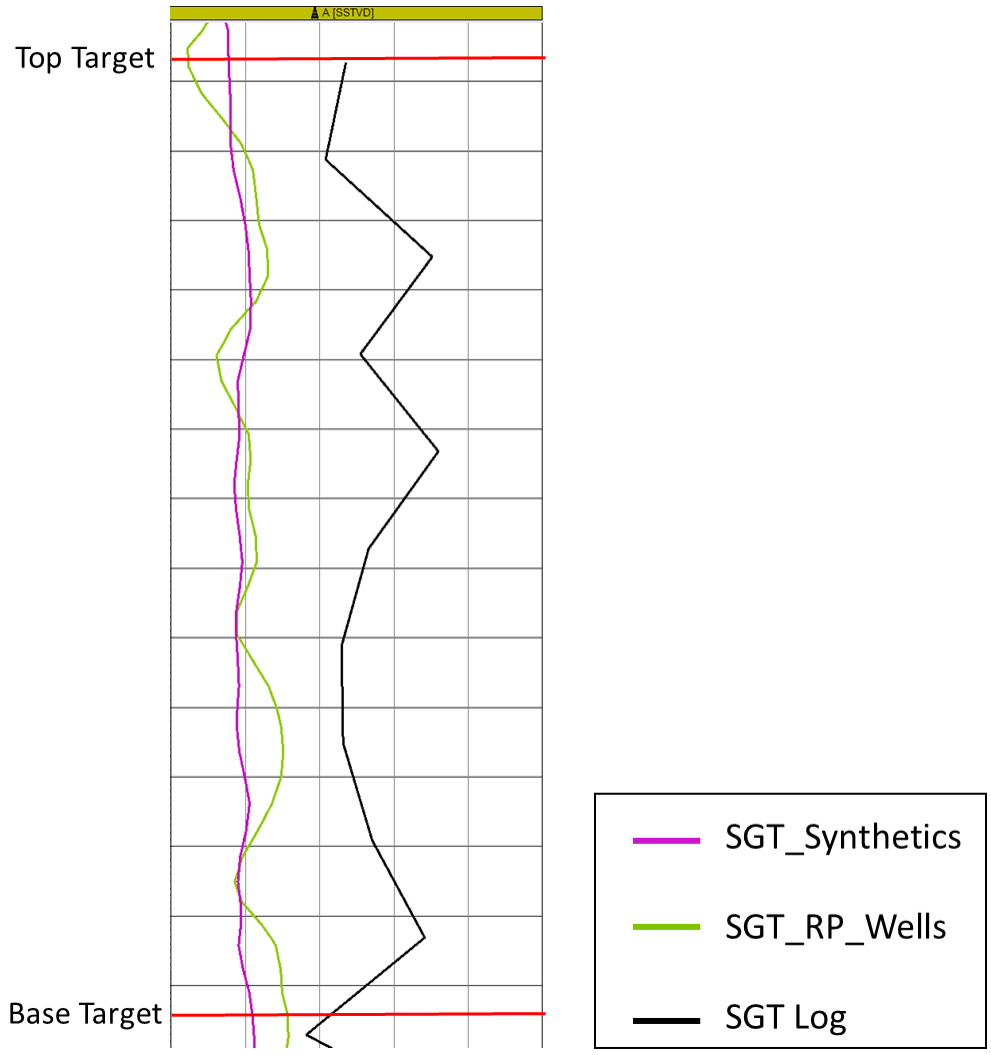

Figure 4.6: Comparison between gas saturation log and the two different inversion estimated gas volumes

From the well logs' comparison at well A, gas saturation derived from synthetics inversion is very similar to the gas saturation derived from actual wells inversion.

4.3 Comparison between Real and Synthetic Wells Inversion

The study results show that all synthetic logs generated by forward modeling of P-wave, S-wave, and density gave less than 10% error when compared to the real well logs.

Generating an inversion from synthetic logs gave similar inversion results when compared to using the original logs. The properties predicted from both inversion results are not recommended to be used in further studies in placing future wells even though their results are matching. Porosity prediction from inversion is not matching well with the porosity logs due to phase inconsistency and noise of the data and that anticipated from the seismic well tie where the synthetics were not matching well with the seismic. Fluid prediction from inversion is not matching with the gas saturation logs. That was early predicted from the AVO feasibility study where the AVA response is not matching in the mid offset between synthetics and seismic gathers. Therefore, fluid prediction from inversion is not going to be accurate.

CHAPTER 5

CONCLUSIONS AND RECOMMENDATIONS

5.1 Conclusions

The study was conducted to test the ability of fluid prediction directly from seismic data. The main findings of this thesis work are:

- The seismic data used in this study was noisy and suffered from phase inconsistency as displayed in the wavelets extractions where the predictability values are low and phase is inconsistent with frequency.
- AVO-friendly processing of the data is needed as seen by the mismatch of synthetics AVA responses from the mid offsets.
- Several methods of wavelet extractions were used to extract the best wavelet for inversion.
- Porosity prediction by neural networks from the real wells' inversion gave good results.
- Porosity prediction from synthetic wells inversion is similar to porosity prediction from the real wells generated by the acoustic impedance relationship. Both of them are not matching closely with the porosity logs.
- Gas saturation prediction from synthetic wells inversion is similar to gas saturation prediction from the real wells generated by rock physics modeling. Both of them are not matching the gas saturation logs.
- Gas saturation prediction by neural networks from the real wells is 56% matching with gas saturation log. It is only recommended to be used as a guidance.

5.2 Recommendations

Based on the outcomes of the study, these are the recommendations on the way forward:

- Reprocess the seismic data gathers from field tapes to enhance the signal to noise ratio using an AVO-friendly processing workflow.
- Apply the synthetic inversion on an area with a better seismic quality where fluid prediction is valid from real well logs inversion.

References

[1] Ali, A., Al-Shuhail, A., "Characterizing fluid contacts by joint inversion of seismic P-wave impedance and velocity," *Exploration Geophysics,* vol.8, no.1, pp. 117- 130, 2017.

[2] Altowairqi, Y., "Seismic Inversion Applications and Laboratory Measurments to Identify High TOC Shale," Doctoral dissertation, Curtin University, 2015.

[3] Barclay, F., Bruun, A., Rasmussen, K., Alfaro, J., Cooke, A., Cooke, D., Salter, D., Godfrey, R., Lowden, D., McHugo, S., Ozdemir, H., "Seismic Inversion: Reading between the lines," *Oilfield Review,* vol.20, no.1, pp. 42-63, 2008.

[4] Craigie, N.W., Rees, A., MacPherson, K., Berman, S., "Chemostratigraphy of the Ordovician Sarah Formation, North West Saudi Arabia: An integrated approach to reservoir correlation," *Marine and Petroleum Geology* vol.77, pp. 1056- 1080, 2016.

[5] Feng, H., Bancroft, J.C., "AVO principles, processing and inversion," CREWES Research Report, , vol.18, pp. 1- 19, 2006.

[6] Foster, D.J., Keys, R.G., Lane, F.D., "Interpretation of AVO anomalies," *GEOPHYSICS,* vol.75, no.5, pp. 75A3- 75A13, 2010.

[7] Kemper, M., "Seismic Inversion," *seismic technology,* p. 10, 2010.

[8] Laboun, A., A., "Paleozoic tectono-stratigraphic framework of the Arabian Peninsula," *Journal of King Saud University (Science),* 2009.

[9] Ma, X., "Simultaneous inversion of Prestack Seismic Data for Rock Properties using Simulated Annealing," *Geophysics,* vol.67, pp. 1877-1885, 2002.

[10] Melvin, J., "Lithostratigraphy and depositional history of Upper Ordovician and lowermost Silurian sediments recovered from the Qusaiba-1 shallow core hole, Qasim region, central Saudi Arabia," *Review of Palaeobotany and Palynology,* vol.212, pp. 3- 21, 2015.

[11] Rutherford, S.R., Williams, R.H., "Amplitude-versus-offset variations in gas sands," *GEOPHYSICS,* vol.54, no.6, pp. 680-688, 1989.

[12] Senlap, M., Al-Duaiji, A.A., "Qasim Formation: Ordovician storm and tide dominated shallow-marine siliciclastic sequences, Central Saudi Arabia," *Geo Arabia,* vol.6, pp. 223- 268, 2001.

[13] Serra, O., “fundamentals of well-log interpretation,” Developments in Petroleum Science, vol.1, 1984.

[14] Varhaug, M., "Basic Well Log Interpretation," *Oilfield Review,* p. 52-53, 2016.

Vitae

Name	: Ahmed Al-Dawood
Nationality	: Saudi
Date of Birth	: 4/4/1989
Email	: ahmed.aldawood89@gmail.com
Address	: P.O. Box 12277 Dhahran 31311, Saudi Arabia
Academic Background	: B.S. in Geophysics from the University of Oklahoma